MULTIBODY SIMULATION OF COUPLED AERODYNAMICS AND STRUCTURAL MODEL OF A HELICOPTER MAIN ROTOR

BİR HELİKOPTERİN ANA ROTORUNUN AERODİNAMİK VE YAPISAL ETKİLER DAHİL EDİLEREK OLUŞTURULMUŞ MODELİNİN ÇOK GÖVDELİ SİMÜLASYONU

Gürkan SERTSOY

SUPERVISOR
Prof. Dr. Volkan PARLAKTAŞ

2nd SUPERVISOR
Assoc. Prof. Dr. Barış SABUNCUOĞLU

Thesis Submitted to

Graduate School of Science and Engineering of Hacettepe University

as a Partial Fulfillment to the Requirements

for the Award of the Degree of Master of Science

in Mechanical Engineering

February 2023

To my family

ABSTRACT

MULTIBODY SIMULATION OF COUPLED AERODYNAMICS AND STRUCTURAL MODEL OF A HELICOPTER MAIN ROTOR

Gürkan SERTSOY

Master of Science, Mechanical Engineering

Supervisor: Prof. Dr. Volkan Parlaktaş

2nd Supervisor: Assoc. Prof. Dr. Barış Sabuncuoğlu

February 2023, 90 pages

The use of helicopters has been on the rise since their invention, particularly due to their ability to perform axial and hover flights. However, designing a helicopter rotor is a complex process, as it involves understanding the aerodynamics and flexible structures of the rotor. The purpose of this thesis is to develop a kinematic rotor model with structural flexibility in a multibody simulation environment, and to perform maneuvers such as hover and forward flight with the model.

The research begins by developing an algorithm using PYTHON to efficiently complete the design, analysis, and post-processing work. The algorithm includes the following steps. First, CAD model of the rotor using Simcenter 3D NX is created. Airfoil profiles are generated using XFOIL software. Then, development of a kinematic multibody model of the rotor using Simcenter 3D Motion software is performed. Flexible models of the rotor blades using the finite element modeling tool of Simcenter 3D are generated.

Finally, aerodynamic parameters of the airfoils using XFOIL software are determined and application of these parameters to the blades are performed using blade element theory.

To verify the model, a FLIGHTLAB model with similar specifications to the Simcenter 3D model is also generated. In verification analyses, a wind tunnel test data is used in aerodynamic model in FLIGHTLAB and Simcenter 3D models. Hover and forward flight maneuver solutions obtained from the FLIGHTLAB and Simcenter 3D rotor models are compared.

Additionally, the thesis examines the effect of various parameters such as twist distribution, wing span, chord length, and material types on the aerodynamic loadings of the rotor blades.

This research contributes to the field of helicopter rotor design by providing a novel approach to simulating aerodynamic loading and structural flexibility in a multibody environment. The results of this thesis can be used to improve the design and performance of helicopter rotors in the future.

Keywords: Simulations, Aerodynamics, Multibody, Elasticity, Loads.

ÖZET

BİR HELİKOPTERİN ANA ROTORUNUN AERODİNAMİK VE YAPISAL ETKİLER DAHİL EDİLEREK OLUŞTURULMUŞ MODELİNİN ÇOK GÖVDELİ SİMÜLASYONU

Gürkan SERTSOY

Yüksek Lisans, Makine Mühendisliği Bölümü

Tez Danışmanı: Prof. Dr. Volkan Parlaktaş

Eş Danışman: Doç. Dr. Barış Sabuncuoğlu

Şubat 2023, 90 sayfa

Helikopterlerin önemi icat edildiklerinden beri sürekli artmaktadır. Özellikle helikopterlerin sahip oldukları eksenel uçuş ve duraksama uçuş yapabilme kapasiteleri onları daha da değerli kılmaktadır. Fakat, oldukça karmaşık aerodinamik ve yapısal elastikiyet etkileri sebebiyle bir helikopterin rotorunu tasarlamak karmaşık bir süreçtir. Bu tezde, çoklu vücut simülasyon ortamında yapısal esnekliği olan bir helikopter kinematik rotor modeli tasarlamak ve modelle hover ve ileri uçuş gibi manevraları gerçekleştirmek amaçlanmaktadır.

Prosedürün ilk adımında, tezde yapılacak olan tüm işleri bir çok farklı tasarım için oldukça verimli ve hızlı tamamlayabilmek adına PYTHON kullanılarak bir tasarım, simulasyon, analiz ve postprocess algotitması geliştirilmiştir. Bu agoritma sırasıyla şunları yapmaktadır. İlk olarak Simcenter 3D NX kullanılarak rotorun CAD modeli

hazırlanmaktadır. CAD modelini hazırlamak için XFOIL kullanılarak gerekli kanat profil şekli oluşturulmaktadır. Daha sonrasında ise, roturun çok gövdeli kinematik modeli Simcenter 3D Motion yazılımı kullanılarak oluşturulmaktadır. Daha sonrasında, elastik pal modelleri, Simcenter 3D yazılımının sonlu elemanlar modelleme aracı kullanılarak oluşturulmaktadır. Son olarak, Simcenter 3D Motion içerisinde aerodinamik model rotor pal genişliği boyunca blade element theory kullanılarak uygulanmaktadır. Kanat profili aerodinamik katsayıları yine XFOIL kullanılarak modele girdi olarak sağlanmaktadır.

Modeli doğrulamak amacıyla FLIGHTLAB programı kullanılarak blade elemet theory ile bir rotor modeli daha oluşturulmuştur. Doğrulama analizlerinde FLIGHTLAB ve Simcenter 3D rotor modellerinde aerodinamik modele literatürden bulunan bir test verisi girdi olarak sağlanmıştır. Askı ve ileri uçuş manevralarında elastik olmayan bladeler kullanılarak bu iki model kıyalanmıştır. Ayrıca elastik rotor modelleri de Simcenter 3D rotor modeli kullanılarak askı ve ileri uçuş manevra koşulları için incelenmiştir.

Ek olarak, pal üzerindeki burkulma açılarının aerodinamik yükleme üzerindeki etkileri elastik olmayan ve elastik tasarımlar için kıyaslanmış ve incelenmiştir. Kanat boyu ve kanat genişliğinin değişiminin rotor katılığı sabit iken aerodinamik yüklere etkileri incelenmiştir. Son olarak ise farklı materya türleri ile üretilen rotorlar incelenmiş, aerodinamik yükleme üzerindeki etkiler tartışılmıştır.

Bu tezde, helikopter rotor tasarımı alanında çoklu vücut ortamında yapısal elastikiyetli simulasyonlar için yeni bir yöntem sunulmaktadır. Bu araştırmadan elde edilen sonuçlar, gelecekte helikopter rotorlarının tasarımını ve performansını iyileştirmek için kullanılabilir.

Anahtar Kelimeler: Simülasyon, Aerodinamik, Çok Gövdeli, Esneklik, Yükler.

ACKNOWLEDGEMENT

This part of my thesis is dedicated to the people who are supporting me during process of my thesis and throughout my life.

I would like to express my special thanks to my supervisors Prof. Dr. Volkan Parlaktaş and Assoc. Prof. Dr. Barış Sabuncuoğlu for their effort, their time and understanding in helping me succeeded in thesis. Their wealth of experience, advice, encouragements and their contribution for generating a thesis topic have inspired me throughout the study.

I would like to express my thanks to Turkish Aerospace for its commercial tool opportunities used in this thesis.

I would like to express my thanks to all the lecturers of Hacettepe University Mechanical Engineering Department. I am always proud of completing my master education in this university with the classes of these very bright people.

I would like to express my thanks to my colleagues in Turkish Aerospace for inspiring me during this thesis and during the job.

Finally, I would like to express my most profound appreciations to my family for their endless support, positiveness and their encourage for arriving to the finish of the thesis.

CONTENTS

FIGURES

TABLES

NOMENCLATURE

R	*Blade Radius*
ζ	*Lead-Lag Angle*
β	*Flapping Angle*
Ω	*Angular Velocity of Rotor*
Ψ	*Azimuth Angle*
m	*Mass*
D	*Drag*
L	*Lift*
F	*Force*
M	*Moment*
α	*Angle of attack of blade section*
θ	*Pitch angle of the blade*
μ	*Advance ratio of blade*
ϕ	*Blade section inflow angle*
U	*Velocity of relative wind*
U_P	*Component of relative wind perpendicular to the tip path plane*
U_T	*Component of relative wind parallel to the tip path plane*
β_0	*Rotor coning angle*
β_{1c}	*Pitch angle of the tip path plane relative to hub plane*
β_{1s}	*Roll angle of the tip path plane relative to hub plane*
θ_0	*Rotor collective pitch angle*
θ_{1c}	*Front to aft change in blade pitch angle*
θ_{1s}	*Side to side change in blade pitch angle*

1. INTRODUCTION

This thesis project focuses on the study of modelling and analysis of a helicopter main rotor. The proposed assembly type of main rotor in this thesis is articulated rotor mechanism assembly.

Since rotorcrafts are initially found during the beginning of 20th century, growing interest has been shown to the rotorcrafts. In fact, since rotorcrafts are aerial vehicles which are capable of performing hover flight and axial flight, there are so many fields requiring rotorcrafts in orders to make their works faster and efficient. Due to this unrivaled capability of rotorcrafts, they are suitable for numerous tasks like providing air medical services, carrying passengers and equipment, firefighting, and other military and civil tasks. For example, military is requiring the utility rotorcrafts in order to carry their armies to some lands which are hard to reach. Also, military is requiring fighter rotorcrafts in order to use them in defense or attack missions. Civil aviation companies are using to carry passengers. Some delivery companies are using in order to deliver the products. Transportation companies are using in order to transport goods, etc. Also, nations are using for so many missions like extinguishing wild fires, polices, office missions, etc.

Since rotorcrafts can be used for wide range of mission types, several rotorcraft types depending on the missions are created. Some types of rotorcrafts are given in Figure 1.

Figure 1: Types of Rotorcrafts [1]

Single main rotor helicopter is operating with one main rotor and one tail rotor in order to compensate the torque created by main rotor. These helicopters are most common helicopters and mainly used for conventional usage or military usage. Tandem helicopters operating with 2 main rotors and are mainly used for cargo transportation missions. These helicopters are mostly using for military. Compound helicopters contains one main rotor and one or more forward thruster propeller or jet engines in order to move the helicopter faster in forward flight and in order to compensate main rotor torque in low speeds. Tilt-rotor helicopters are operating with double tilting rotors. These helicopters perform hover axial and high-speed forward flight capability. Coaxial helicopters are operating with double main rotor rotating in the same axis.

Usage of rotorcrafts also brings their expenses in contrast. This expense mostly comes from operating with high energy consumption of main rotor systems in order to keep the rotorcrafts in the air. The high energy consumption is mostly requiring during the hover operations. Due to this challenge, more efficient rotorcrafts are tried to be developed and it is highly researched up to today in order to investigate the parameters on rotor system of helicopters. The wide area of this research is dedicated to parameters on a helicopter main rotor during some maneuvers which are forward flight and hover flight.

1.1.Aim of the Study

The aim of this study is to create a helicopter main rotor and investigate some design parameters on the helicopter main rotor with multibody dynamic simulations approach in Simcenter 3D using elastic and rigid modeling of blades and using aerodynamic loads on blades. Then, wide range of design solutions according to some design parameters of blades are investigated in the thesis. Firstly, aerodynamic and structural loads on blades are investigated according to effect of material types. Effect of flexibility on angle of attack and flap angle distribution on blades due to material types are investigated. Then, effect of chord length and wingspan for constant solidity of rotor are also investigated in this thesis. Finally, effect of different twist angle distribution on aerodynamic loads in rigid and elastic bodies are investigated. In order to perform the investigations, the simulations are performed at forward flight and hover flight load cases.

Simcenter 3D is a multibody kinematic and dynamic simulation tool like a wide known tool named as MSC ADAMS. The boot tools are providing solving some equations of motions for static, kinematic and dynamic simulations. MSC ADAMS is commonly used

software in the literature and there are significant number of studies in the literature about solving kinematic and dynamic simulations of helicopter rotor or some other mechanisms with MSC ADAMS whereas there are very limited number of studies for Simcenter 3D Motion software and almost no studies are observed up to now for helicopter rotors. In addition, generation of a CAD model and kinematic and dynamic flexible analyses of this CAD model cannot be performed directly using most well-known tools like CAMRAD or FLIGHTLAB. Therefore, the main rotor model is created using Simcenter 3D in this thesis. Then, a simulation of rotor mechanism with Simcenter 3D are tested by investigating rotor motion parameters in Simcenter 3D and by comparing the rotor model with FLIGHTLAB rotor model created with the same specifications in Simcenter 3D rotor model.

As it is stated above, for Simcenter 3D Motion software, there are very limited number of studies in the literature. Due to this lack of source, the other rotor modelling approaches are searched in the literature mostly. In the literature, the rotor models are mostly created flexible and beam models are mostly preferred in order to make flexible simulations. For example, there are couple of studies of euler-bernoully beam theory for creating beam models. In the present study, elastic beam are created with FEM modelling and nonlinear mode shapes are used in order to create flexible blades.

Finite element tool of Simcenter 3D motion named as Simcenter Pre-Post tool is used in order to make elastic beam model with FEM. This tool provides generation of 1D, 2D and 3D finite element modeling of a CAD model using Simcenter Nastran module of Simcenter 3D. Blades are modelled as flexible whereas other rotor components are kept as rigid. For different design options and for different rotor simulation cases, elastic behaviors, loads and angles of blades and loads of other rotor components according to flap up and down conditions are investigated. The major rotor forces are aerodynamic and centrifugal forces and almost all amount of these forces on the rotor are created by blades. Therefore, in this thesis, design parameters of rotor blades are mostly concerned. Different designs of blades are affecting the stress distributions, aerodynamic loads and loads of rotor components. Therefore, loads and stress distributions of different blade structures depending on material, twist distribution, airfoil shape, chord length and wing span are investigated.

In this study, investigation of different rotor model simulations with aerodynamic loads are main objective. Therefore, aerodynamic load creation method is essential. In general,

main source of following loads on a rotor mechanism are aerodynamic forces and moments.

- Torque on main rotor shaft,
- Lift and drag forces on blades,
- Bending moments on blades in lead-lag and flapping directions,
- Axial forces on hinges,
- Bending moments on blades due to Coriolis effects,

In the literature, there are couple of methodologies for aerodynamic loads application. In some papers, aerodynamic behavior of a blade at each angle of attack and sideslip angles are calculated in CFD or some other aerodynamic tools. Unsteady aerodynamic effect, dynamic stall effect and free wake effects can also be implemented. Then, this information are inputted to an aeromechanical analyses tool like CAMRAD II, FLIGHTLAB, etc. Lifting line theory, CFD coupling methods, blade element theories are also some aerodynamic load application methods which are used in literature. CFD coupling methods require coupling methodologies with flexible multibody model. Coupling methodologies requires more powerful computers and too much time for calculation with FEM at each design. Since wide number of different designs are considered in this thesis, these methodologies are not intended to be performed and these methodologies are considered as future study. Application of database of unsteady aerodynamic, dynamic stall, and free wake models is also considered as future study since it requires some CFD tools and a comprehensive analyses tool. In the present study, blade element theory implementation on blade is considered for aerodynamic load calculation. The method is implemented to the rotor model in Simcenter 3D Motion software.

A rotor model in FLIGHTLAB is also generated and used in order to verify the rotor model in Simcenter 3D. FLIGHTLAB is a comprehensive rotorcraft or rotor analyses tool [24]. There are significant number of studies in the literature about modelling, analyzing, verifying, and validating of rotorcraft or rotor models using FLIGHTLAB. Then this tool is selected for verification of rotor model in Simcenter 3D.

In this thesis a rotor model with multibody aerodynamic and structural approach is generated in Simcenter 3D software. Using this model different design of blades are solved and some parameters like angles, forces and stress distributions of different

designs are investigated. Using the generated database, one can get idea about the effect of different design solutions of a helicopter rotor loads.

1.2.Working principles of Helicopter Rotors

Rotorcrafts are air vehicles which are flying with rotary wing systems. In order to utilize required lift, helicopters utilize rotating airfoils or rotors, instead of fixed wings. The rotary wing systems are varying according to the helicopter types. Most of the helicopters have main and tail rotor systems which are conventional type helicopters, but some helicopters do not have tail rotor system (e.g., coaxial rotor types [2]) as discussed. In this thesis, the concerned helicopter types are conventional helicopters. Main rotor system provides aerodynamic lift which is required for a helicopter to take off and fly. Main rotor systems are also creating a reactional torque exerted on the fuselage. Tail rotor systems are mechanisms which create a counter reactional torque to the main rotor systems. In this thesis, only main rotor system will be concerned. Some main rotor types of conventional helicopters are given in Figure 2.

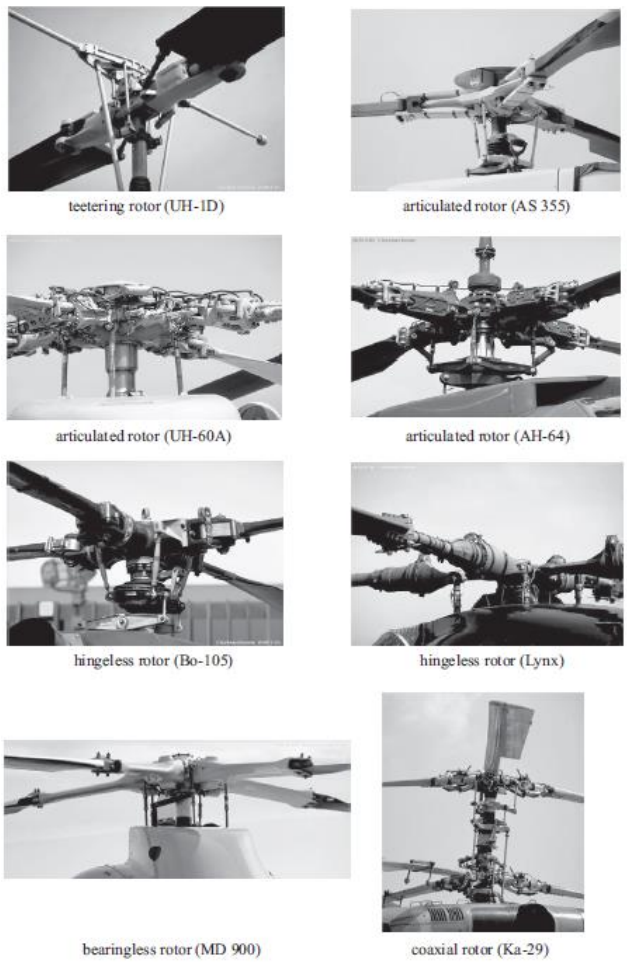

Figure 2: Some Main Rotor Types of Helicopters [1]

Main rotors types differ according to the hinge types in the rotor head.

In order to keep the helicopter in the air, rotor systems on helicopters create high number of forces and moments coming from undetermined and complex aerodynamic phenomenon. In general, 6 types of forces and moments on a helicopter main rotor can be analyzed. General forces on a helicopter main rotor can be represented as in Figure 3.

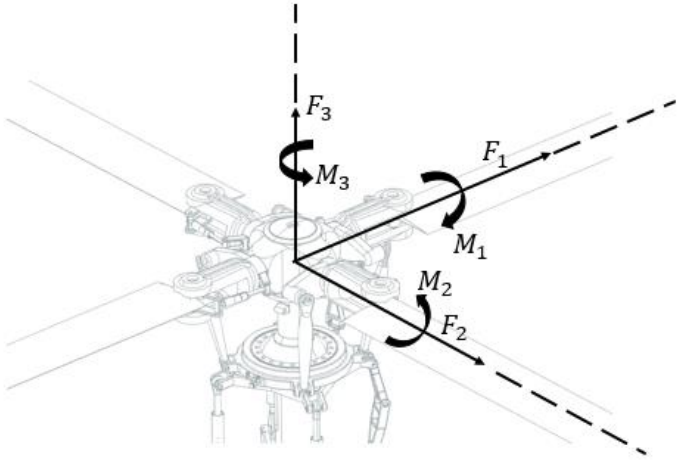

Figure 3: Forces and Moments on a Helicopter Rotor

The contributors of these forces and moments are lift, drag and centrifugal forces which are created during rotation of main rotor system and, pitch, flap, and lead lag motions of main rotor blades as discussed in Figure 4. The behavior of forces and moments become completely different at different maneuvers. In addition, the forces and moments exerted on a blade of main rotor are different at each azimuth position during a maneuver other than hover maneuver, but forces and moments on each blade can be observed as very close to each other at the same azimuth positions.

As mentioned, 3 different DOFs of blade motions can be discussed for a helicopter main rotor system. These are flapping, lead-lagging, and feathering motions as presented in Figure 4.

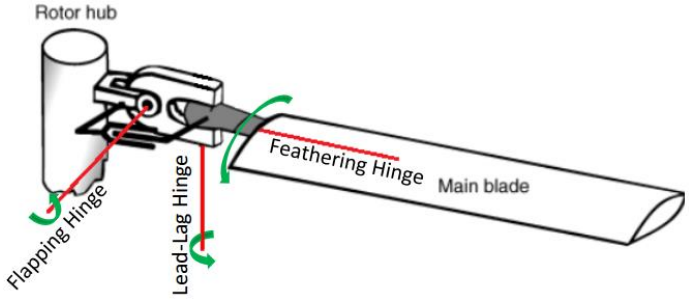

Figure 4: Motions of a Helicopter Blade

Flapping hinge is providing a flapping motion to the blades. With the help of this motion, helicopter can respond to lateral and longitudinal cyclic inputs. Longitudinal and lateral cyclic inputs provide pitch and roll motions to the helicopter. Due to flapping motion, Coriolis effect is seen on blade. This Coriolis effect results lead-lag motion on blades. The lead-lag motion is a problem itself because of its low natural damping. Therefore, lead-lag dampers are used in order to increase damping capability. Feathering hinge provides pitch up and pitch down motion to the blades. Complete view of rotor hub assembly is shown in Figure 5.

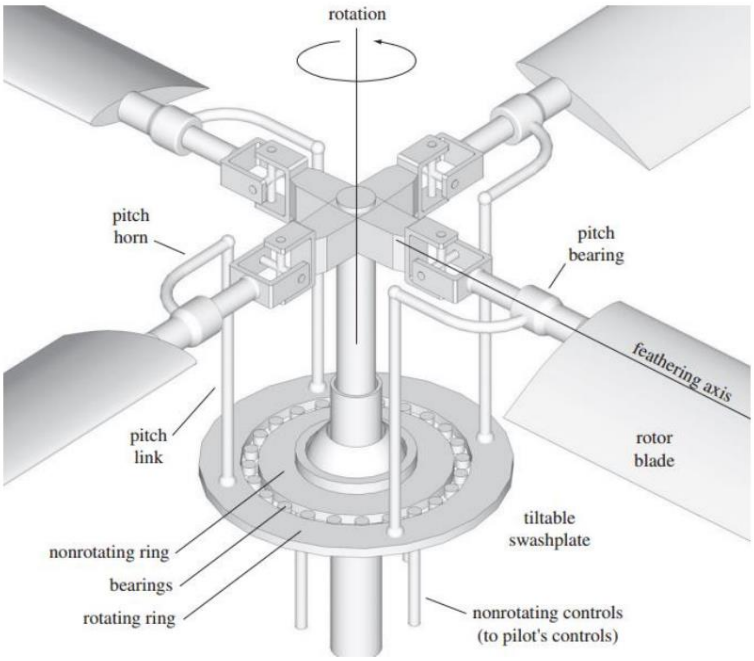

Figure 5: Representation of Rotor Hub [1]

1.3.Literature Review

In the literature, several research projects have been focused on modelling and/or analyzing the dynamics of the helicopter main rotor system. Some of research project are discussed as following in this part.

Yaakub, Wahab, Abdullah and Mohd [3] created an aerodynamic model of a helicopter main rotor using Blade Element Theory. They are modelled each section of blade as quasi-2D airfoil with NACA 0012 airfoil aerodynamic data. The airfoil data is obtained from a NASA paper [4]. Blade pitch, flapping, lead lag motions and blade velocity is dynamically used in the model in order to create angle of attack of blade sections. They compared the angle of attack distributions in forward flight condition along the rotor disc with an existing data. Comparisons show good correlations.

Juho Ilkko, Jaakko Hoffen and Timo Siikonen are performed a flow simulation analysis on UH-60A helicopter isolated main rotor in order to validate flow solver code FINFLO [5]. In this paper, a development of a rotor simulation in Finland is discussed.

In the mechanic model of this study, rigid blade bodies oscillating about root hinges are implemented in the model. Therefore, two degree of freedom moment equations which are flapping and lagging equations are implemented. The equations are as below.

$$(1) \quad \ddot{\beta} = \frac{-m(r_{cg}-eR)}{I_\beta} eR\Omega^2 cos\zeta\ sin\beta - sin\beta cos\beta\left(\Omega - \dot{\zeta}\right)^2 + \frac{Q_\beta}{I_\beta}$$

$$(2) \quad \ddot{\zeta} = \frac{-m(r_{cg}-eR)}{I_\zeta cos\beta} eR\Omega^2\ sin\zeta\ - 2\ tan\beta\left(\Omega - \dot{\zeta}\right)\dot{\beta} + \frac{Q_\zeta}{I_\zeta cos^2\beta}$$

In the simulation, the aerodynamic solver produces some aerodynamic moments. These moments are applied in the equations of motion. The spring and damping systems of each blade are modelled. The resulting moments are added into 2 degree of freedom equations. Centrifugal moments are also included in the equations. The equations are solved with Runge-Kutta integration.

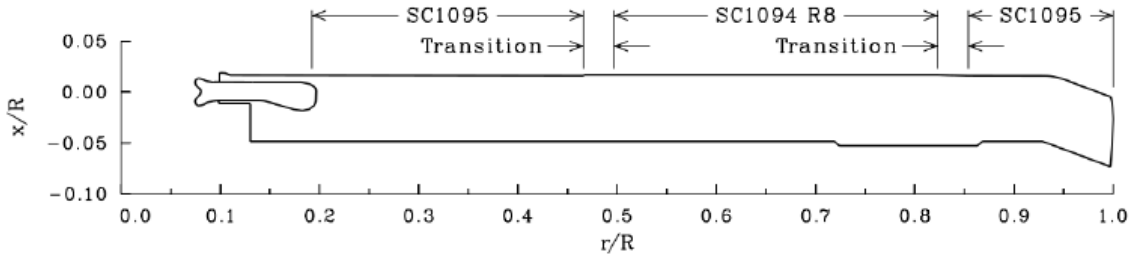

Figure 6: Shape of the Blade in the FINFLO Solver

The results of the simulations are compared with some reference data of the UH-60A helicopter. The FINFLO results show a great correlation with the reference data.

K. Skiba is performed a preliminary design of a helicopter 3-blade rotor model in Simcenter NX 12.0 program. [6] A kinematic model is also created and structure is checked for its strength using NX Nastran software. Also, in order to investigate the basic advantages and disadvantages of developed rotor design with other rotors, a comparative analysis of the modelled rotor was carried out. The solid CAD model of a rotor is represented in Figure 7

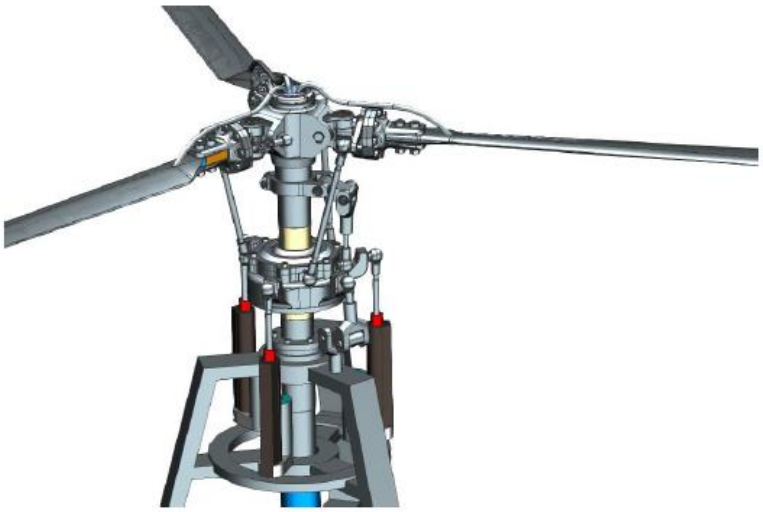

Figure 7: CAD Model of Skiba's Rotor

Equivalent aerodynamic and centrifugal forces, and torsional moments are applied to each blade base. The strength analyses are performed while the rotor is rotating at maximum speed. Maximum performance is investigated by changing rotor configurations. Behaviors of rotor components under high rotor forces are investigated.

Persson, Weinerfelt and Saab Aeronautics are presented a coupled aerodynamic and structral simulation model of a helicopter named Skeldar V200 in ADAMS software [8]. The model is shown in Figure 8.

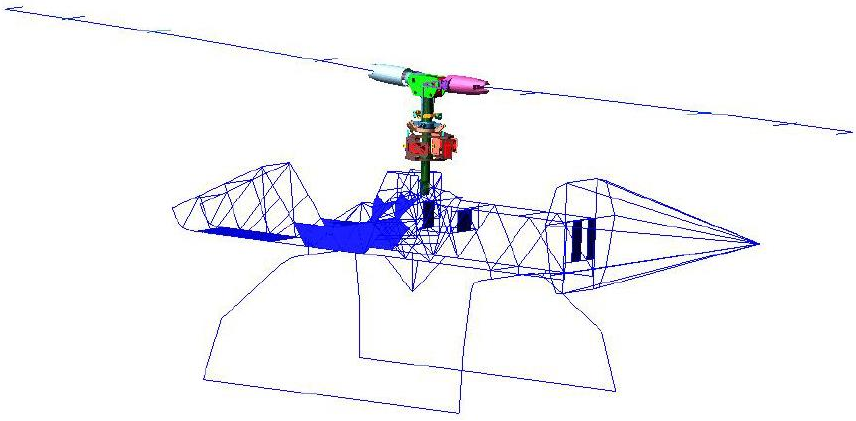

Figure 8: Skeldar V200 Simulation Model

The all simulation of the model is performed with structural model for the helicopter airframe, aerodynamic and elastic models of helicopter rotor blades, models for servos, swash plate and the control linkages which are providing transfer of control inputs between swash plate and blades. The structural dynamics, aerodynamics and control systems are coupled in order to perform the simulations. The structural parts are modelled

in CATIA and imported into Adams. Smaller parts like bolts, plates etc. are omitted. For efficiency reasons, blades are implemented by a beam model. Aerodynamic forces and moments are adopted to the model using lifting line theory [9], [10]. Following equations are used.

$$F = \int \begin{bmatrix} D\cos\phi + L\sin\phi \\ 0 \\ L\cos\phi - D\sin\phi \end{bmatrix} dy$$

$$M = \int \begin{bmatrix} y(L\cos\phi - D\sin\phi) \\ -x_{cp}(D\cos\phi + L\sin\phi) \\ -y(D\cos\phi + L\sin\phi) \end{bmatrix} dy$$

Where,

$$L = \frac{1}{2}\rho U^2 c \bullet c_{l,\alpha} \bullet \left(\underbrace{\theta + \phi}_{\alpha} - \alpha_0 \right)$$

$$D = \frac{1}{2}\rho U^2 c \bullet c_d$$

The simulation parameters of model are compared with rig test and flight test data and the great correlation are shown.

Patrick M. Shinoda tested a full-scale four bladed UH-60/Wide Chord Blade rotor system in the NASA Ames 40-by 80-foot wind tunnel in order to support future rotor developments and rotor analyses improvements [11].

Figure 9: UH-60 Blades in NASA Ames 40-by 80-foot Wind Tunnel [11]

Hub, spindles, swash plate and blades are putted in the wind tunnel as a model. CAMRAD 2 rotor analyses models are also used in order to compare the rotor performance data. An isolated rotor of a wide chord blade rotor model is used. This model consists elastic blades which are created with nonlinear finite elements. Free-wake analyses, which are using second order lifting line theory, are included in aerodynamic model. Lift, drag, and moment values of SC2110 and SSCA09 airfoils are used. CAMRAD 2 rotor analyses show a great correlation for main rotor power with wind tunnel test data. However, some improvements are required at hover and low advance ratio cases. This paper is a sample of modelling a rotor in an analyses tool and validation of rotor model.

J-S. Park is performed a flexible multibody analyses of a helicopter main rotor [13]. DYMORE is used in order to analyze aeromechanics and performance of full-scale utility helicopter main rotor in forward flight load cases. Multibody modelling of rotor in DYMORE is shown in Figure 10.

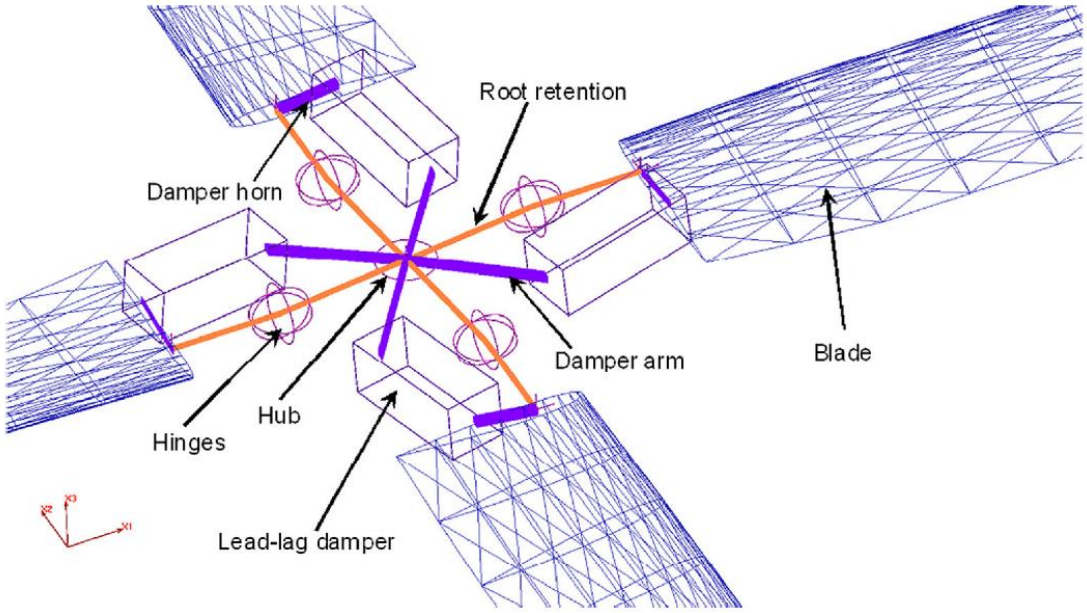

Figure 10: DYMORE Modelling of Main Rotor [13]

The model consists of root retention, blade, hydraulic lead-lag damper, damper arm, damper horn and hub. In order to create articulated rotor system, flap, lead-lag and feathering hinges are created with three collocated revolute joints. For rotor control system stiffness, torsional spring is used for feathering hinge. In addition, the blade is modeled with 10 cubic beam elements. Damper arm and damper horn are created with rigid body structure. Hydraulic damper is used for lead lag damper. In order to calculate air loads on blades, airfoil tables are imported. Performance parameters of full-scale

utility helicopter main rotor, aerodynamic loads on blades, some control angles and structural loads of blades are correlated with wind tunnel test data and flight test data. In low advance ratio flight, the figure of merit is corrected well but at high thrust cases, the results are decided as over predicted. Rotor power with the sweep of the rotor lift corrected well.

Donald L. Kunz and Henry E. Jones designed AH-64 Apache rotor system models with different modelling approaches in an aeromechanical analysis tool named CAMRAD II [14]. Two different load model named as single load path model and multiple load path model are generated. The models differ due to the joint types and elastic modelled parts. Pitch link loads generated in the models are compared with flight test data of the helicopter. Then he decided best one depending on flight test data. In this project, depending on the comparison of pitch link loads with flight test, models created with CAMRAD II shows a great correlation.

Sun T., Tan J., and Wang H. are performed an aeroelasticity analyses of rotor blade and rotor control systems [15]. In order to predict rotor pitch link and swash plate servo loads, multibody dynamics analyses models of UH-60 and SA349/2 helicopter rotors is utilized. Representation of multibody structural model of rotor blades and coupled rotor swashplate system mechanism are shown in Figure 11 and Figure 12.

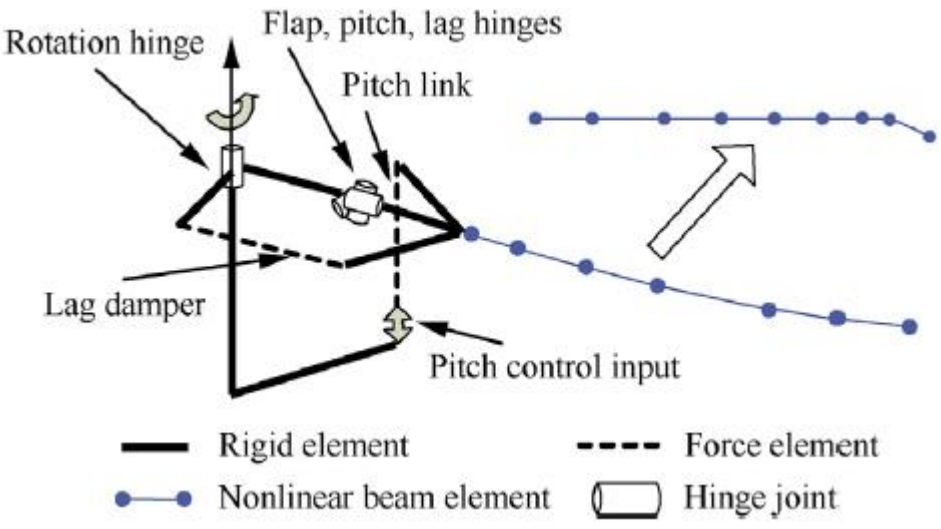

Figure 11: Multi-body Structural Model of Rotor Blades.

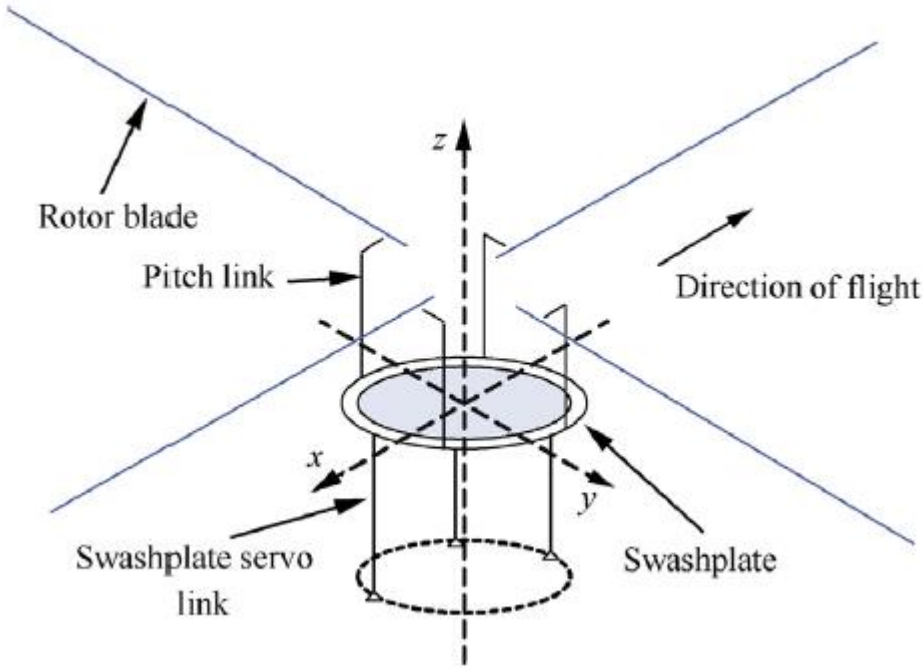

Figure 12: Representation of the coupled rotor/swashplate system model.

An isolated rotor model is established. The components of the rotor are given as below

- Rigid body elements: Rotor hub and pitch horn.
- Flexible beam elements: Blades.
- Hinge Joints: All of the nonlinear beam elements in the rotor model are connected with hinge joints and boundary nodes.
- Force elements: Pitch link and lag damper are created as linear spring and damper force elements.

Lifting line method is used in order to generate aerodynamic forces and moments on blades. It is stated that CFD/CSD coupling method is not used due to efficiency problems. The analyses are compared with flight test data and CAMRAD II results and present analyses results show great agreement with the flight test data and CAMRAD II.

2. ARTICULATED HELICOPTER ROTOR SYSTEM

2.1.Components of Articulated Helicopter Rotor System

In this project, articulated main rotor system of a helicopter is considered. Therefore, parts of the articulated helicopter rotor system will be investigated in this part. Main rotor is composed of rotor hub assembly and rotor blades. Main rotor hub assembly is also composed of the following rotor components:

- Rotating Swashplate,
- Stationary Swashplate,
- Actuators,
- Scissor Links,
- Pitch Links,
- Pitch Horns
- Dampers,
- Drive Shaft

Composed components of rotor hub and blades are shown in Figure 13.

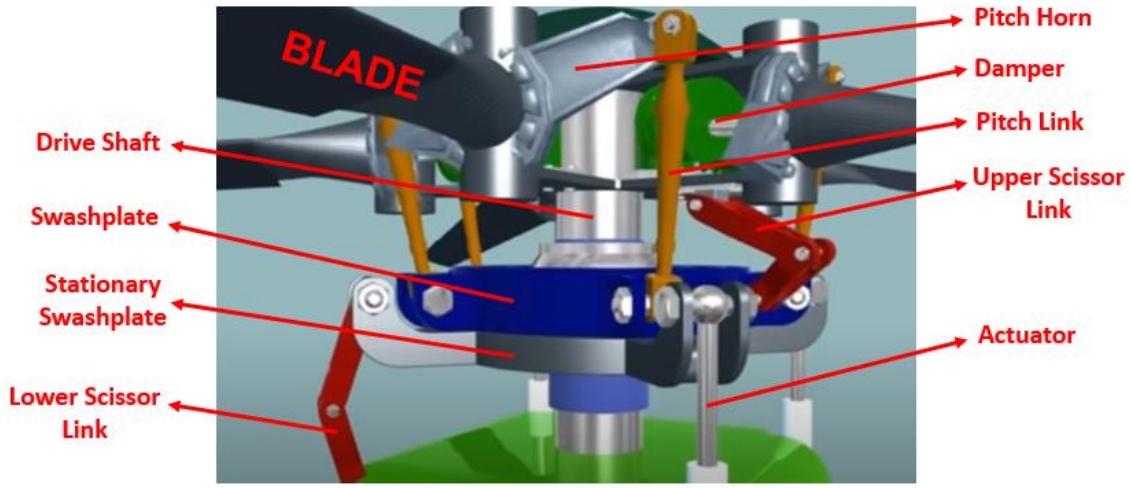

Figure 13: Articulated Main Rotor Hub Assembly [16]

In the articulated rotor system, the blades are attached to the hub with flap and lag hinges [1]. In addition, pitch motion is accomplished by feathering hinge. No bending moments are transferred to the hub from the blades by hinges. Representation of hinges of articulated rotor system are shown in Figure 4. The components of rotor system are deeply investigated in the following subchapters.

Swashplate:

Swashplate is a mechanism which allows to transfer pilot inputs to the blades. The swashplate mechanism has 2 main parts which are stationary and rotating swashplates. Rotating swashplate is assembled on the stationary swashplate with a bearing and the rotating swashplate is rotating on stationary swashplate at the same RPM with blades. Stationary swashplate is linked to main rotor mast with lower scissor link and it is connected to cyclic and collective controls by actuators. In order to transfer the cyclic inputs to the blades, actuators tilt stationary swashplate. This results to tilt rotating swashplate. In order to give collective pitch inputs or in order to increase or decrease the pitch angle of all blades, actuators move both of the swashplates upwards or downwards.

Actuators:

Actuators are mechanisms which transfer collective and cyclic inputs to the swashplates through slider joints. Upper ends of the actuators are connected with universal joints to stationary swashplate but lower ends of the actuators are connected with spherical joints to base.

Scissor Links:

Upper scissor link connects the blades with rotating swashplate and this prevents the rotating swashplate from rotating at different RPM of the blades. In addition, lower scissor link connects the stationary swashplate with main rotor mast. This prevents the rotation of stationary swashplate. Torques are carried scissor links and torques are not exerted on actuators or pitch links. Lower end of lower scissor link and upper end of upper scissor link are connected with revolute joint. Whereas swash plate linking of scissor links are connected with spherical joint.

Pitch Links and Pitch Horns:

Pitch links transfer collective and cyclic pitch inputs to the blades through pitch horns. Lower ends of pitch links are connected with universal joints to rotating swashplate whereas upper ends of pitch links are connected with spherical joints to pitch horns. Pitch horn connects blade to pitch link.

Dampers:

Lead-lag motion of blade has low natural damping so that it is a problem itself since amount of drag changes in the plane of rotation are small whereas flapping motion has much bigger amount of lift changes therefore flapping motion is inherently well damped. Even in the ground condition, an unstable lead lag motion can be observed. Therefore, the helicopter can be destroyed with ground resonance. This requires an auxiliary

damping unit for lead-lag motion. Connecting a damper mechanism to the root part of each blade, the problem tried to be solved. Therefore, the damper units must be modeled in any rotor simulations although rigid blades are taken into account. The unit also contains a spring that increases the natural frequency of lead-lag motion. One end of the unit is connected with a universal joint whereas the other end of the unit is connected with a spherical joint.

Drive shaft

Shaft provides power transmission of engine to the rotor. Rotational motion of rotor is maintained by a shaft torque created by engine. Drive shaft is connected to the rotor hub by fix joint.

2.2.Kinematic Joint Types on Helicopter Rotor

Used joint types on helicopter rotor model are discussed in this part. Following joint types are used in the model.

- Universal Joint
- Fixed Joint
- Spherical Joint
- Slider Joint
- Revolute Joint

Usage of joints in the model are discussed in chapter 2.5

2.2.1. Universal Joint

Universal joint is combination of a 2 revolute joint. This allows 2 degree of freedom rotational motion between 2 motion bodies. Representation of universal joint is shown in Figure 14.

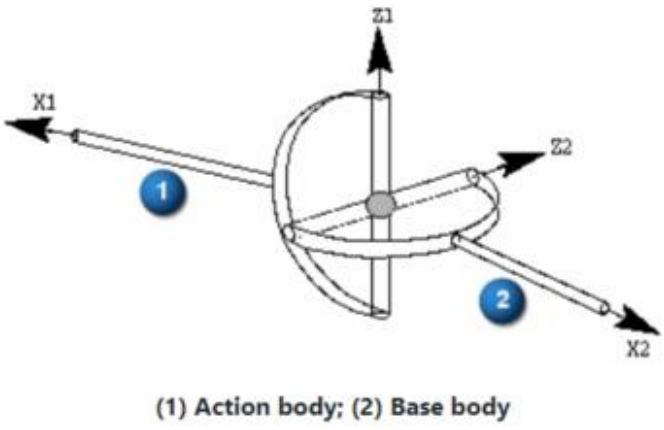

Figure 14: Representation of Universal Joint [17]

Joint features and constraints are as below.

- Rotational motions are performed around perpendicular Z axes.
- Origins of rotation of each motion body are coincidence of Z1 and Z2 axes.
- No translation between motion bodies is observed.

2.2.2. Fixed Joint

A fixed joint merges 2 motion body and no translation and no rotation are observed between 2 motion bodies. Therefore, this joint allows zero degrees of freedom.

2.2.3. Spherical Joint

A spherical joint connects 2 motion bodies with three degrees of freedom rotational motion. A spherical joint is also called as ball-and-socket joints. Representation of spherical joint is shown in Figure 15.

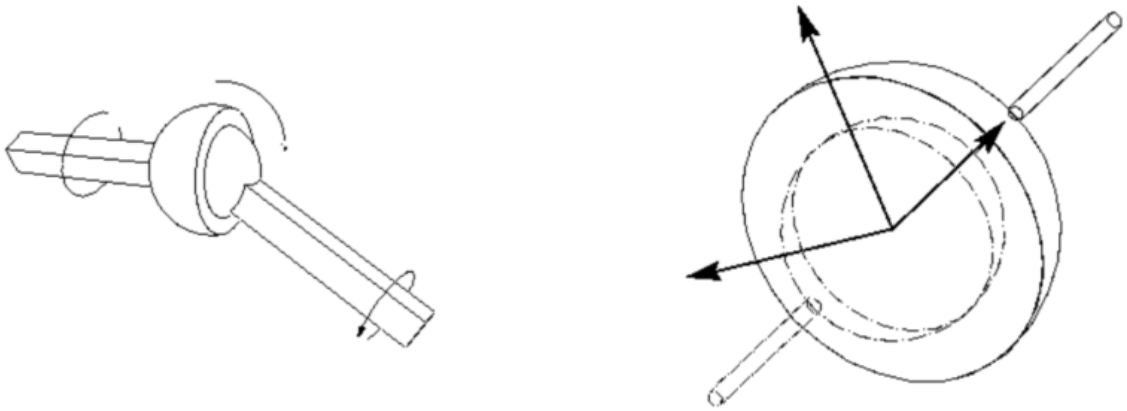

Figure 15: Representation of Spherical Joint [17]

Joint features and constraints are as below.

- Rotational motion is observed around X, Y, and Z axis.
- Origins of joints on each motion body are coincident.
- No translation between motion bodies is observed.

2.2.4. Slider Joint

A slider joint, which connects 2 motion bodies, allows 1 degree of freedom translation between bodies. Representation of slider joint is shown in Figure 16.

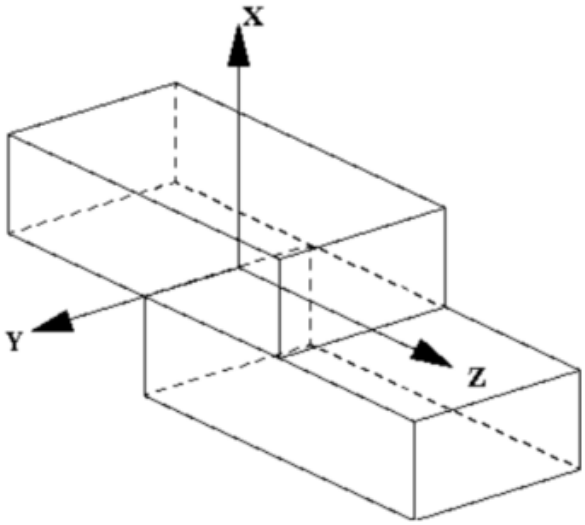

Figure 16: Representation of Slider Joint [17]

Joint features and constraints are as below.

- Only translation along the Z axis occurs and no rotation is observed.
- The translation axes (Z) are colinear, and the X-axes and Y-axes are aligned.

2.2.5. Revolute Joint

One rotational degree of freedom motion along Z axis between two motion bodies is allowed in revolute joint. Representation of revolute joint is shown in Figure 17.

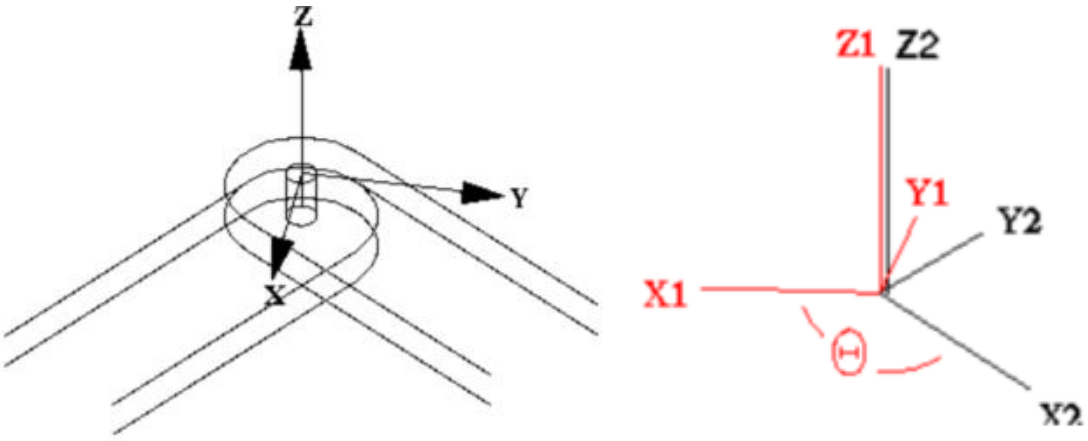

Figure 17: Representation of Revolute Joint [17]

Joint features and constraints are as below.

- In the specified coordinate system in Figure 17, rotation is about the Z axis.
- Origin of rotation of both motion bodies is coincident.
- No translation is allowed between two moton bodies.
- Rotation axes (Z axes) of each motion bodies are colinear or parallel.

2.3.Calculation of Rotor Loads

General forces and moments on a helicopter rotor is represented in Figure 3 in section 1.2. In this thesis, rotor loads are calculated using blade aerodynamic, inertial and centrifugal forces. Hover flight and forward flight maneuvers will be performed in this thesis. Therefore, loads on blades are represented for hover and forward flight as given in Figure 18 and Figure 19.

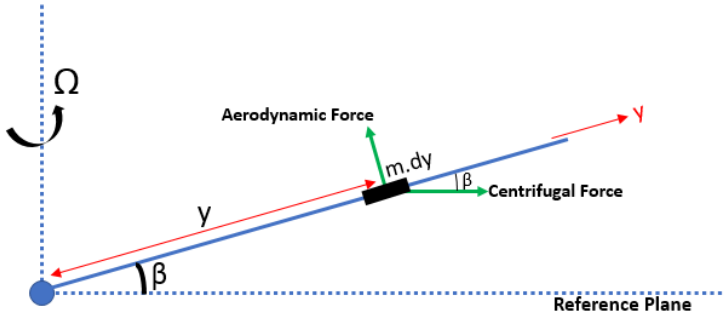

Figure 18: Forces on Rotor Blades in Hover Flight

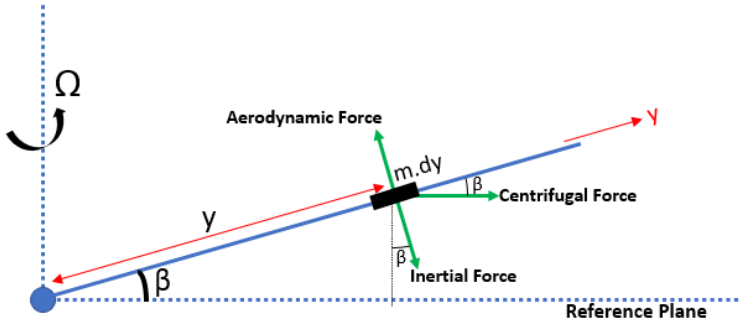

Figure 19: Forces on Rotor Blades in Forward Flight

In Figure 18 and Figure 19, aerodynamic, inertial, and centrifugal forces applied on an infinitesimally small blade element are represented. For hover flight, blades are not flapping but for forward flight, blades are performing flapping motion. Therefore, in forward flight, inertial forces due to flapping are also observed opposite to aerodynamic forces.

2.3.1. Rotor Aerodynamic loads

Aerodynamic loads on blades are main concerns of working principles of helicopters. In addition, as discussed in the introduction part, aerodynamic loads on rotor are a very complex phenomenon. Therefore, it is required to calculate aerodynamic loads with an aerodynamic load calculation methodology. In this thesis, rotor aerodynamic loads are calculated using blade element theory [1] with some assumptions. Aerodynamic loads are

calculated at each blade or wing segment in blade element theory as represented in Figure 20. In this thesis, aerodynamic loads are calculated at each segment of a blade as shown in Figure 20. In this figure, lift and drag forces are applied to the blade at some equally spaced segments. Chord length and area specifications of segments are used for calculation.

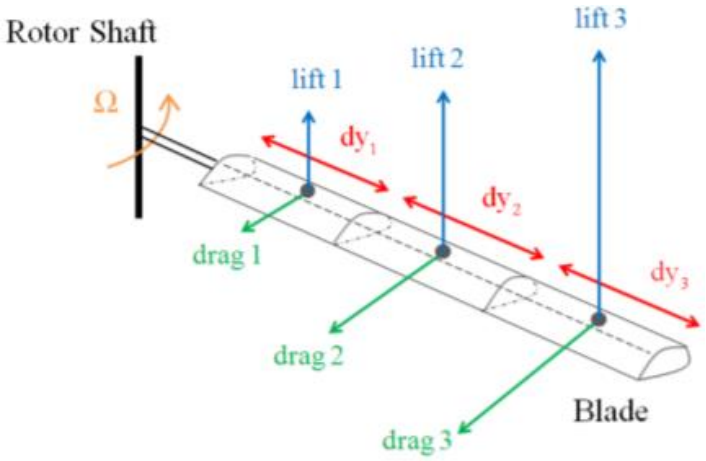

Figure 20: Forces on Rotor Blades [18]

This blade section aerodynamic forces are calculated using blade section aerodynamic parameter and airfoil aerodynamic coefficients. The airfoil aerodynamic coefficients are generated using XFOIL software and these parameters are supplied into Simcenter 3D. During a solution of a simulation, blade section aerodynamic parameters are generated at each step of solution by Simcenter 3D. Simcenter 3D uses blade section aerodynamic parameters for selecting suitable airfoil aerodynamic coefficients during a solution. Then, the forces are created during the solution at each step of solution. Aerodynamic parameters at each blade section are shown in Figure 21.

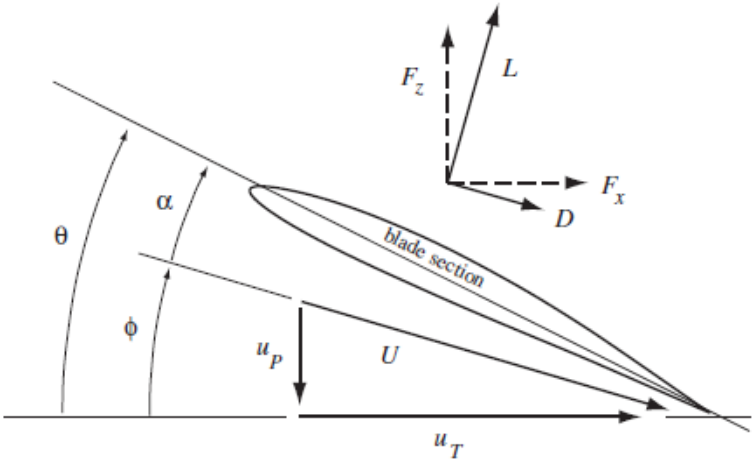

Figure 21: Blade Section Aerodynamics [1]

The parameters in the figure are described as below [1],

- α : Angle of attack of blade section
- θ : Pitch angle of the blade
- μ : Advance ratio of blade
- ϕ : Blade section inflow angle.
- U : Velocity of relative wind.
- U_P : Component of relative wind perpendicular to the tip path plane.
- U_T : Component of relative wind parallel to the tip path plane.

(3) $U = \sqrt{U_T^2 + U_P^2}$

(4) $\phi = tan^{-1}\frac{U_P}{U_T}$

Air velocity of blade is also calculated as below [1].

- Ω : Angular velocity of blade
- β : Flapping angle of blade

(5) $U_T = \Omega R + \mu\Omega R \sin\psi$

(6) $U_P = r\dot{\beta} + \mu\Omega R \sin\beta \cos\psi$

- μ : is advance ratio of rotor

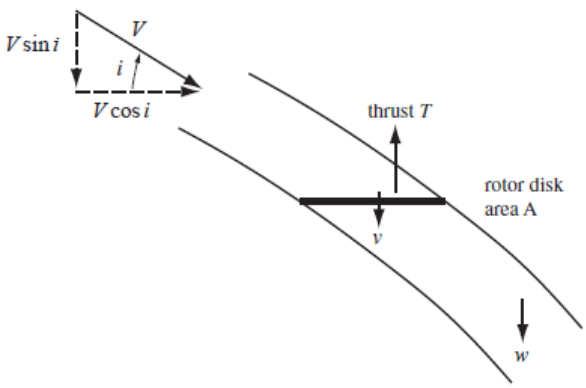

Figure 22: Flow Model in Forward Flight [1]

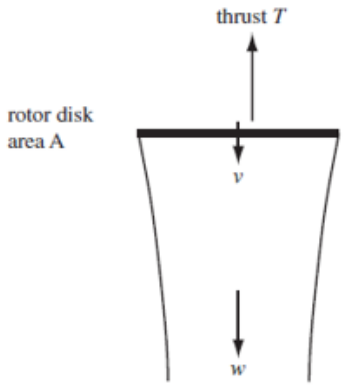

Figure 23: Flow Model in Hover Flight[1]

(7) $\mu = \frac{V\cos i}{\Omega R}$

where, V is the velocity of air coming to the rotor, i is the incidence angle of tip path plane.

- D : Drag force on blade section (parallel to relative wind velocity).
- L : Lift force on blade section (perpendicular to relative wind velocity).

Then, total aerodynamic forces normal and parallel to the tip path plane are given as below [1],

(8) $F_Z = L\cos\phi - D\sin\phi$

(9) $F_X = L\sin\phi + D\cos\phi$

Where,

(10) $L = \frac{1}{2}\rho U^2 c.c_l$

(11) $D = \frac{1}{2}\rho U^2 c.c_d$

In addition, moment equation is given in equation (12) below [1],

(12) $M = \frac{1}{2}\rho U^2 c.c_m$

In equations 3 and 4, ρ is density of air, c is chord length of airfoil in the concerned section, and c_l, c_d, and c_m are airfoil section 2D lift and drag coefficients respectively. The lift and drag coefficients are complicated functions of angle of attack.

Therefore thrust, torque, and power on rotor blade are given as below [1],

(13) $dT = NF_Z dr$

(14) $dQ = NF_x r dr$

(15) $dP = \Omega dQ = \Omega N F_x r dr$

2.3.1.1.Rotor Aerodynamic Load Calculation in Simcenter 3D

Rotor aerodynamic loads are calculated in Simcenter 3D Motion software by using function and marker tools. It is possible to enter some equations and methods to Simcenter 3D Motion using function tool. The aerodynamic load calculation methods and equations are applied to the rotor model in Simcenter 3D Motion using markers and functions. Markers are added to rotor blades at some locations in spanwise and chordwise directions. These markers trace aerodynamic parameters like angle of attack and sideslip angles of blades and these parameters are supplied to equations in functions at each step of solutions dynamically. The markers are putted on to the blades at some trailing edge and leading-edge locations in spanwise direction. The blade with markers is represented in Figure 24. In this figure, the markers are applied to the blade from trailing edge and leading edge at 6 equally spaced stations in spanwise direction. The aerodynamic parameters at each section differ from each other since they are applied from different stations and the blade has twist. In addition, since the blade is simulated elastically, shape change of blade also affects the aerodynamic parameters. The effect of number of stations are also investigated in the following sections.

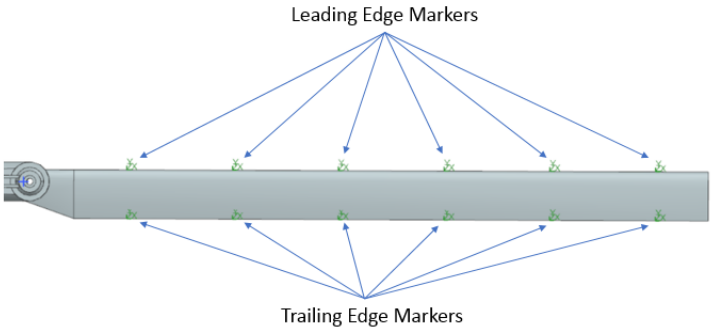

Figure 24: Markers on Blade

The parameters, which markers are tracing at each station, are given below,

- Flap angle (β),
- Velocity of flapping ($\dot{\beta}$),
- Pitch angle (θ),
- Velocity of pitching ($\dot{\theta}$),
- Velocity coming to blade section (V),
- Azimuth angle at each section (ψ),
- Angle of attack of blade section (α),

With the velocity coming to each blade sections and angle of attack of each blade sections, equation numbers (10), (11), and (12) are solved in functions in Simcenter 3D Motion during solution. Airfoil aerodynamic coefficients, which are Cl Cd and Cm curves, are calculated using XFOIL at the outside of Simcenter 3D. XFOIL is also explained in the next chapter. The coefficients generated by XFOIL can also be found from [7]. These coefficients are given as profiles depending on the angle of attack and are supplied to Simcenter 3D Motion. Since markers are tracing the angle of attack, the coefficients at each solution steps are calculating using linear interpolations in functions. Therefore, calculated coefficients are applied to the equations in functions at each solution steps. Therefore, the aerodynamic loads are calculated. In this thesis, NACA 23015 airfoils is used in design. The used coefficient tables of these airfoils are given in figures in chapter 2.3.1.2.

2.3.1.2. Aerodynamic Coefficients Generation with XFOIL

XFOIL is an interactive program for the design and analysis of subsonic isolated airfoils [23]. Aerodynamic coefficients and coordinate points of airfoil profiles are generated using XFOIL tool. Airfoil profile used in blade design is given in Table 1.

Table 1: Airfoil Profiles

Airfoil	Type of Airfoil
NACA 23015	Cambered (non-symmetric) Airfoil

NACA23015 airfoil coordinates are generated in XFOIL and they are plotted in Figure 25. Aerodynamic coefficients of the airfoil are also generated using XFOIL and are plotted in Figure 26 to Figure 28.

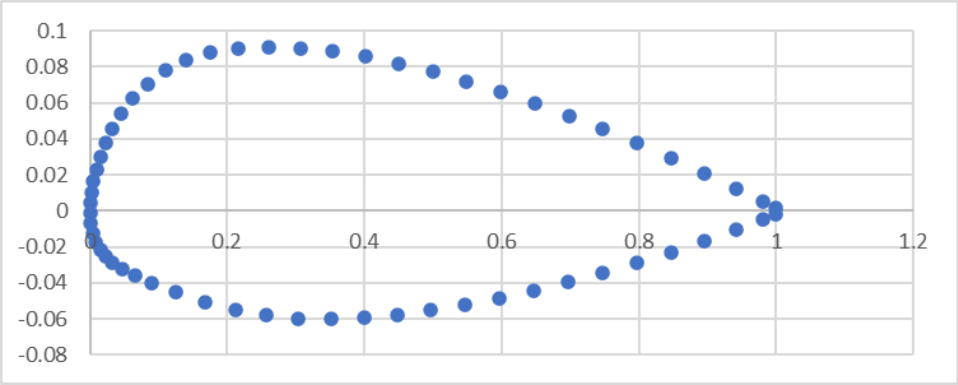

Figure 25: NACA23015 Airfoil Profile

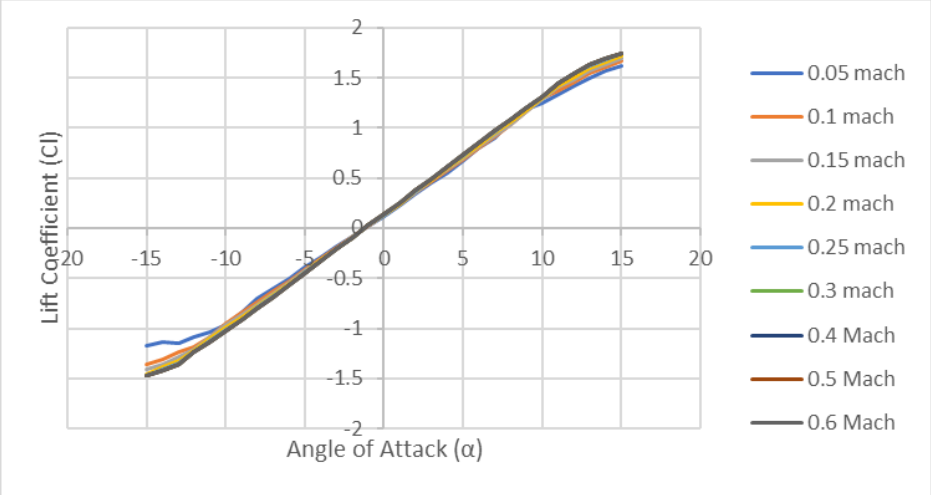

Figure 26: NACA23015 Cl vs. α Plot

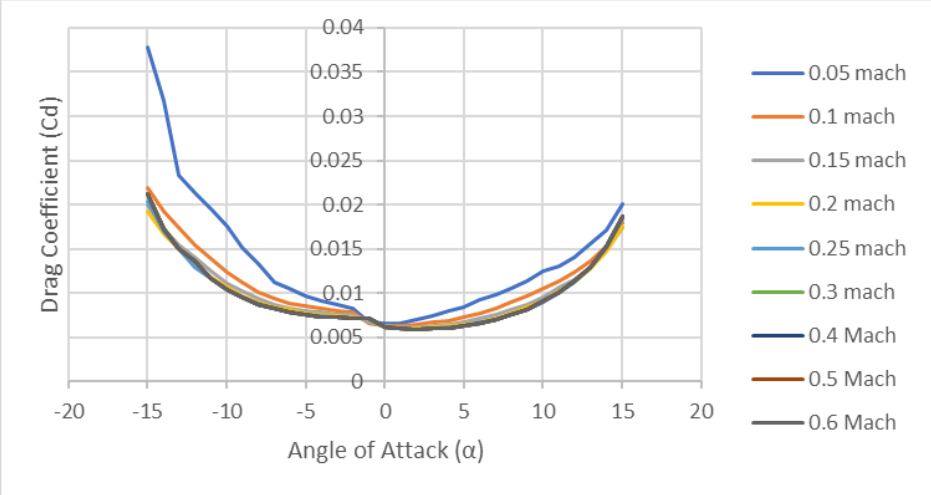

Figure 27: NACA23015 Cd vs. α Plot

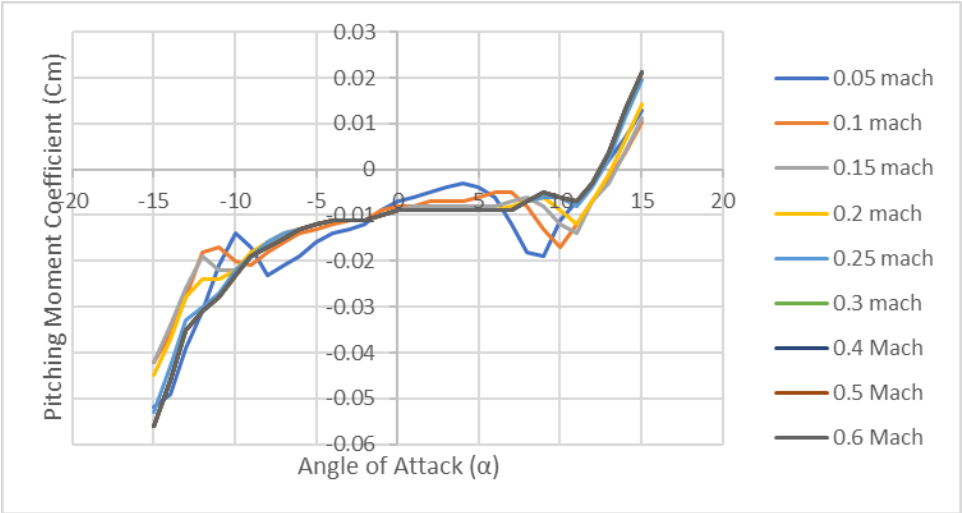

Figure 28: NACA23015 Cm vs. α Plot

Since XFOIL is better converging between +15˚ and -15˚ range, the simulations are performed between these ranges. In addition, since XFOIL is not working for subsonic compressible region, the coefficients for this region are created with extrapolation.

2.4.Rotor Control

Rotor control is provided by collective pitch, longitudinal and lateral cyclic pitch inputs. The inputs are provided to the rotor by changing the orientation of swashplate. Swashplate movements for collective inputs and sample swashplate orientation for cyclic inputs are shown in Figure 29 and Figure 30 respectively.

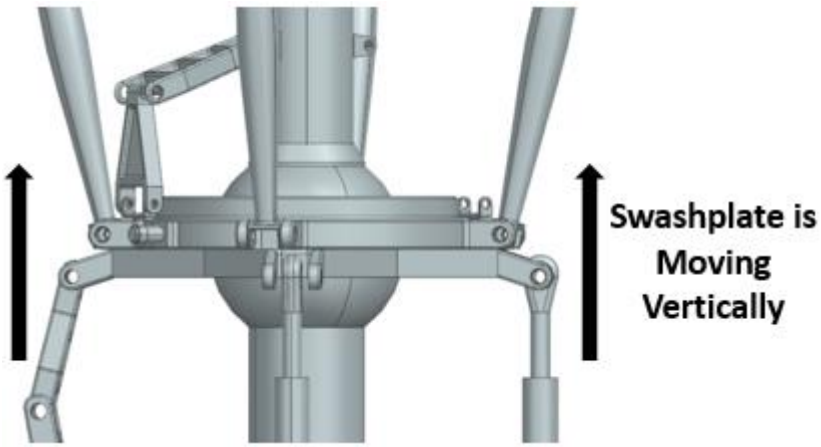

Figure 29: Movement of Swashplate for Collective Pitch Inputs

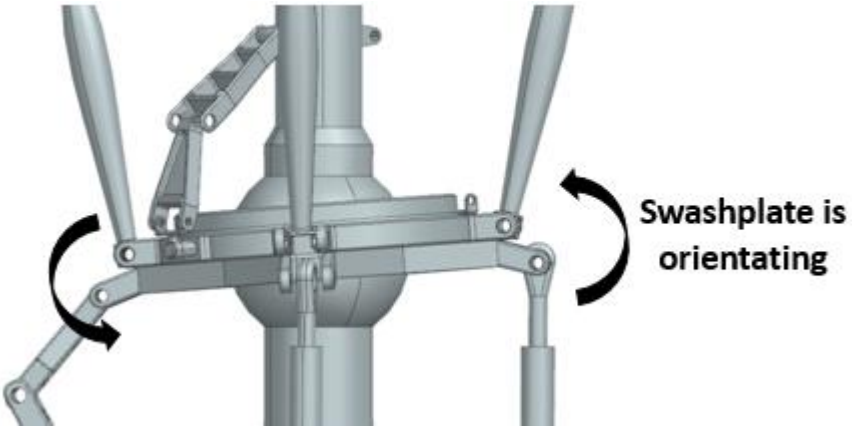

Figure 30: Orientation of Swashplate for Cyclic Inputs

By giving these inputs, periodic motions of blades are observed. These periodic movements are changing the rotor blade angles as below.

In collective pitch control (θ_0), pitching up motion in feathering axis is applied to all blades at all azimuth angles. Therefore, all blades have flapping up motion at around flapping hinge at all azimuth angles as shown in Figure 31.

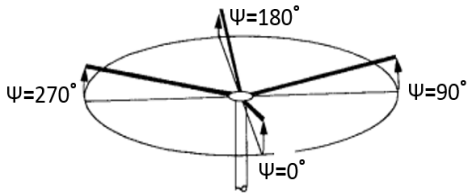

Figure 31 Orientation of TPP with Collective Pitch Control [19]

In Longitudinal cyclic pitch control (θ_{1s}), the pitching up motion is given to blades at 90˚ and 270˚ azimuth angles. Therefore, all blades have flapping up and down motion at around flapping hinge near 0˚ and 180˚ azimuth angles as shown in Figure 32.

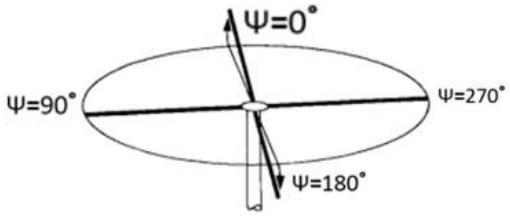

Figure 32 Orientation of TPP with Longitudinal Cyclic Pitch Control [19]

In Lateral cyclic pitch control (θ_{1c}), the pitching up motion is given to blades at 0˚ and 180˚ azimuth angles. Therefore, all blades have flapping up and down motion at around flapping hinge near 90˚ and 270˚ azimuth angles as shown in Figure 33.

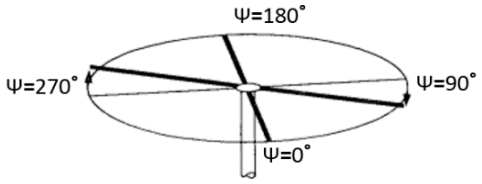

Figure 33 Orientation of TPP with Lateral Cyclic Pitch Control [19]

For the steady state operation of rotor system, periodic blade motion around the azimuth angle (ψ) is performed and this can be expanded as Fourier series in (ψ) as below [19],

(16) $\beta = \beta_0 + \beta_{1c}\cos\psi + \beta_{1s}\sin\psi + \beta_{2c}\cos\psi + \beta_{2s}\sin\psi + \cdots$

(17) $\zeta = \zeta_0 + \zeta_{1c}\cos\psi + \zeta_{1s}\sin\psi + \zeta_{2c}\cos\psi + \zeta_{2s}\sin\psi + \cdots$

(18) $\theta = \theta_0 + \theta_{1c}\cos\psi + \theta_{1s}\sin\psi + \theta_{2c}\cos\psi + \theta_{2s}\sin\psi + \cdots$

The mean and first harmonics of the blade motion are important and 2nd order harmonics can be neglected in the equations. This parameters for rotor performance and control are important. The description of mean and first harmonics are given below,

- β is flapping angle.
- β_0 is the rotor coning angle.
- β_{1c} is the pitch angle of the tip path plane relative to hub plane.
- β_{1s} is the roll angle of the tip path plane relative to hub plane.
- ζ is blade lagging angle. Lagging is positive when opposite to the direction of rotation of the rotor.
- θ is blade pitch angle, or feathering motion.
- θ_0 is rotor collective pitch angle.
- θ_{1c} is front to aft change in blade pitch angle.
- θ_{1s} is side to side change in blade pitch angle.

2.5. Multibody Modelling in Simcenter 3D Motion

Representation of kinematic model in Simcenter 3D Motion software is shown in Figure 34. In this model, base bodies are connected to ground with fixed joints. Drive shaft is linked to base bodies with revolute joint and both of the swashplates are connected to drive shaft with spherical joints. Rotating swashplate is connected to stationary swashplate with revolute joint. Lower scissor link connects stationary swashplate with base and upper scissor link connects rotating swashplate with shaft. Actuators are giving collective and cyclic inputs to swashplates. Pitch links transfer collective and cyclic inputs to the blades through pitch horns. Blades are connected to hub and hub is connected to shaft with fixed joint. Dampers connect blades to pitch horn body (represented as

orange color). Dampers are created with some stiffening and damping coefficients. Details are given in the following sections.

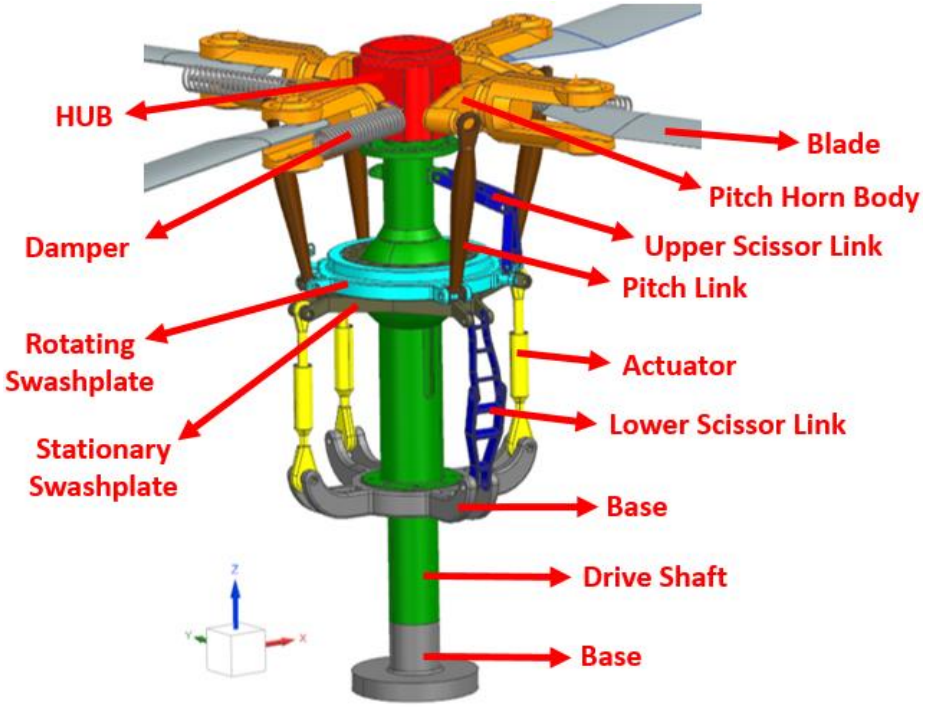

Figure 34: Representation of Multibody Kinematic Model in Simcenter 3D Motion

In addition, mid joints of upper and lower scissor links are created as revolute joint as shown in Figure 35.

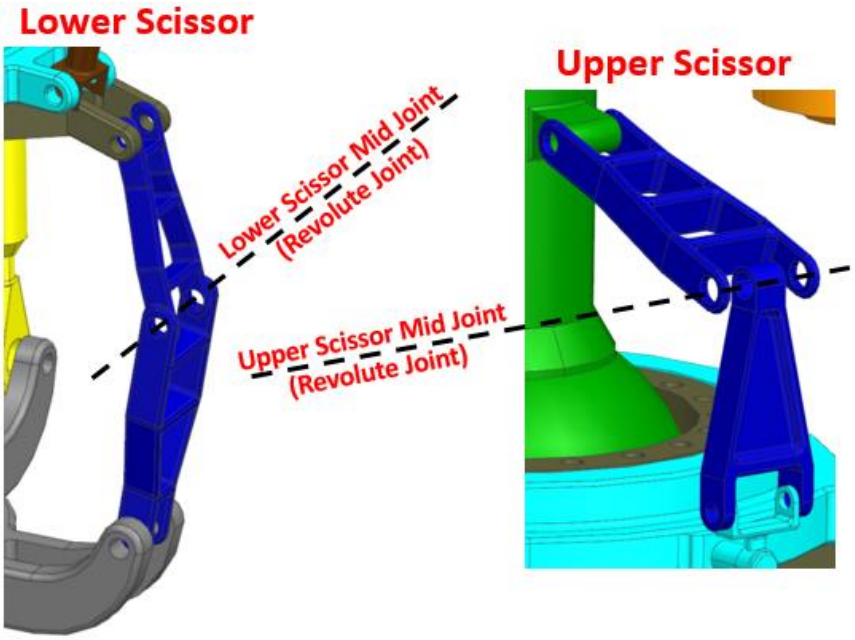

Figure 35: Mid Joints of Scissor Links

Hinges of rotor system are also represented in Figure 36. Since this is an articulated rotor system, the model contains flapping, feathering, and lead-lag hinges. All of the hinges are created with revolute joints.

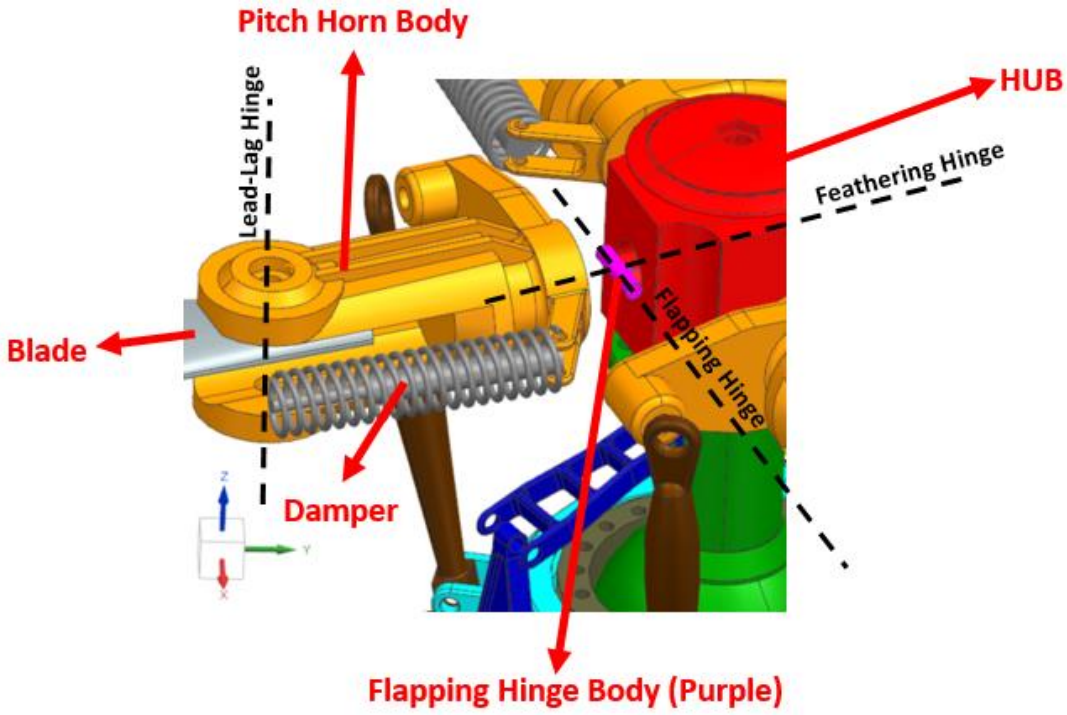

Figure 36: Hinges of Articulated Rotor System in Simcenter 3D Motion

Joints are also defined in Table 2. In this table, joint types and connected bodies with these joint types are listed.

Table 2: Joints and Connectors in the Multibody Model

Joints and Connectors	First Body	Second Body
Fix	Base	Ground
Revolute Joint	Drive Shaft	Base
Revolute Joint	Base	Lower Scissor
Revolute Joint	Lower Scissor	Stationary Swashplate
Revolute Joint	Stationary Swashplate	Rotating Swashplate
Spherical Joint	Drive Shaft	Stationary Swashplate
Universal Joint	Stationary Swashplate	Actuator
Spherical Joint	Actuator	Base
Universal Joint	Rotating Swashplate	Pitch link
Spherical Joint	Pitch Link	Pitch Horn Body
Universal Joint	Pitch Link	Rotating Swashplate
Revolute Joint	Upper Scissor Link	Drive Shaft
Spherical Joint	Upper Scissor Link	Rotating Swashplate
Revolute Joint	Upper Scissor Mid Joint	
Revolute Joint	Lower Scissor Mid Joint	
Revolute Joint (Lead-Lag Hinge)	Blade	Pitch Horn Body
Revolute Joint (Feathering Hinge)	Flapping Hinge Body	HUB
Revolute Joint (Flapping Hinge)	Pitch Horn Body	Flapping Hinge Body
Damper	Pitch Horn Body	Blade

2.6. Elastic Blade Models

Helicopter blades are long, narrow shape mechanisms. The blades are also called as rotating wing with high aspect ratio that minimizes the drag from tip vortices. Since complex aerodynamic phenomenon are observed on rotor blades, in detailed rotor dynamic simulations, the elasticity of blades must be taken into account. In this part, the blade elasticity methodologies, which are used in this project, are discussed.

Rotor blades are made out of various materials which are steel, aluminum, composite structure and titanium. In addition, an absorption shiel is used on the leading edge of blades. In the early days of aviation, since the technology of the time allows wooden fabric materials, the rotor blades are made out of wooden materials. These rotor blades consist of main spar, ribs and covering wooden material skins. The blades were also fabricated as symmetric airfoils since it is easy to build and high lift versus drag was created during operations.

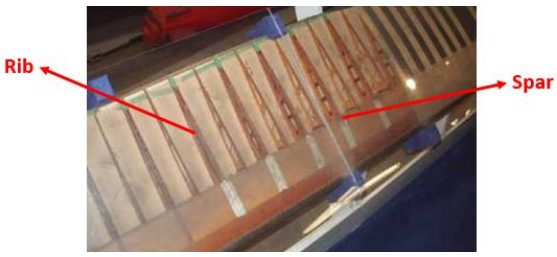

Figure 37: Typical Construction of Blades in the Past [20]

Since the wooden blades could be damaged beyond repair and since they are not resistant to water, metal blades began to appear. This allowed easier to repair process since individual blades can be repaired instead of whole set. The metal blades are also introduced honeycomb with combination to metal skins. This provides good strength and increased performance.

Figure 38: Honeycomb with Metal Blades [20]

However, the metal blades came with an important disadvantage. A metal blade can experience a catastrophic failure if the blade was damaged from a critical area. Due to the

disadvantages of metallic and wooden blades, researchers introduced composite (non-metallic) blades. The composite blades offered a non-catastrophic failure mode. Whereas the metal and wooden blades experience sudden fails like crack, composite blades would not experience sudden failure. In addition, blades are constructed with high stiffness with low weight. A sample composite blade structure is shown in Figure 39.

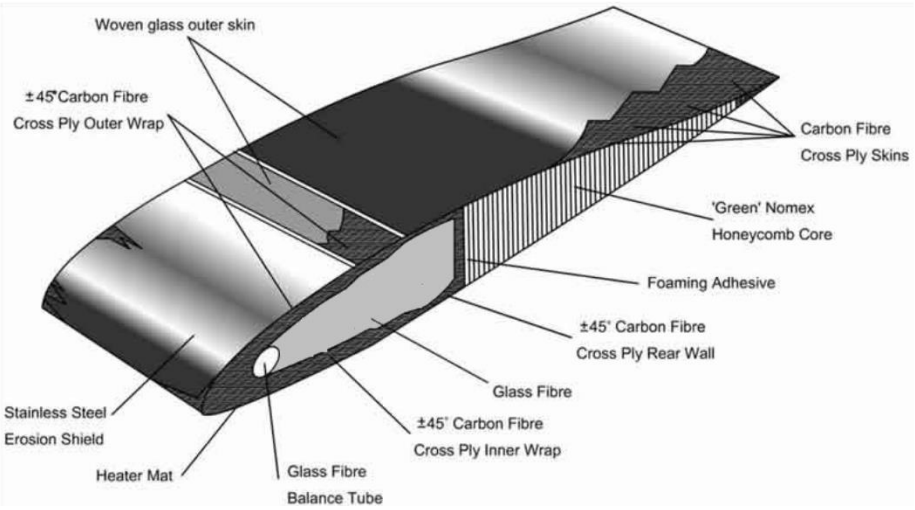

Figure 39: Sample Composite Rotor Blade Construction [21]

In the present, complex blade shapes are also introduced. Blades are created with non-symmetrical airfoil profiles, swept wing shapes, twist angles, etc. Some sample airfoil profiles of non-symmetric and symmetric airfoils are shown in Figure 40.

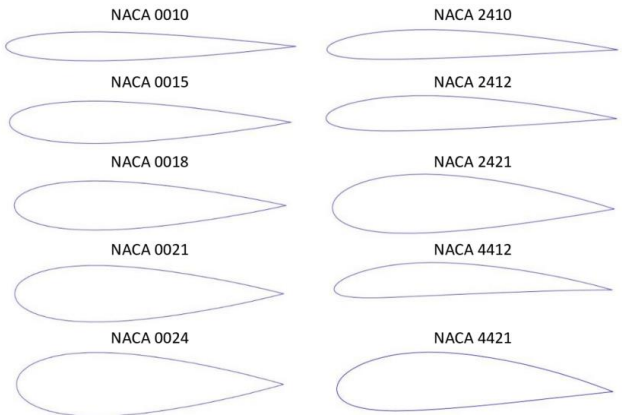

Figure 40: Sample Airfoil Profiles for Non-Symmetric and Symmetric Airfoils [22]

In the present study, NACA23015 airfoil profile is analyzed and investigated for different materials and twist angles. The aerodynamic loads and aerodynamic angles of designs are tabulated.

As discussed in chapter 1.1, elasticity methodology approach, which is finite element modelling, is used in this thesis. The applications are discussed in following subchapters.

2.6.1. Elastic Blade with Finite Element Modelling

Finite element modelling of blades is generated using Simcenter 3D pre-post tool. Other parts of rotor mechanism kept rigid. In the thesis, it is required to generate database for so many distinct designs. For that reason, the time required for designing, analyzing and post-processing of a blade should be as little as possible. The blades are generated with some rotor blade radiuses which are not bigger than 2.5-meter radius in this thesis. This size of rotor blades can be suitable for small scale helicopters i.e., RC helicopters. Therefore, it is enough to design the rotor blades with 1 single solid body with 1 material. This is good for decreasing the time required for designing and analyzing. In addition, Tetrahedral meshing with 4 grid points is utilized to the solid blade body. Tetrahedral meshing of CTETRA (10) is used with 6 mm width of elements. Sample meshing information for a blade, which is given in Table 3, are given in Table 4.

Table 3: Blade Specifications

Airfoil Profile	NACA23015
Chord Length (m)	0.120
Rotor Radius (m)	2
Linear Twist (˚)	4 at the root, -2 at the tip

Table 4: Meshing Information of the Blade

Type of Mesh	3D
Type of Element	CTETRA (10)
Average Elements size (mm)	6
Number of Elements (Per 2m Radius Rotor Blade)	82577
Number of Nodes (Per 2m Radius Rotor Blade)	144556

General view of the blade discussed above is shown in Figure 41. Visualization of blade with tetrahedral mesh is shown in Figure 43.

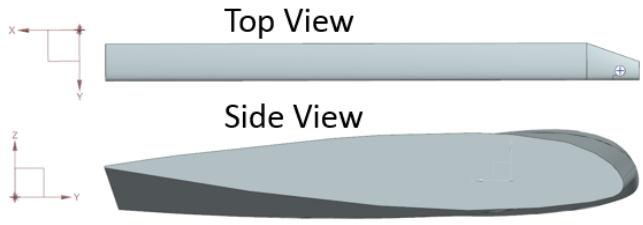

Figure 41: The Blade given in Table 3

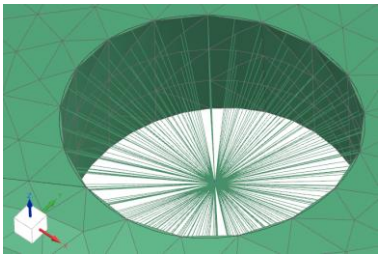

Figure 42: Connection with RBE3 Element in Simcenter 3D Pre-Post

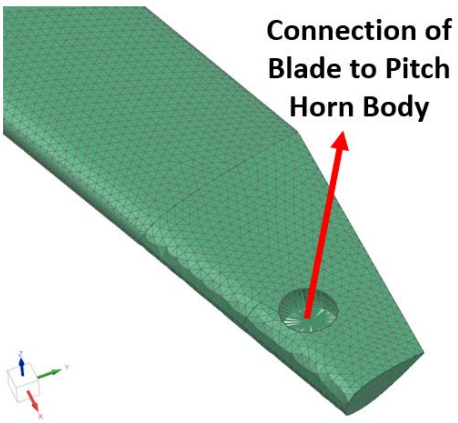

Figure 43: Tetrahedral Mesh for the Blade

In order to connect the blade to pitch horn body, which is given in Figure 34, RBE3 element of Simcenter 3D Pre-Post tool is used. RBE3 is the rigid body element feature of Simcenter Pre-post tool. RBE3 element utilizes the connection between each projected node and nodes on target edge. RBE3 element is an elastic element and load applied at the projected node is distributed to the nodes on target edge with weighted average. RBE3 element connection is shown in Figure 42.

Aerodynamic loads are applied to the blade from equally spaced locations in spanwise direction and at ¼ of the chord from leading edge. The sample application of aerodynamic loads points is shown in Figure 44. In this figure the aerodynamic loads are applied from 6 equally spaced points. For 2.5m long blade, the aerodynamic loads are applied from 8 equally spaced points.

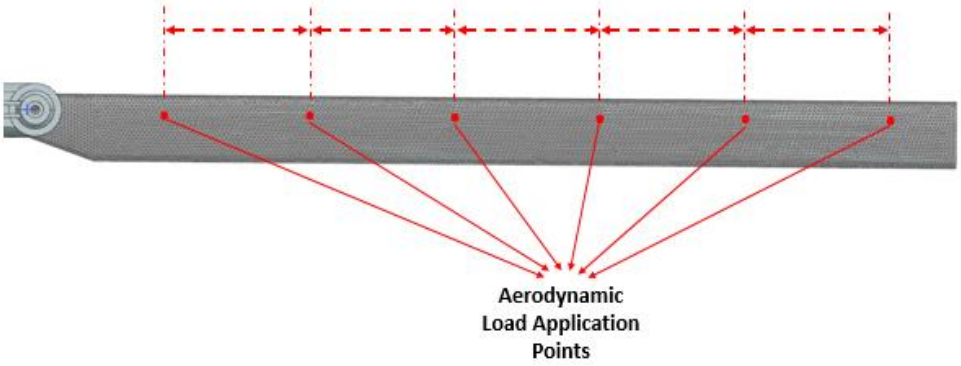

Figure 44: Aerodynamic Load Application Points

After application of aerodynamic loads in hover maneuver (see Figure 23), von-misses stress distribution on blade and nodal displacement from undeformed position are created and are given in Figure 45 and Figure 46. In hover maneuver, the stress distribution becomes almost the same in every azimuth position. Therefore, the distribution plot can be taken in any azimuth position. The pilot inputs and parameters of the simulation are given in Table 5.

Table 5: Pilot Inputs and Simulation Parameters

Rotor RPM [rad/sec]	80
Collective input [deg]	11
Cyclic input [deg]	0
Forward Velocity [m/s]	0

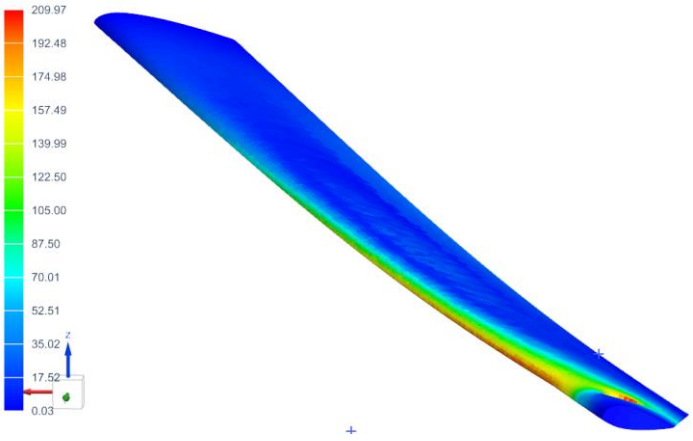

Figure 45: Von-Misses Stress Distribution in [MPa]

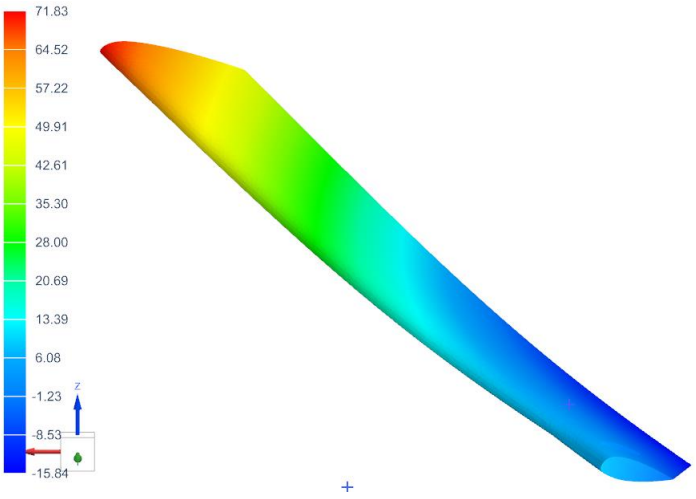

Figure 46: Nodal Displacement from Undeformed Position in [mm]

Since stress distribution and nodal displacements on blade are smoothly distributed, it is enough to apply aerodynamic forces and moments from 6 equally spaced points in spanwise direction for 2m long blade.

2.7. Rotor Simulation Tool (PYTHON Tool)

A tool is generated in order to perform design, analyses, and post process procedures. PYTHON is used in order to perform all of procedures in a loop for so many different blade designs. The PYTHON tool is performing the following operations in order.

- Inputs of the design, analyses and simulation procedures, are imported to the tool from input.txt file.
- NACA airfoil type is inputted to XFOIL and XFOIL is run in order to generate polar files and airfoil shape profiles. Polar files include angle of attack (α), velocity of flow in Mach number, Reynolds number of flow, lift coefficients (Cl) (given in Figure 26), drag coefficients (Cd) (given in Figure 27), moment

coefficients (Cm) (given in Figure 28). Airfoil shape profile files include 2D coordinates of airfoil profiles given in Figure 25.

- Point coordinates in airfoil shape profile files are manipulated in order to create 3D wing as shown in Figure 47. The blades are created at specified span of the wing, twist distribution, angle of incidence, and chord length in Simcenter 3D NX.

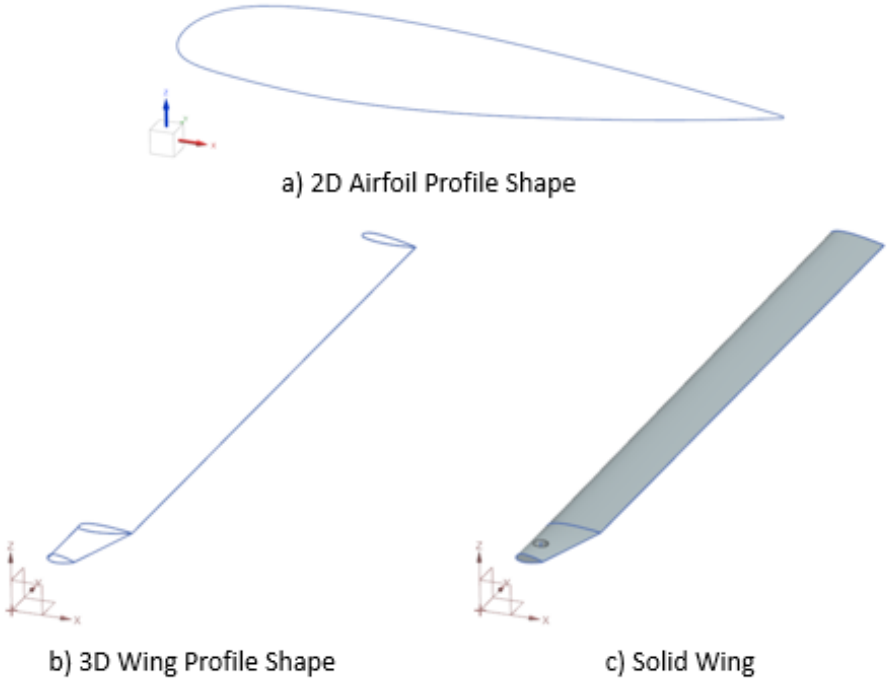

Figure 47: 3D Wing from Airfoil Profile Coordinates.

- Coordinates of leading edge, trailing edge, and ¼ of the chord for designed wing are calculated and stored. Markers are created in these locations. Markers provide necessary inputs like geometric angle of attack (α) and free stream velocity at each station to the force and moment calculation equations.
- Cl, Cd, and Cm profiles are inputted to Simcenter 3D Motion. Then, force and moment equations are created using function tool of Simcenter 3D Motion.
- Created CAD model of blade is inputted to flexible body creation module named Simcenter 3D Pre/Post. 3D meshing, blade connectivity to HUB, and number of modes and mode shapes are stored to a file (.op2). The OP2 file of Simcenter 3D contains all necessary information of flexibility of body. This file is inputted to Simcenter 3D motion for making blade flexible and performing the simulation with flexible blades. The mode shapes used in simulation are given in Figure 48 and Figure 49.

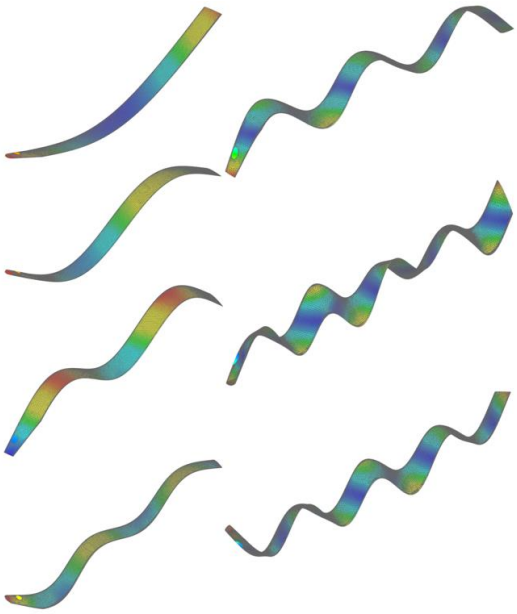

Figure 48: Transverse Bending Mode Shapes (Flapping Modes)

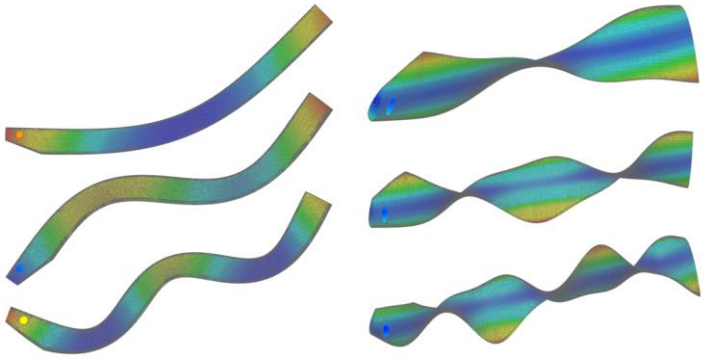

Figure 49: Lateral Bending (Lead-Lag) and Torsional Mode Shapes

- Collective and cyclic pitch inputs are given to the rotor by displacing the actuator pistons under the swashplate. Then, simulation is run.
- Simulation parameters are exported. Postprocess is performed.

The flowchart of all process of the PYTHON tool is given in Figure 50. The processes presented in this chapter and the flowchart are performed repetitively up to amount of given input sets. Some sample input sets are given in Table 6. If a user gives this input set to the PYTHON tool, the tool will perform for set1 and set2 maneuvers sequentially.

Table 6: Sample Input Sets

Number of Sets	Airfoil Profile	Material	Chord Length [m]	Wing Span [m]	Twist Angle (root, end) [deg]	RPM (rad/sec)	Actuator Piston Displacements (1, 2, 3) [mm]	Relative Velocity [m/sec]
Set 1	NACA 23015	AISI 410 SS	0.121	2.0	4.2, -2	80	-25, -25, -25	50
Set 2	NACA 0012	Aluminum 2014	0.2	1.5	2.2, -4	70	-25, -10, -25	30

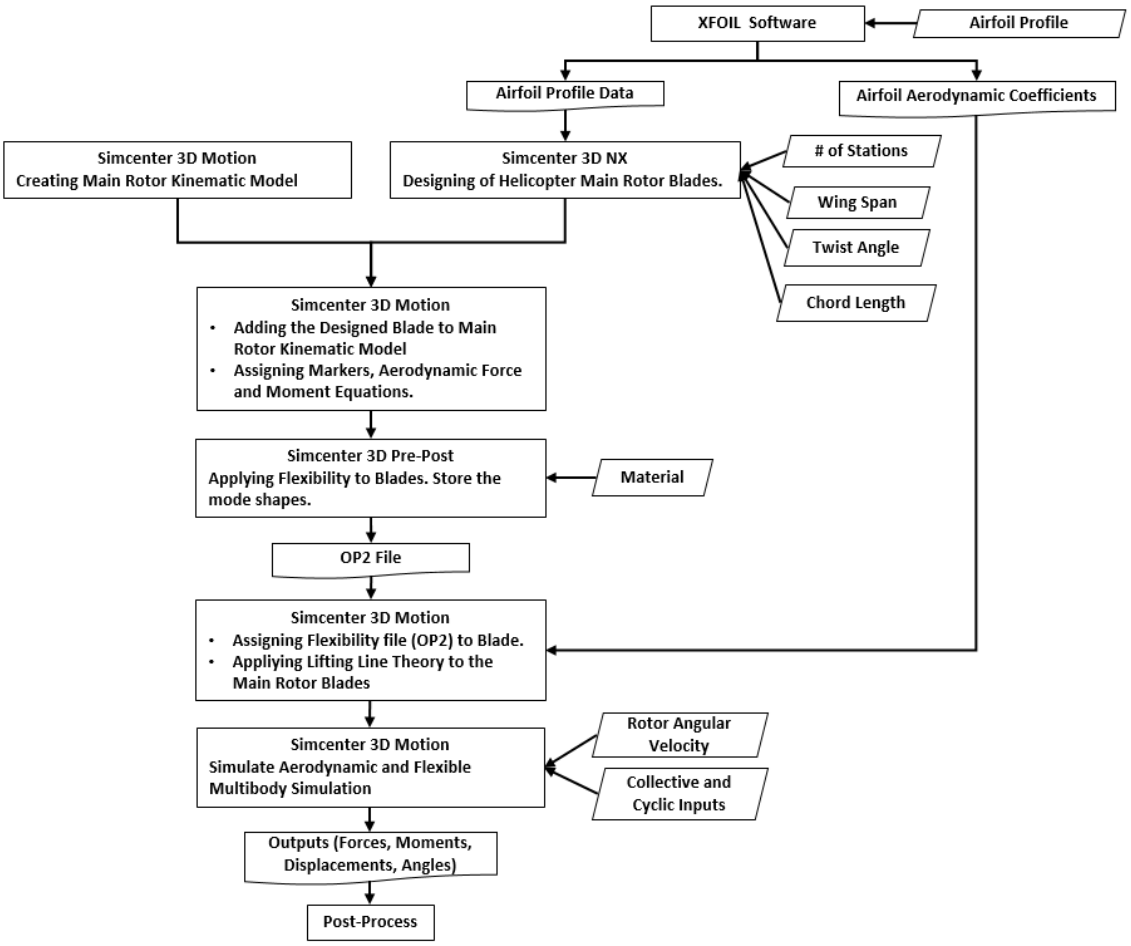

Figure 50: Flowchart of the PYTHON Tool

2.8. Isolated Rotor Model in FLIGHTLAB

An isolated rotor model is also created in a comprehensive real-time simulation software named FLIGHTLAB in order to verify the Simcenter 3D rotor model. FLIGHTLAB is a comprehensive modeling and analysis software for rotorcrafts [24]. This tool is used for almost 40 years in order to modeling and analyses of rotorcraft and helicopter models [24]. There are so many papers and works in order to verify or validate full rotorcraft or isolated rotor models. Due to this wide variety of usage of FLIGHTLAB, it is decided to verify the Simcenter 3D rotor model with FLIGHTLAB rotor model.

The FLIGHTLAB rotor model is created with fully articulated rotor hub system. The blades are modeled as rigid. Blade element theory options provided in FLIGHTLAB is selected as aerodynamics implementation methodology. All flap, lead-lag, and pitch degrees of freedom is opened and no stiffness and damping parameters are assigned to hinges. The same chord length, wing span, twist, and airfoil profiles are used in

FLIGHTLAB with Simcenter 3D rotor model. Twist and chord distribution along the radius is given in Figure 51.

No dynamic inflow model is implemented in FLIGHTLAB since no inflow model is assigned in Simcenter 3D rotor model. Hinge offset value is assigned as Simcenter rotor model and torque offset value is given as 0 in both models. Hinge offset is a distance to hinge points from rotor rotation axis.

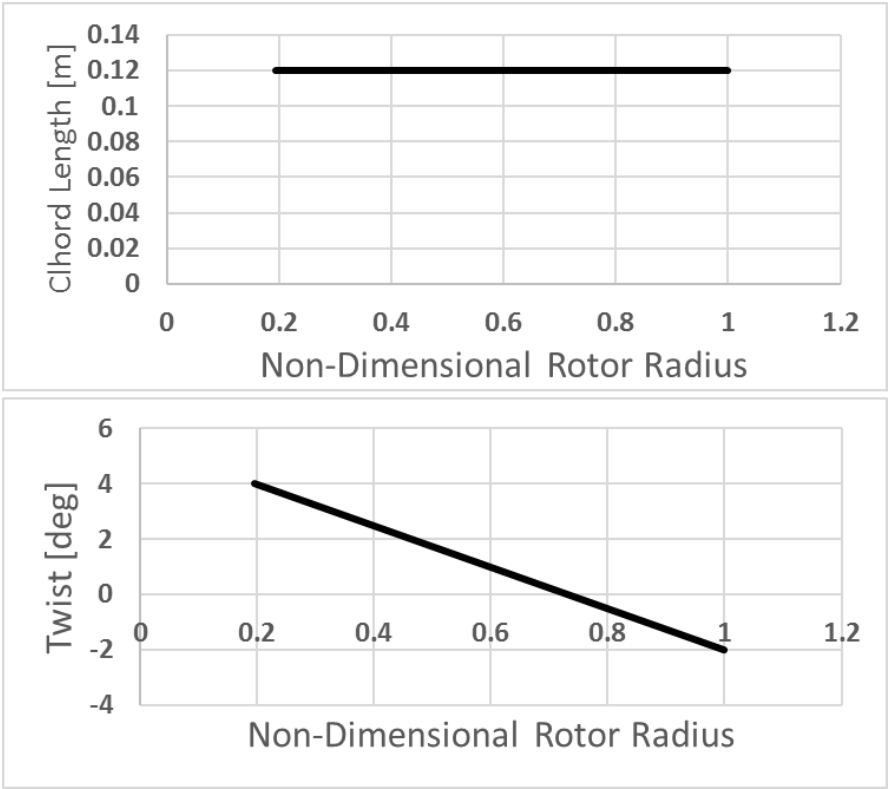

Figure 51: Twist and Chord Distribution of Blade in FLIGHTLAB model

The hinge offset values are given in Table 7 from the rotation center of rotor.

Table 7: Hinge offset

Hinge	Hinge Offset [m]
Flapping	0.08
Feathering	0.08
Lead Lag	0.33

All blade hinges and blade mass are assigned on the line of %25 of chord from leading edge as shown in Figure 52. Mass and inertia values are located to 1 meter from rotation center. Mass and inertia values of blade are given in Table 8.

Table 8: Mass and Inertia of Blade in FLIGHTLAB Model

Hinge	Hinge Offset [m]
Mass [kg]	5.9300
Ixx [$kg.m^2$]	60
Iyy [$kg.m^2$]	60
Izz [$kg.m^2$]	60

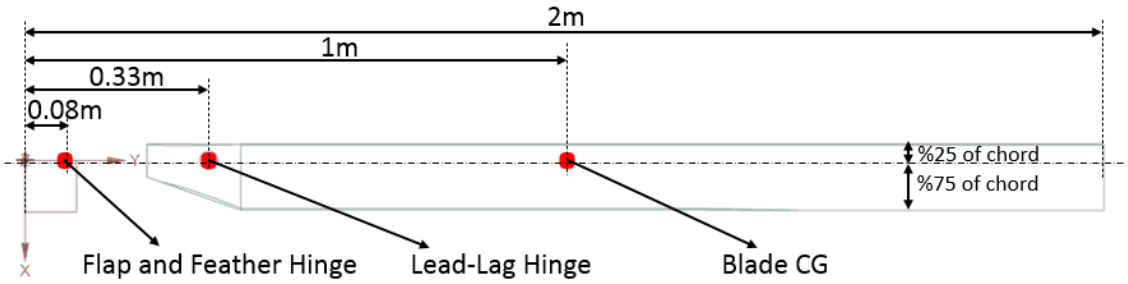

Figure 52: Hinges and Blade mass in FLIGHTLAB Model

NACA 23012 airfoil profile and airfoil aerodynamic data [25] are used in order to design blade and generate aerodynamic model. Fuselage, tail rotor, vertical tail, horizontal tail, landing gears etc. options are closed since isolated rotor model is created. Aerodynamic interferences of blades or other components are not implemented in aerodynamic model. Some hover trim maneuver results and forward flight simulation maneuver results are generated using FLIGHTLAB rotor model and are compared with Simcenter 3D rotor model simulation results. The comparisons of solutions are discussed in chapter 3.2.

3. ROTOR SIMULATIONS

In this part, rotor simulations performed in this thesis and analytical verification of rotor simulation model are discussed. Rotor model in this thesis is investigated with 1 blade due to decrease the complexity of helicopter rotor simulation and due to decrease the simulation duration. The rotor simulations are performed for forward flight and hover flight conditions. Simulations in these flight conditions are also explained in the following subchapters.

3.1. Background of Simulations

Fixed wing aircrafts and helicopters are differing according to their aerodynamic loadings on lifting machines. For fixed wing aircrafts, total lifts on both wings are almost equal during a standard forward level flight condition. In helicopters, the flight condition is more complex than fixed wing aircrafts. The cyclic movements of the rotor disk are performed at the starting and during the forward flight conditions. Moving the longitudinal cyclic forward makes the helicopter nose down motion and this concludes decreasing some altitude of helicopter. By moving the longitudinal cyclic forward, thrust vector of helicopter rotor is tilted to forward and the helicopter started to move forward by gaining speed. In order to maintain the altitude constant, the collective (power) is increased since the tilting of thrust vector decrease the vertical component of thrust vector. In contrast, moving the longitudinal cyclic back makes the helicopter nose up and slow the helicopter down. At this time, vertical component of thrust vector is increased since the lift of the rotor is increased during forward flight. This makes helicopter climb and the collective input should be decreased in this situation in order to make the altitude constant. Applying these coupled inputs, which are up collective plus forward cyclic and down collective plus back cyclic, causes change in the relative speed of rotorcrafts with respect to ground while helicopter is trying to maintain altitude constant.

During the forward flight, the blade motions are also important in helicopters. Helicopter rotors are rotating mechanisms at some rotational velocities. Loads on each blade are almost equal during hover flight conditions but in forward flight, blade loads are changing during each azimuth positions since relative air velocity coming to rotor blades are manipulating the lift distribution on blades at each azimuth positions. In addition, drag forces on blades are also changing at each azimuth positions. While a rotor is performing

hover flight and forward flight, blade airflow distribution in advancing side and retreating side of rotor are shown in Figure 53 and Figure 54.

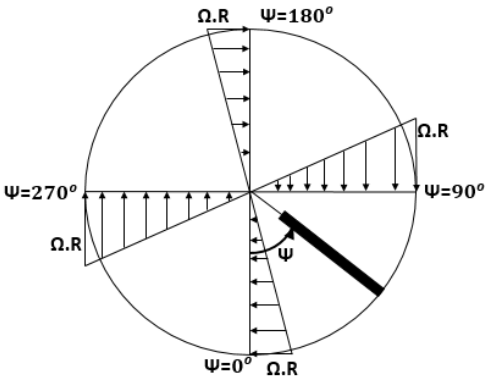

Figure 53: Airflow Distribution on a Rotor Blade in Hover Flight

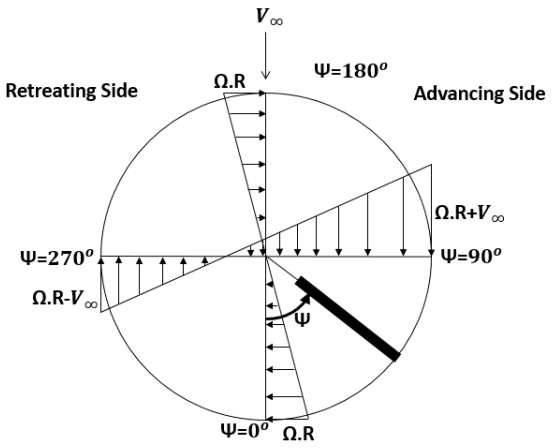

Figure 54: Airflow Distribution on a Rotor Blade in Forward Flight

Airflow velocity in a point on rotor is almost the same at each azimuth position while hover flight is performing. However, in forward flight, airflow velocity on a point on rotor increases while a blade is moving through advancing side and decreases while blade is at the retreating side of rotor. This flow velocity difference causes unsymmetrical load distribution throughout rotor disk. In advancing side, lift and drag forces are increasing whereas decreasing in retreating side. This causes flapping motion. Flapping motion also cause lead-lag motion due to Coriolis effect. Flap (β) and lead-lag (ζ) motions are expressed as Fourier series given in equations (16) and (17).

$$(16)\ \beta = \beta_0 + \beta_{1c}\cos\psi + \beta_{1s}\sin\psi + \beta_{2c}\cos\psi + \beta_{2s}\sin\psi + \cdots$$

Where β_0 is the coning angle, β_{1c} is the longitudinal tip-path plane-tilt and β_{1s} is lateral tip-path plane-tilt as shown in Figure 55.

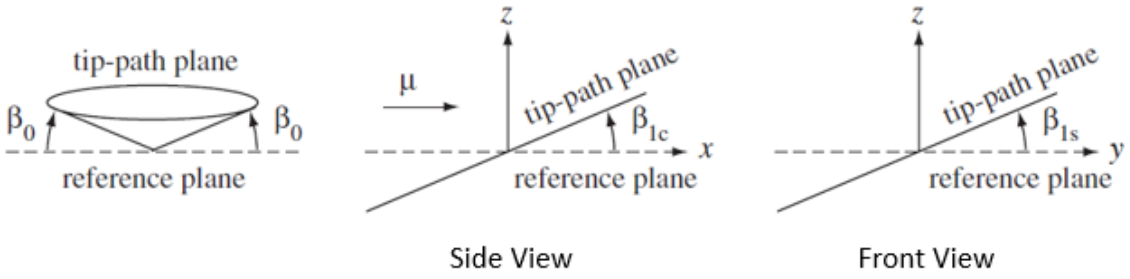

Figure 55: Blade Flapping Harmonics [1]

$$(17)\ \zeta = \zeta_0 + \zeta_{1c}\cos\psi + \zeta_{1s}\sin\psi + \zeta_{2c}\cos\psi + \zeta_{2s}\sin\psi + \cdots$$

Where ζ_0 is mean lag angle of the blades relative to the rotor hub and shaft, ζ_{1c} is first harmonic lateral cyclic lag of the blades and it produces lateral shift of the blades. This causes lateral shift of rotor center of gravity. When $\zeta_{1c} > 0$ the lateral shift is through to the left. Similarly, ζ_{1s} is first harmonic longitudinal cyclic lag of the blades. This produces longitudinal shift of blades in plane of rotation so that longitudinal shift of center of gravity of rotor. When $\zeta_{1s} > 0$ the aft shift is observed. The lag harmonics is represented in Figure 56.

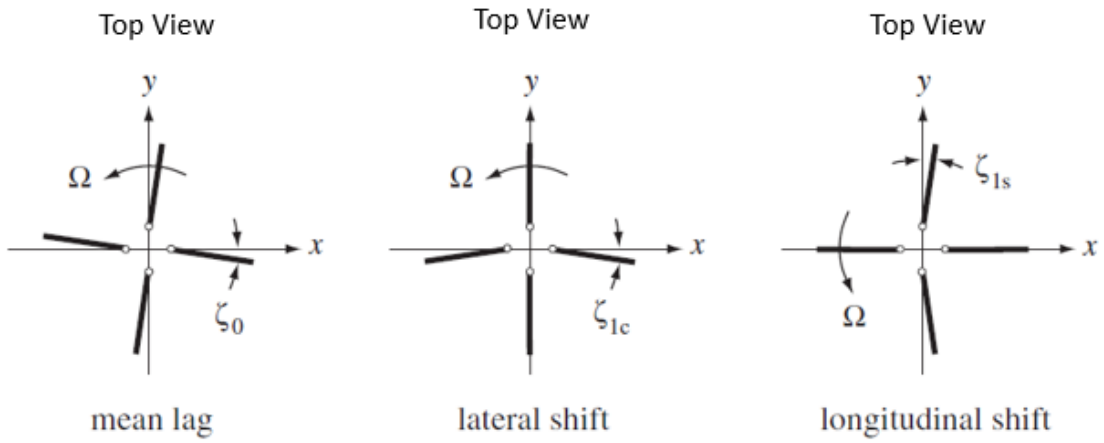

Figure 56: Blade Lag Harmonics [1]

The Fourier series expansion of pitch motions of blades are also shown in equation (18).

(18) $\theta = \theta_0 + \theta_{1c}\cos\psi + \theta_{1s}\sin\psi + \theta_{2c}\cos\psi + \theta_{2s}\sin\psi + \cdots$

The representations of the blade pitch angles are discussed in Figure 31, Figure 32, and Figure 33. Elastic deformation of control system and blade and pilot inputs causes pitch motions of blades. Due to pitch motions, large lift changes because of angle of attack changes are observed. This causes the flap and lag motions.

3.1.1. Rotating Blade Axis

In the load parameter generation, the rotating blade axis is used in the thesis. The loads are generated in rotating blade axis as shown in Figure 57. The axis is attached to the HUB and rotated with the hub during the simulation. However, the blade flapping, lead-lag and pitching motions are not affecting the orientation of rotating blade axis.

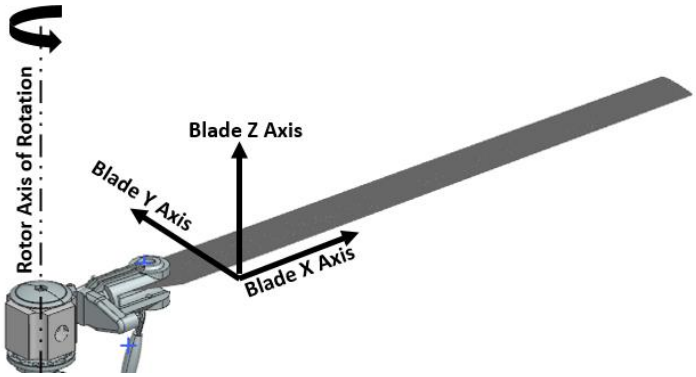

Figure 57: Representation of Rotating Blade Axis

The axis definitions are given as following,

- The Blade X Axis is through spanwise direction of the blade.
- The Blade Y Axis is from trailing edge to leading edge of the blade.
- The Blade Z Axis is in the same direction with rotor axis of rotation.

3.1.2. Global Axis

The global axis system is shown in Figure 58. The axis is fixed to space (non-rotating). Blade flapping, lead-lag and pitching motions are not affecting the orientation of the axis.

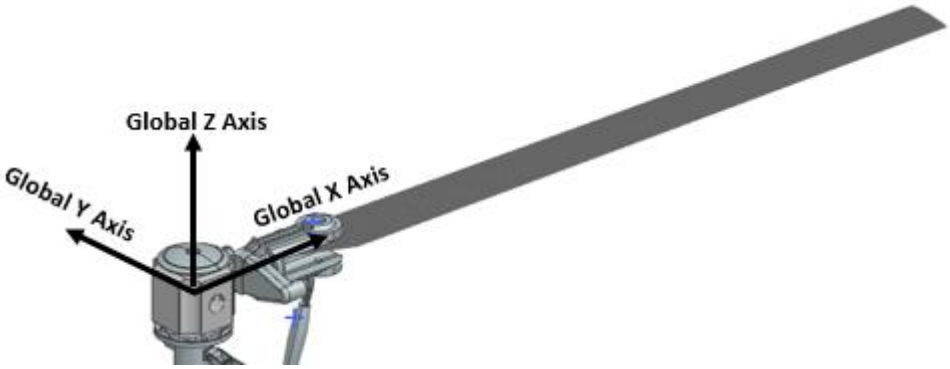

Figure 58: Representation of Global Axis

The axis definitions are given as following,

- The Blade X Axis is through spanwise direction of the blade.
- The Blade Y Axis is from trailing edge to leading edge of the blade.
- The Blade Z Axis is in the same direction with rotor axis of rotation.

3.1.3. Rotor System Bending Moment Calculation Point

In the following subchapters, bending moment created by the aerodynamic and inertial forces of rotor blade are also investigated. Calculation point of this bending moment is selected as rotor system - space connection point given in Figure 59.

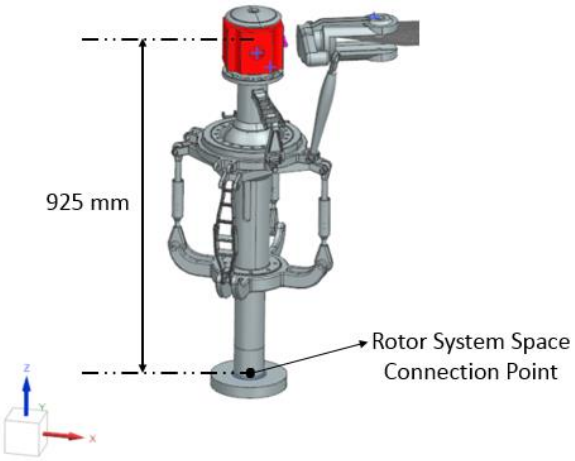

Figure 59: Rotor System Space Connection Point

3.2. Comparison of FLIGHTLAB and Simcenter 3D Rotor Models

In this part, rotor model solutions generated with Simcenter 3D is compared with rotor model solutions created in FLIGHTLAB in order to verify the Simcenter rotor model. For comparison, both of the models are created with rigid blade body parts and same specifications described in section 2.8 are used in both models.

Some hover trim solutions are performed in FLIGHTLAB. Trim targets of maneuvers are defined as blade thrust values and are given in Table 9.

Table 9: Trim Targets

Maneuvers	Trim Target Fz [N]
Hover 1	453
Hover 2	657
Hover 3	879
Hover 4	1100
Hover 5	1323
Hover 6	1545

The hover maneuvers for the same trim targets are also simulated in Simcenter rotor model. Pitch and flap angle for same trim targets are compared as shown in Figure 60 and Figure 61 respectively. In the figures, dashed lines are representing FLIGHTLAB trim maneuver results whereas solid lines are representing Simcenter 3D simulation results which are trimmed to specified trim targets.

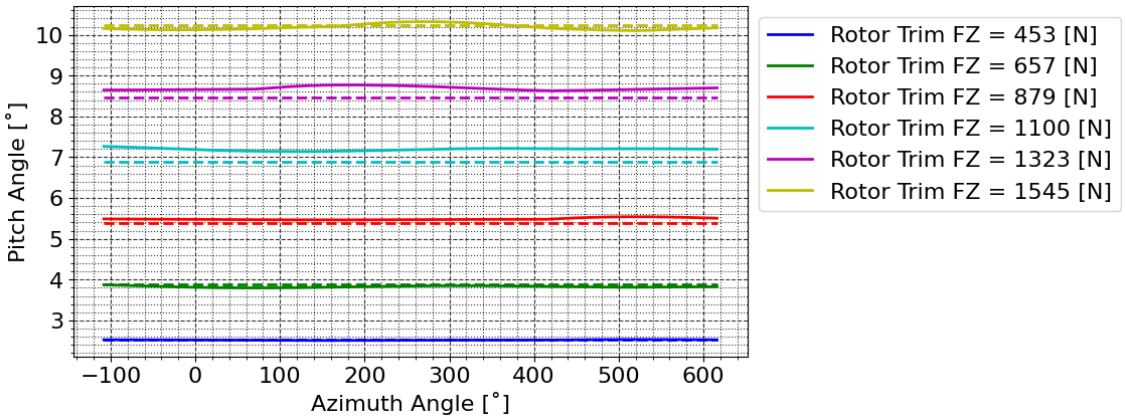

Figure 60: Pitch Angle Comparison of FLIGHTLAB and Simcenter Rotor Models in Hover Maneuver.

Pitch angles are showing great correlations with FLIGHTLAB trim solutions. Some slight differences are seeing due to calculation methodology difference of both models. These results showing that the airfoil profile usage and modelling of aerodynamics and kinematics are correct in Simcenter 3D rotor model.

Flap angles are also showing a great correlation but some slight differences are seeing in Figure 61. These differences are mostly observed in very high and very low thrust trim maneuvers. The cause of differences are some numerical solution errors and due to some differences of blade element method implementations. In addition, whole simulations are shown with Simcenter 3D solutions but trim instants to trim targets are shown in FLIGHTLAB solutions. This is also a reason why Simcenter 3D solutions are not perfectly matching with trim solutions in Figure 61.

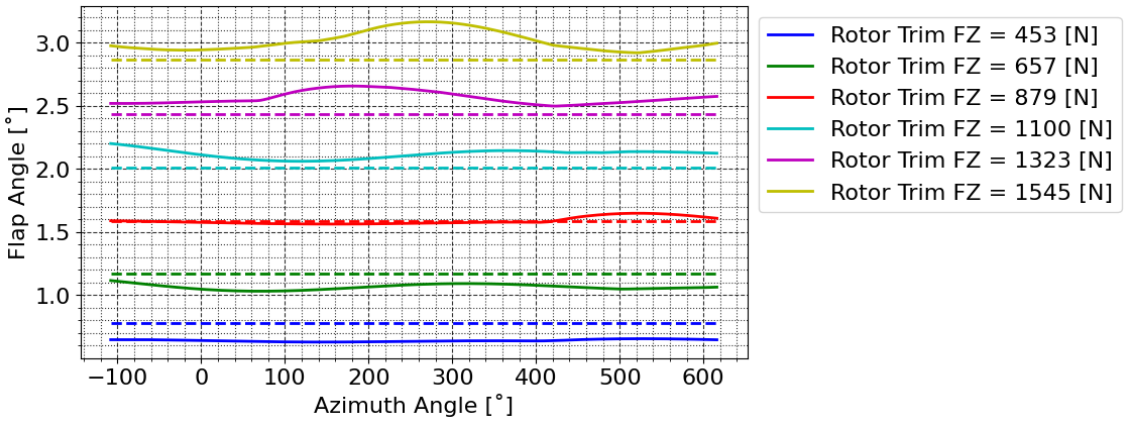

Figure 61: Flap Angle Comparison of FLIGHTLAB and Simcenter Rotor models in Hover Maneuver.

Some forward flight simulation results are also compared for Simcenter 3D and FLIGHTLAB rotor models. In these simulations, collective pitch input is kept the same

in each simulation but longitudinal cyclic inputs are varying. The inputs in each simulation are given in Table 10.

Table 10: Simulation Inputs for Comparison Study

Maneuvers	Collective Pitch [deg]	Longitudinal Cyclic Pitch [deg]
Maneuver 1	5	2.86
Maneuver 2	5	4.30
Maneuver 3	5	5.73
Maneuver 4	5	7.16
Maneuver 5	5	8.59

Since the collective pitch input is not changing, the blade thrust value is calculated as almost the same in each maneuver and the value is approximately 750N. Pitch and flap angles are compared as shown in Figure 62.

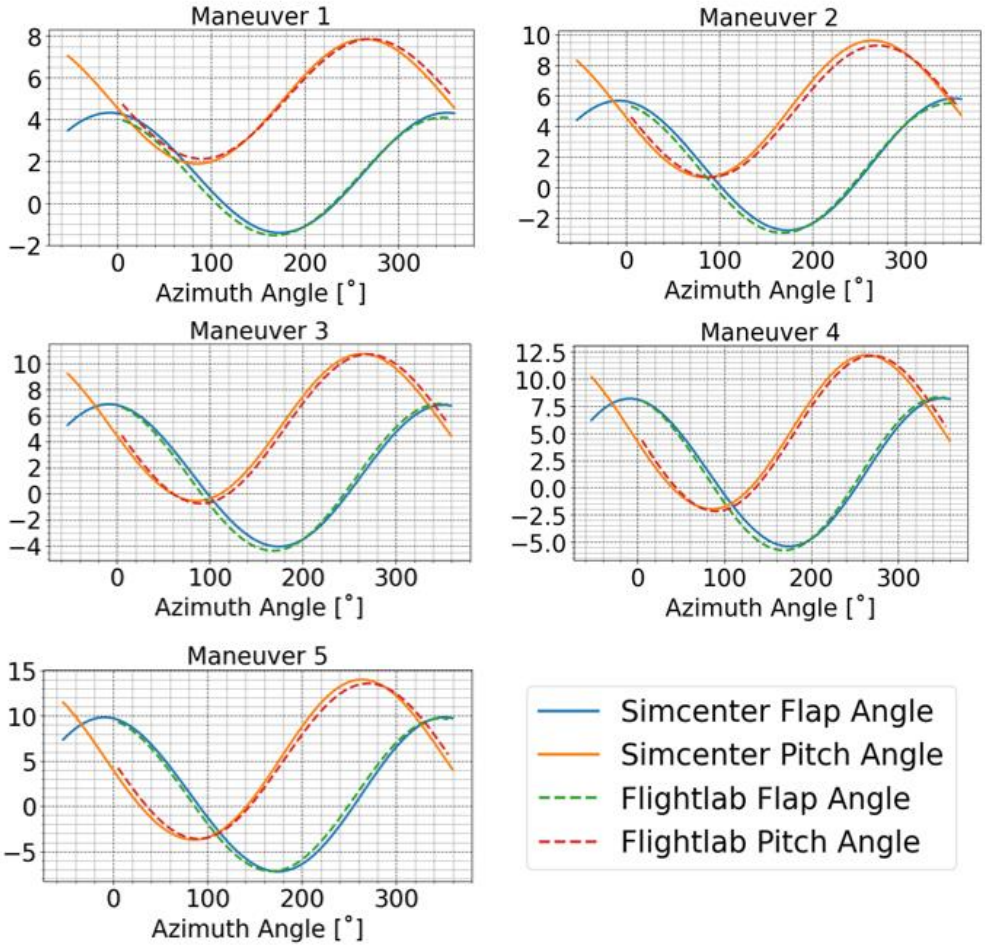

Figure 62: Flap and Pitch Angle [Degrees] Comparisons of Forward Flight Simulations with FLIGHTLAB and Simcenter Rotor models.

In the figures, dashed lines are representing FLIGHTLAB simulation maneuver results whereas solid lines are representing Simcenter 3D simulation results. The comparisons are showing that great correlations are observed for both of the models in forward flight simulations.

The comparison of results in both hover and forward flight maneuvers are motivated in order to continue to the flexible blade modelling parts. In the next sections, behaviors and parameters of flexible blade modelling under aerodynamic loadings are discussed.

3.3. Elastic Rotor Modeling in Simcenter 3D

In this part blades are modelled as flexible. Aerodynamic interactions of blades and any aerodynamic loadings caused by other rotor system components are neglected. Therefore, rotor system with only one blade is investigated. Some parameters of the helicopter rotor kinematic and aerodynamic model, and structural specifications are investigated under different flight scenarios. The investigated aerodynamic and structural parameters are listed in Table 11 and Table 12.

Table 11: Aerodynamic Parameters

Parameter Types
Angle of attack of blade sections
Flap, lag and pitch angles of blade
Aerodynamic Forces and Moments
Rotor System Bending Moment

Table 12: Structural Parameters

Parameter Types
Von misses stress in blade sections
Deformation in blade sections

The analyzed blade design specifications and simulation inputs are given in Table 13.

Table 13: Blade Design Specifications and Rotor Rotational Velocity

Number of Stations	6
Airfoil Profile	NACA23015
Material	Aluminum_2014
Chord Length (m)	0.2
Rotor Radius (m)	2
Root cut-out (m)	0.27
Linear Twist (˚)	4 at the root, -2 at the tip
Rotational Velocity (rad/sec)	80

Stiffness and damping values in flapping, lag-lag and feathering hinges are given in Table 14.

Table 14: Stiffness and Damping at Hinges

Hinge	Stiffness (Nm/rad)	Damping (Nm sec/rad)
Feathering Hinge	800	70
Flapping Hinge	3000	300
Lead-Lag Hinge	3000	300

Lead-lag damping curve of lead-lag damper is given as in Figure 63.

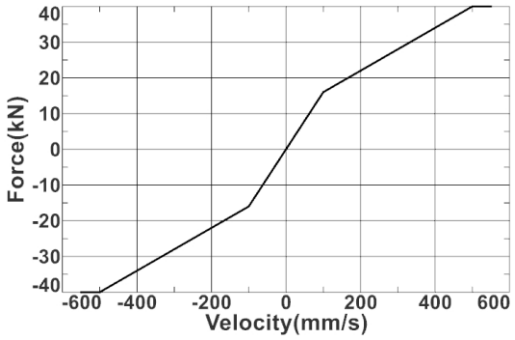

Figure 63: Lead-Lag Damper Profile

Distance of each blade station to the flapping hinge is also given in Table 15. In addition, blade hinge locations in Global Axis are given in Table 16.

Table 15: Distance of Blade Stations to Flapping Hinge

Station Number	Displacement (mm)
Station 1	617
Station 2	877
Station 3	1137
Station 4	1397
Station 5	1657
Station 6	1917

Table 16: Blade Hinge Locations in [mm]

Hinge Type	X [mm]	Y [mm]	Z [mm]
Flapping Hinge	75	30	0
Feathering Hinge	75	30	0
Lead-Lag Hinge	308	121	0

Pilot inputs are given to blades using actuator displacements in kinematic model. A sample actuator displacement representation is shown in Figure 64.

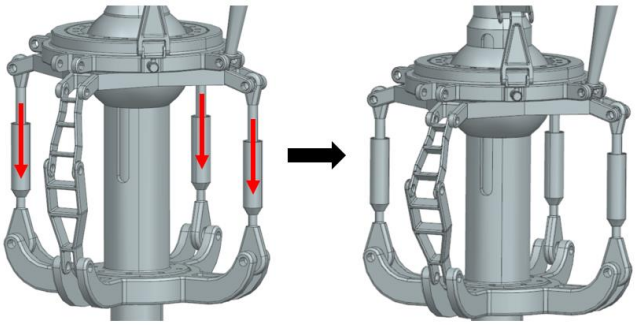

Figure 64: Actuator Movement for given Pilot Collective Inputs

In Figure 64, only collective (θ_0) input is given to the blade. Therefore, all 3 actuators are displacing with same magnitude. In Chapter 3.3.1, simulation parameters of rotor model under these types of inputs are investigated whereas in Chapter 3.3.2, collective (θ_0) input together with longitudinal cyclic pitch (θ_{1c}) input are given to system.

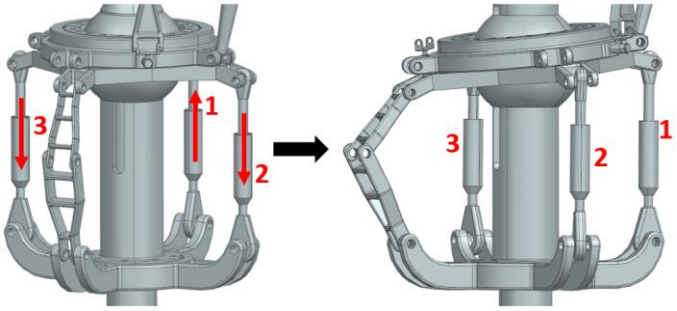

Figure 65: Actuator Movement for given Pilot Collective and Longitudinal Cyclic Pitch Inputs

At this time the orientation of rotor system is observed as shown in Figure 65. Due to difference in actuator displacement, the swashplate is orientating. This is a sample longitudinal cyclic pitch input given to blade.

3.3.1. Rotor Parameter Investigation in Hover Flight

Simulation parameters with respect to azimuth angle at each station in hover flight are investigated in this section. In hover flight, since there is no forward velocity, the parameters are expected to be almost the same at each azimuth stations.

- Angle of attack should be constant at each azimuth station and should always be less at the tip since the blade has 6-degree linear twist.
- Blade pitch, lead lag and flap angles should be almost constant at all stations after pilot input entry was finished as shown in Figure 66. Therefore, aerodynamic force and moments should be constant at all stations during steady phases.

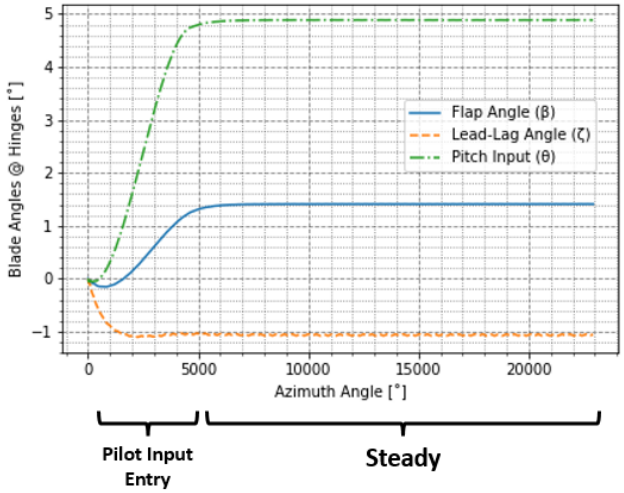

Figure 66: Blade Angle Variations During Pilot Input Entry and Steady Phases

- Aerodynamic forces should increase from blade root to tip since linear velocity at each section on blade is increasing from root to tip.
- Aerodynamic damping is high in flapping direction whereas the low aerodynamic damping is observed in lead-lag motion direction. Therefore, lead-lag oscillation of blade can be more visible.

2 hover maneuver analyses are performed. The blade is designed with the parameters given in Table 13.

3.3.1.1. Hover Simulation with 4° Pitch Input

In this part, only collective pitch input, is given to the blade and forward velocity is not given to the rotor. Pitch angle, flap angle, lead lag angle, aerodynamic forces and moments and angle of attack parameter variations at each blade stations during the simulation are shown in Figure 67 to Figure 72. In this simulation, only 4-degree pitch input is given to blade. In Figure 67, lead-lag angle and flap angle response of blade to 4-degree pitch input are shown.

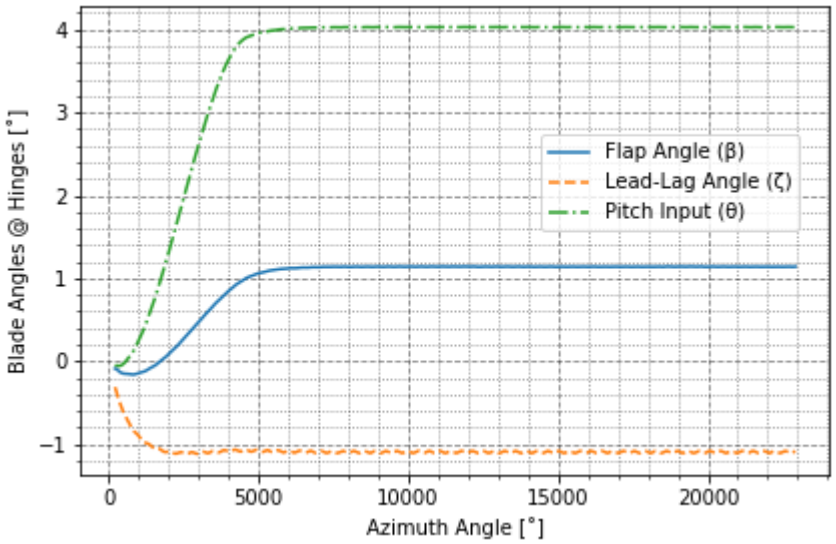

Figure 67: Pitch, Lead-Lag and Flap Angles of Blade

In Figure 68,angle of attack distribution on blade at each blade stations are shown for 4-degree collective pitch input.

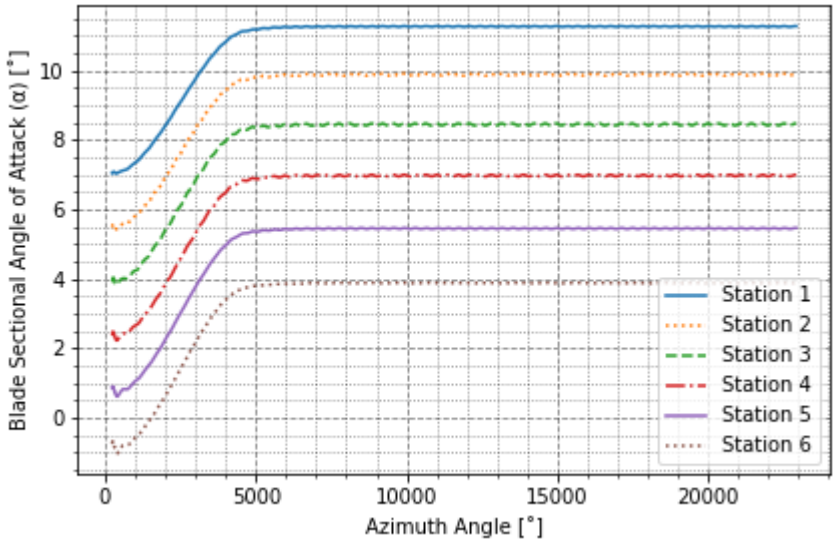

Figure 68: Angle of Attack

Since 4-degree pitch input is given to the blade, angle of attack values are increasing about 4-degree at each stations. The starting angle of attack of the blades are varying due to blade twist angle and the angle of attack values of each section are always distinct values during simulation.

In Figure 69, vertical aerodynamic loads (lift) at each station on blade are shown for 4-degree collective pitch input.

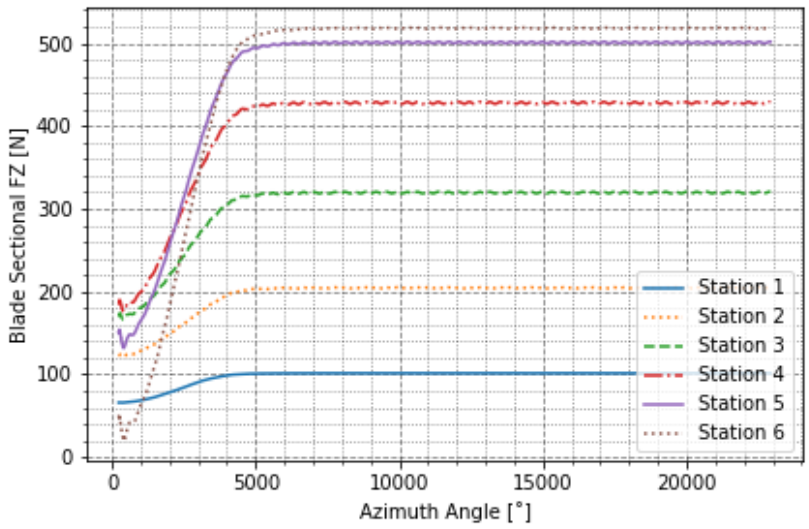

Figure 69: Aerodynamic Force Components in Z direction in Rotating Blade Axis

Although, angle of attack at the tip is less due to twist angle, lift force is more at the tip of blade. In addition, increasing of lift is more at station 6 since linear velocity is more at the tip compared to root. Also, lift coefficient Cl is 0 between -1 and 0 angle of attack

range. Since blade incidence @ station 6 is (-), lift is close to 0 at the station 6 at low pitch angles (at the starting of simulation).

In Figure 70, horizontal aerodynamic loads parallel to rotor disk (drag) is shown for 4-degree collective pitch input.

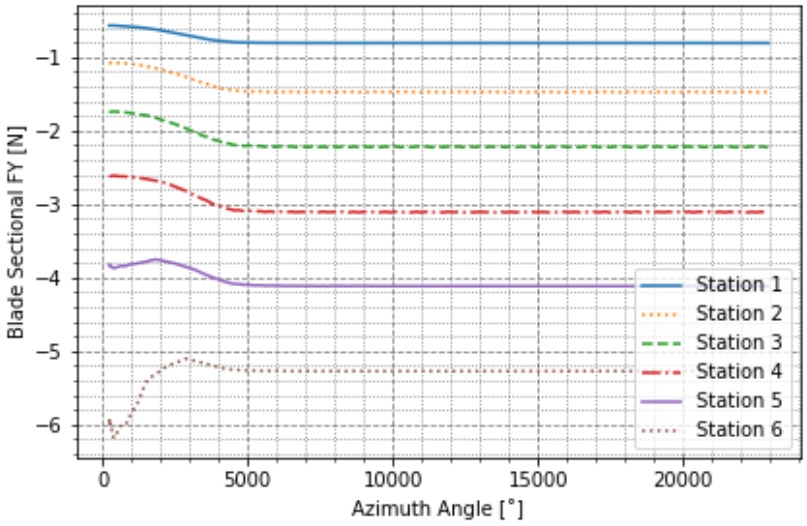

Figure 70: Aerodynamic Force Component in Y direction in Rotating Blade Axis

Since the airfoil is generating low drag coefficient, the drag forces at each section are very low compared to lift force. In addition, pitching moment generation is also low as shown in Figure 71.

In Figure 71, aerodynamic pitching moments on each station of rotor blade are shown for 4-degree collective pitch input.

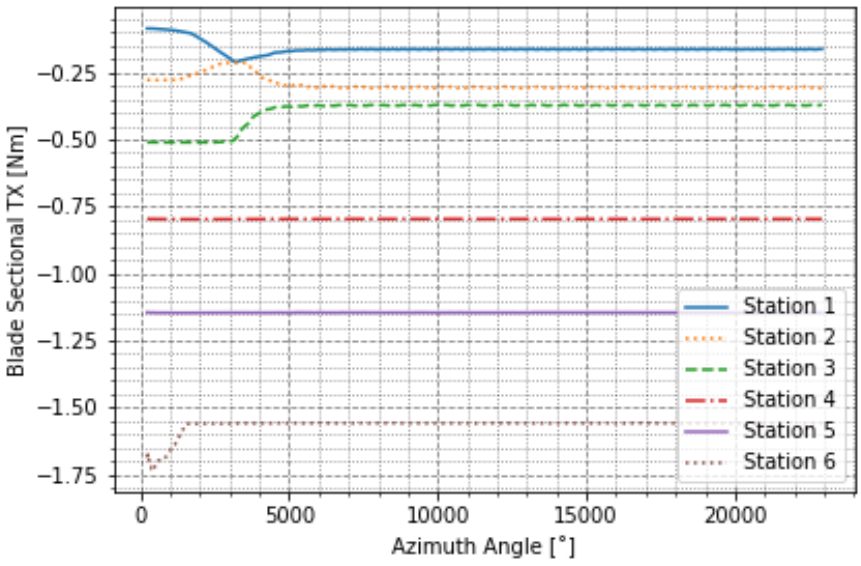

Figure 71: Aerodynamic Moment Component in X direction in Rotating Blade Axis

Bending moment created by rotor blade on rotor system space connection point in rotating blade axis is shown in Figure 72. Centrifugal force of blade and aerodynamic forces and moments on blade contribute the bending moment of rotor blade system.

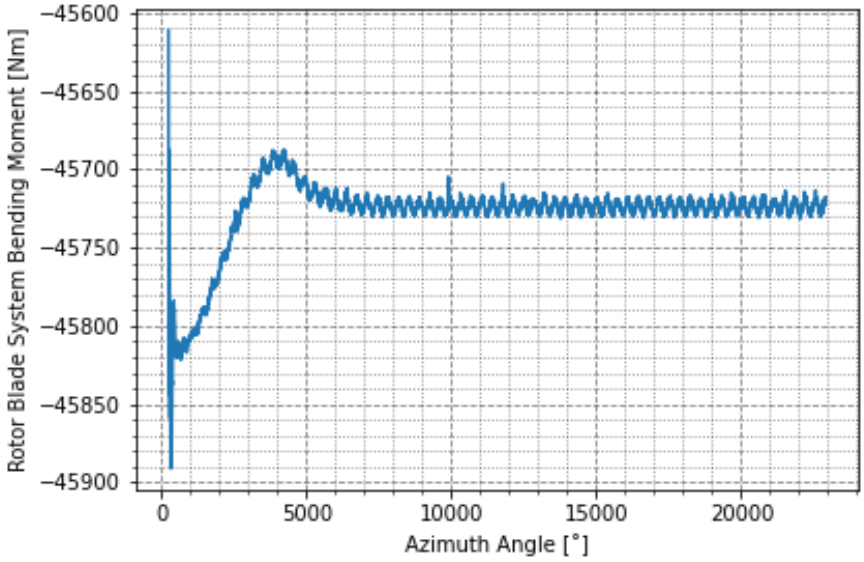

Figure 72: Rotor Blade System Space Connection Point Bending Moment in Y direction in Rotating Blade Axis for 4-degree Collective Pitch Input

Von-Misses Stress Distribution on blade is also shown in Figure 73.

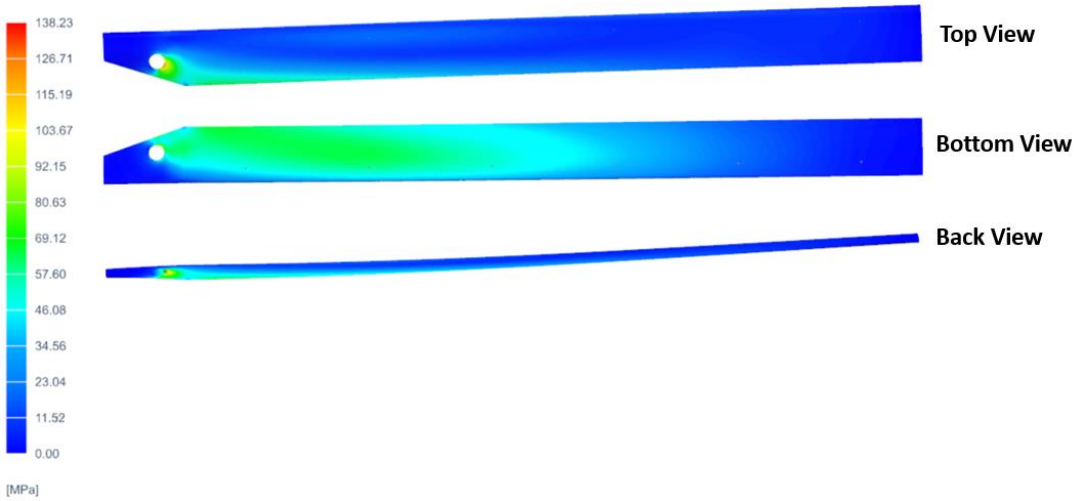

Figure 73: Von-Misses Stress Distribution on Blade

Due to lift force on blade, the blade makes flapping up at each azimuth angle. Therefore, lower side of blade is exposed to tension and von-misses stress distribution on tension side is more than compression side. It is not necessary to investigate flapping up and down motions separately in hover flight since these motions are not expected to observe.

3.3.1.2. Hover Simulation with 8˚ Pitch Input

Hover simulation is also performed with an 8-degree pitch input. The forward velocity is not given in this simulation either. The simulation parameters are investigated in to Figure 79. In Figure 74, lead-lag angle and flap angle response of blade to 8-degree pitch input are shown.

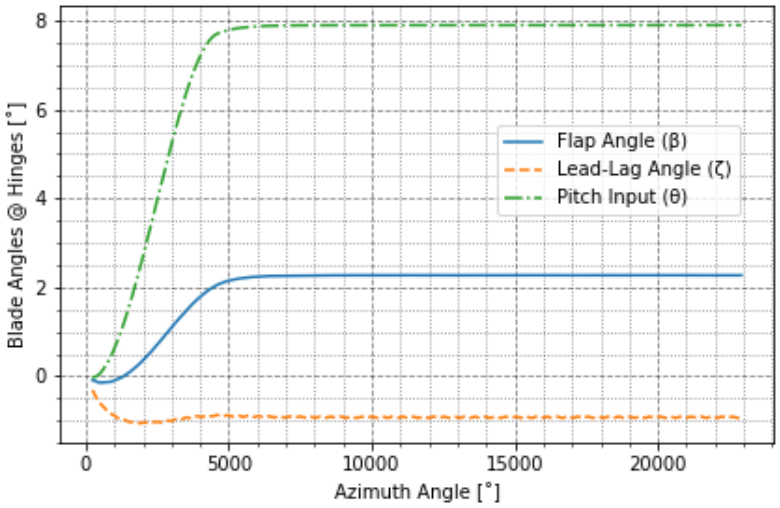

Figure 74: Pitch, Lead-Lag and Flap Angles of Blade

Pitch angle parameter comes to 8 degrees as expected and flap angle is almost doubled compared to 4-degree pitch input maneuver. The change in lead lag angle is not visible since drag force on blade is not significant compared to lift force.

In Figure 75, angle of attack distribution on blade at each blade stations are shown for 8-degree collective pitch input.

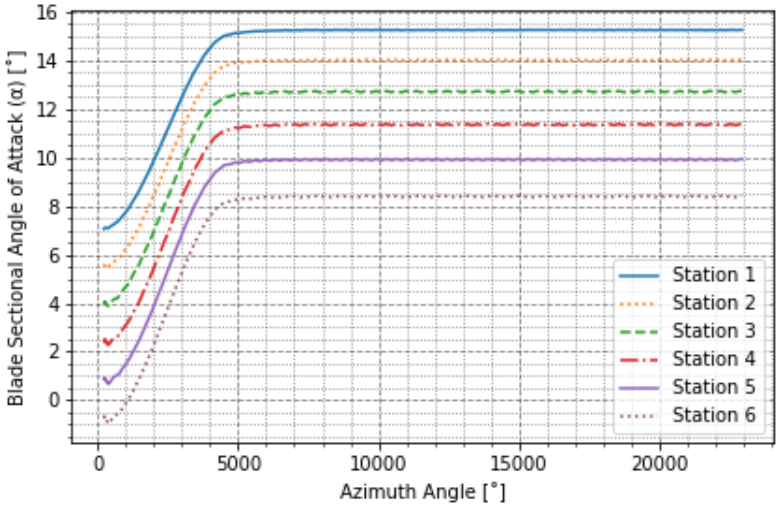

Figure 75: Angle of Attack

Change in angle of attack values at each section are about 8 degrees as shown in Figure 75. Due to twist angle, the blade angle of attack values are varying at each sections.

In Figure 76, vertical aerodynamic loads (lift) at each station on blade are shown for 8-degree collective pitch input.

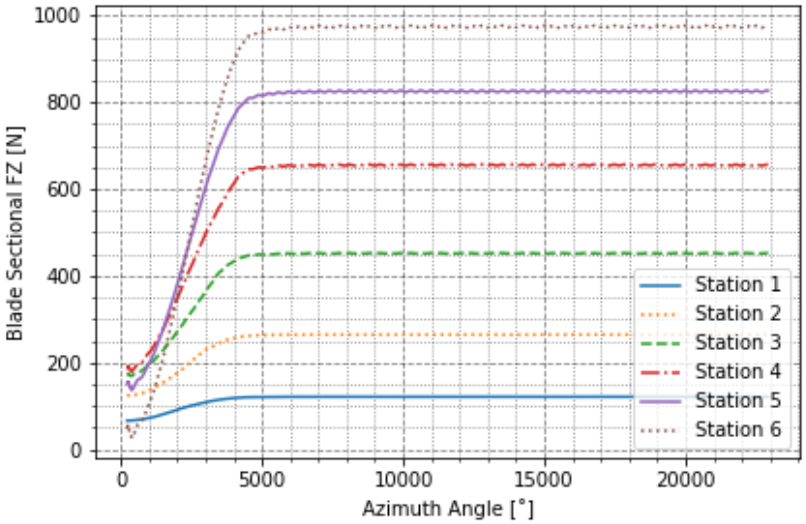

Figure 76: Aerodynamic Force Component in Z direction in Rotating Blade Axis

Sectional lift forces are also increased compared to 4 degrees pitch input case. The increasing of lift forces is more at the tip compared to root due to dynamic pressure since dynamic pressure is related with the square of freestream velocity coming to blade sections.

In Figure 77, horizontal aerodynamic loads (drag) at each station on blade are shown for 8-degree collective pitch input.

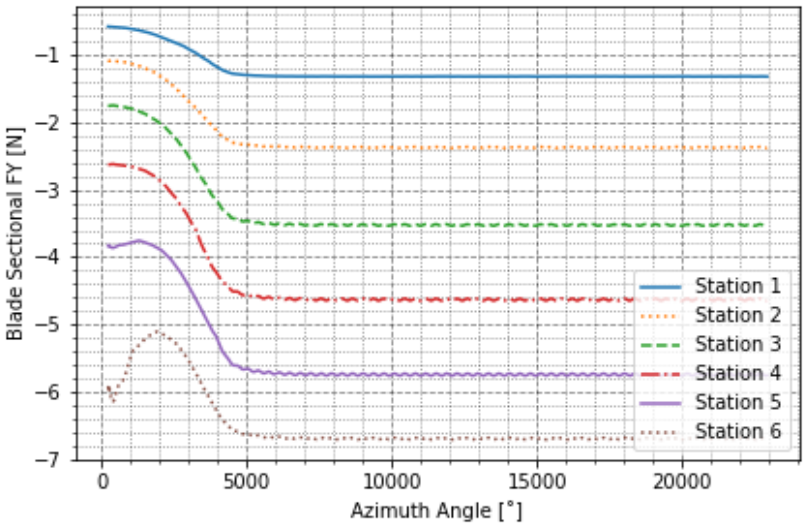

Figure 77: Aerodynamic Force Component in Y direction in Rotating Blade Axis

An increasing in drag force is observed compared to 4-degree pitch input case but still the drag force is not significant as shown in Figure 77.

Aerodynamic pitching moments at each section on blade for 8-degree pitch input are shown in Figure 78.

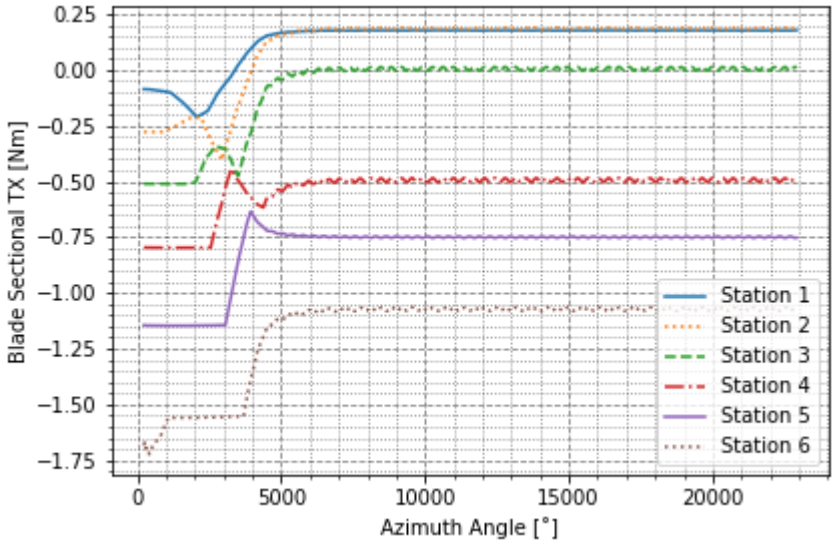

Figure 78: Aerodynamic Moment Component in X direction in Rotating Blade Axis

Bending moment observed on rotor blade system space connection point is investigated in Figure 79 for 8-degree collective pitch input.

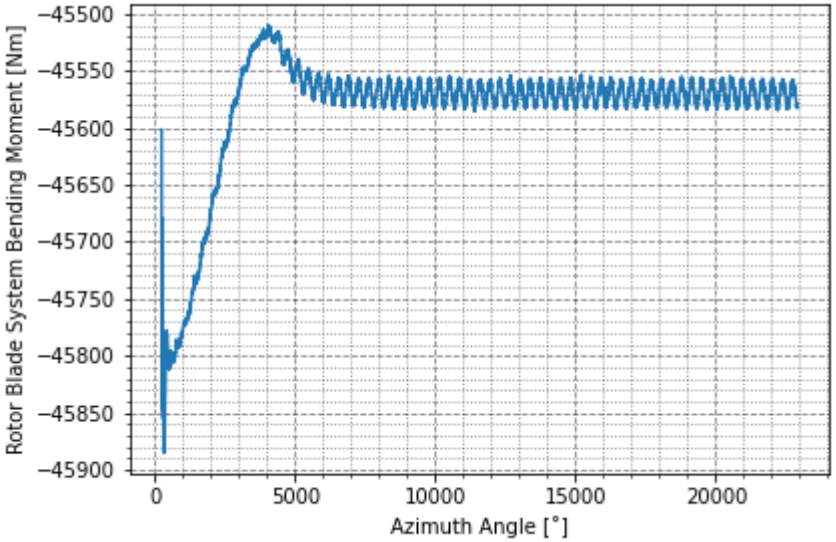

Figure 79: Rotor Blade System Space Connection Point Bending Moment in Y direction in Rotating Blade Axis for 8-degree Collective Pitch Input

It is seen that the magnitude of bending moment is decreased. Reason of this decreasing is discussed in Free Body Diagram of blade in hover which is given in Figure 80.

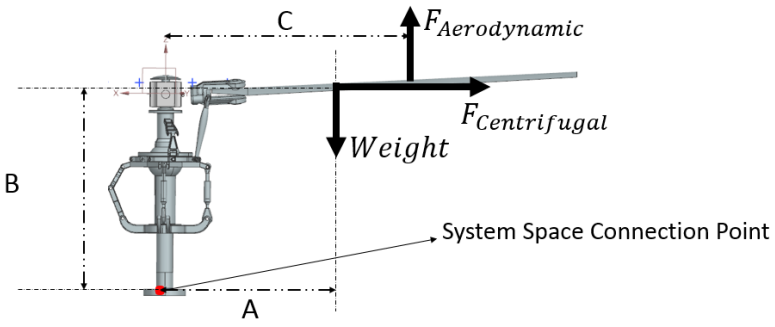

$$M = F_{Aerodynamic}\, x\, C \; - Weight\, x\, A \; - F_{Centrifugal}\, x\, B$$

Figure 80: Free Body Diagram of Blade in Hover

- Due to more flapping, horizontal distance between cg of the blade and rotation axis of rotor decreases. This decreases the moment arm of aerodynamic force. But in overall, moment contribution of aerodynamic force is increasing in counter clockwise direction since aerodynamic force are increasing.
- horizontal distance between cg of the blade and rotation axis of rotor are also decreasing. This decreases the moment created by weight in clockwise direction.
- The decrease in distance between cg of the blade and rotation axis of rotor also decreases the magnitude of centrifugal force since centrifugal force is proportional with the square of velocity and velocity is proportional with the distance to rotor rotational axis. In addition, vertical distance between cg point to system space connection point is increasing proportional with the distance. As a result, moment created by centrifugal force is decreasing in overall in clockwise direction.

As a result, moment is decreasing in clockwise directions. Since centrifugal force is major contributor of moment created in system space connection point, the moment decreases in the point.

In addition, stress distribution on blade and blade shape during steady phase is given in Figure 81.

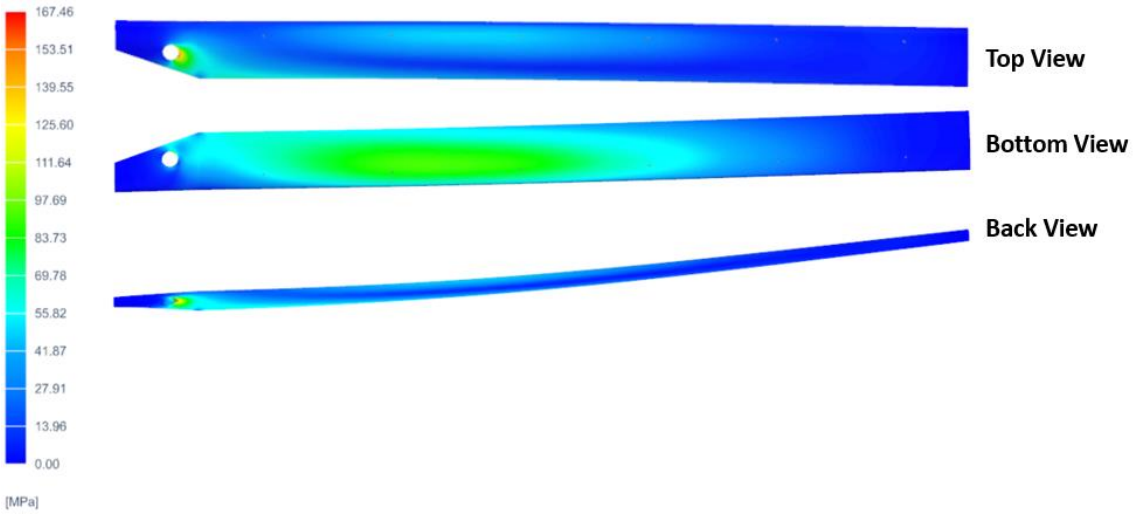

Figure 81: Blade Von-Misses Stress Distribution on Blade

Magnitudes of nodal von-misses stress distribution on blade are increasing compared to 4-degree pitch input since aerodynamic forces and moments on blade is increasing with increasing of angle of attack. This corresponds to more bending moment on blade.

3.3.2. Rotor Parameter Investigation in Blade Flapping Maneuvers

Rotor performs flapping motion with longitudinal cyclic pitch input, lateral cyclic pitch input and with relative flow coming to the rotor disk. Simulation parameters with respect to azimuth angle at each station in flapping motion are investigated in this section. In simulation, blades perform flapping motion in forward to aft or side to side of rotor disk. Therefore, the blade angles are not expected to be same at each azimuth angles in flapping condition. However, blades are performing almost the same angles at the same azimuth angles in pure longitudinal or lateral cyclic pitch inputs, or in constant relative velocity situations. This makes a harmonic motion of blades. This motion is discussed in detail in following subchapters.

- Angle of attack is changing at each azimuth angle and still expected to be less at the tip compared to root since the blade has 6-degrees linear twist. However, this situation can change due to structural flexibility of blades.
- Blade pitch, lead-lag and flap angles vary at all stations during the pilot input entry and steady phases with respect to the azimuth angle. Therefore, aerodynamic forces and moments are varying at all stations during steady and pilot input entry phases. Sample blade angle representations are shown in Figure 82. In Figure 82, longitudinal cyclic pitch input is given to the blade. Therefore, rotor is expected

to perform the motion given in Figure 32. Therefore, the blade flap directions should be as shown in Figure 32 in corresponding azimuth angle.

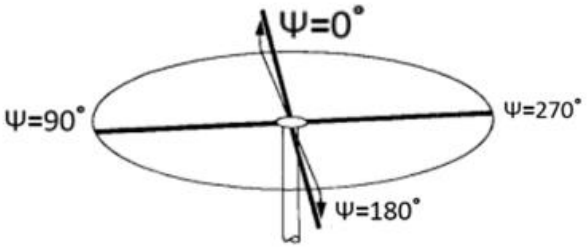

Figure 32 Orientation of TPP with Longitudinal Cyclic Pitch Control [19]

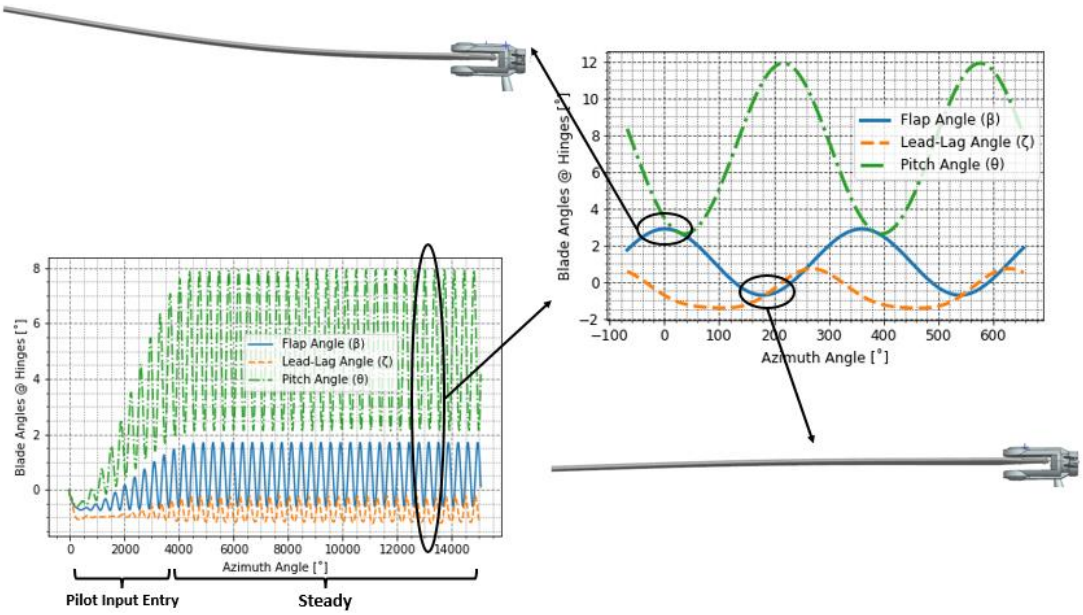

Figure 82: Blade Angle Variations During Pilot Input Entry and Steady Phases for Longitudinal Cyclic input

It is shown in Figure 82 that the blade is flapping up near 0 degree and flapping down near 180 degrees. Therefore, rotor is tilting forward to aft direction.

- As in hover flight, aerodynamic forces should increase from blade root to tip since linear velocity at each section on blade is increasing from root to tip.
- Lead-lag oscillation of blade can be more visible compared to hover flight due Coriolis effect in flapping motion.

3.3.2.1. Investigation of longitudinal Cyclic Pitch Input

In this simulation, longitudinal cyclic pitch input together with collective pitch input is given to rotor blade. The pitch angle of blade is varying according to the equation (18).

(18) $\theta = \theta_0 + \theta_{1c}\cos\psi + \theta_{1s}\sin\psi + \theta_{2c}\cos\psi + \theta_{2s}\sin\psi + \cdots$

Therefore, the parameters in the equation and actuator piston displacements in the model are given as below,

(19) $\theta_0 = 5.0$ (5-degree collective pitch input)
(20) $\theta_{1c} = 5.0$ (5-degree longitudinal cyclic pitch input)
(21) $\theta_{1s} = 0$ (0-degree lateral cyclic pitch input)

$Actuator\ Piston\ 1 = 14mm$ in -Z Direction in Global Axis

$Actuator\ Piston\ 2 = 2mm$ in +Z Direction in Global Axis

$Actuator\ Piston\ 3 = 14mm$ in -Z Direction in Global Axis

Pitch angle variation of Simcenter 3D rotor model simulation and analytical calculations using the equation (18) are compared in Figure 83. Since θ_0, θ_{1c}, and θ_{1s} are kinematic variables, the rotor model is solved in a vacuum situation which is aerodynamic forces and moments are neglected.

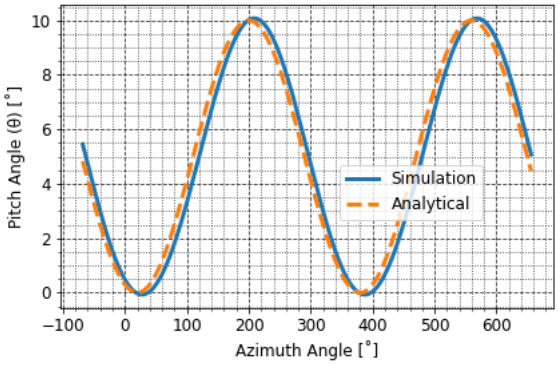

Figure 83: Comparison of Blade Pitch Angles Generated from Analytical Calculation and Simulation

The analytical calculation and simulation show great correlation. The simulation results under the aerodynamic forces and moments effect are shown in Figure 84 to Figure 91. Pilot input entry part is not investigated in this part, since it is already discussed. Parameters are investigated in some 720-degree azimuth angle range in steady part.

Sectional velocities of blade are changing smoothly with azimuth angle as shown in Figure 84 since there is no rotor forward velocity implementation. Reason of smooth changes is the Coriolis effect which is created by flapping motion. The Coriolis effect creates lead-lag motion. When lead-lag motion given in Figure 85 and velocity of blade station 6 given in Figure 84 are traced, it can be seen that the parameters are decreasing

or increasing together at the same azimuth angle. Variations of blade station velocities are more visible in relative velocity implementation. (See chapter 3.3.2.2)

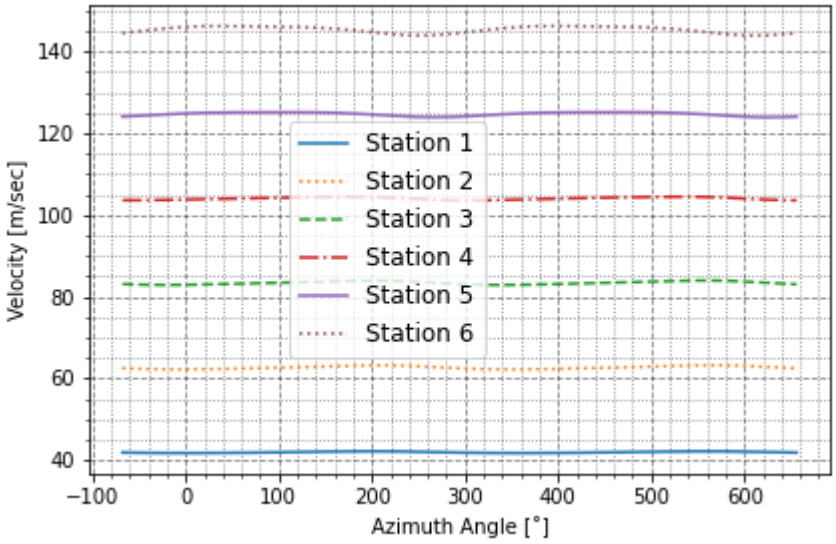

Figure 84: Velocity of Blade Sections

In Figure 85, blade is started to perform flapping up from 180-degree to 360-degree azimuth angle. At around 180-degree azimuth, the pitch angle of the blade is highest and it starts to decrease while blade is performing flapping up. At around 360-degrees, the pitch angle of blade is at its lowest value. Therefore, the lift created by the wing is around its lowest values and this makes the blade flapping down till around 540-degree azimuth angle. While the blade is going to flapping down, the pitch angle of blade is increasing. This creates highest lift of blade. Therefore, the blade again started to create flapping up. While the blade is performing the flapping up and down motion, cg of the blade getting closer and far from the rotation axis of rotor disk. This creates Coriolis effect and this Coriolis effect creates lead-lag motion.

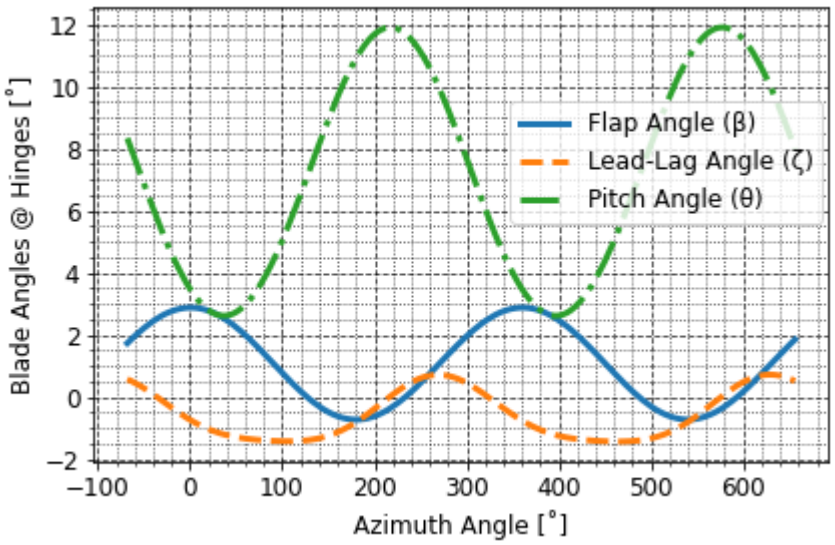

Figure 85: Pitch, Lead-Lag and Flap Angles of Blade

Angle of attack variation of each section of blade in longitudinal cyclic pitch input case is shown in Figure 86.

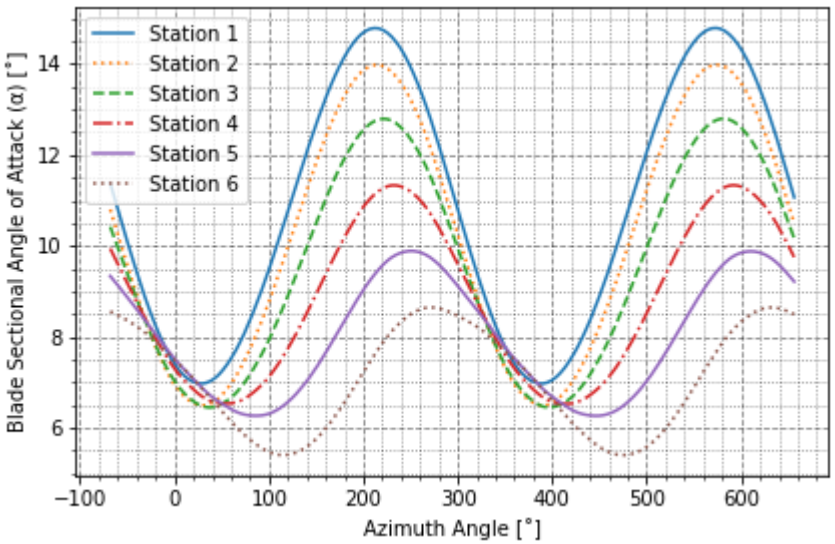

Figure 86: Angle of Attack

According to pitch angle variation, the angle of attack of blades at each section are also changing parallel to the pitch angle as shown in Figure 86.

Aerodynamic force component in Z direction in each station is shown in Figure 87 for longitudinal cyclic pitch inputs.

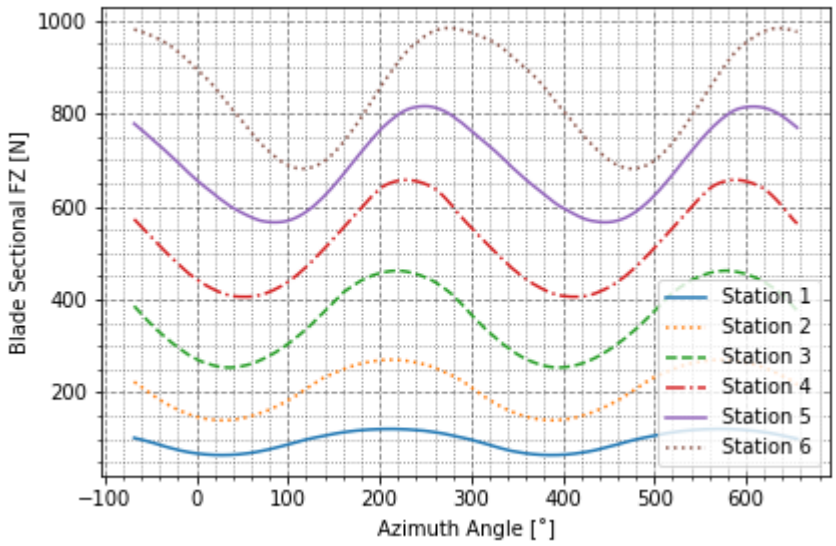

Figure 87: Aerodynamic Force Component in Z direction in Rotating Blade Axis

Horizontal aerodynamic forces and pitching moments given in Figure 88 and Figure 89 are also changing according to the blade sectional angle of attack. While angle of attack is increasing, the lift and drag forces and pitching moments are increasing.

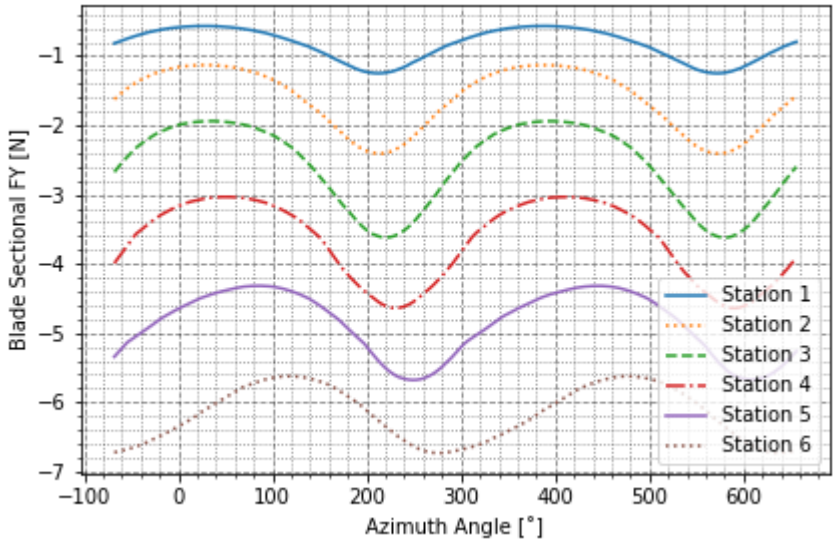

Figure 88: Aerodynamic Force Component in Y direction in Rotating Blade Axis

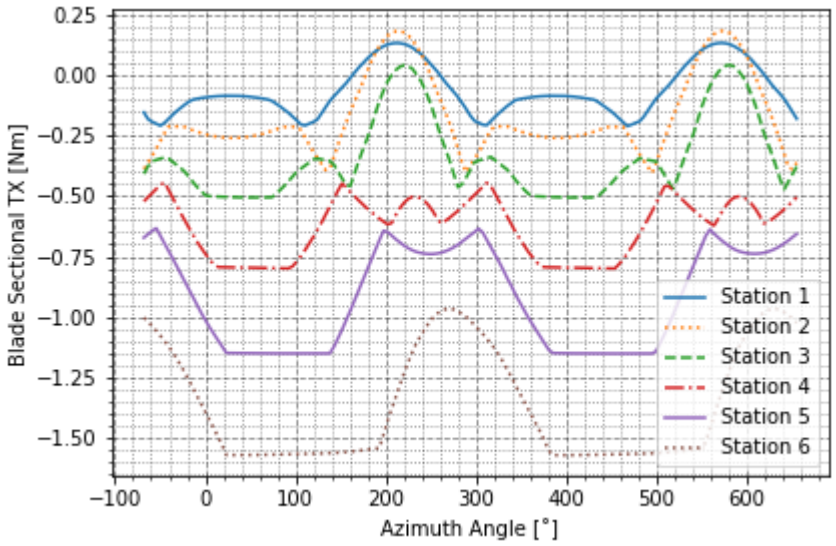

Figure 89: Aerodynamic Moment Component in X direction in Rotating Blade Axis

Bending moment observed on rotor blade system space connection point is investigated in Figure 90 for longitudinal pitch input.

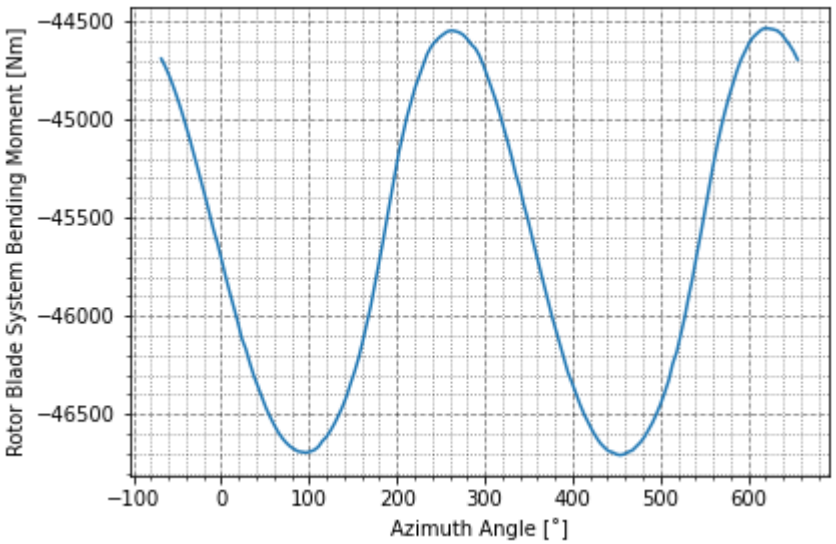

Figure 90: Bending Moment in Y Direction in Rotor Blade System Space Connection Point in Rotating Blade Axis for Longitudinal Cyclic Pitch Input

Amplitude of bending moment variation was approximately 20 Nm in hover flight but here is approximately 2000 Nm due to flapping.

Stress distribution on blade and blade shape during flapping up and down phases are given in Figure 91 and Figure 92 respectively.

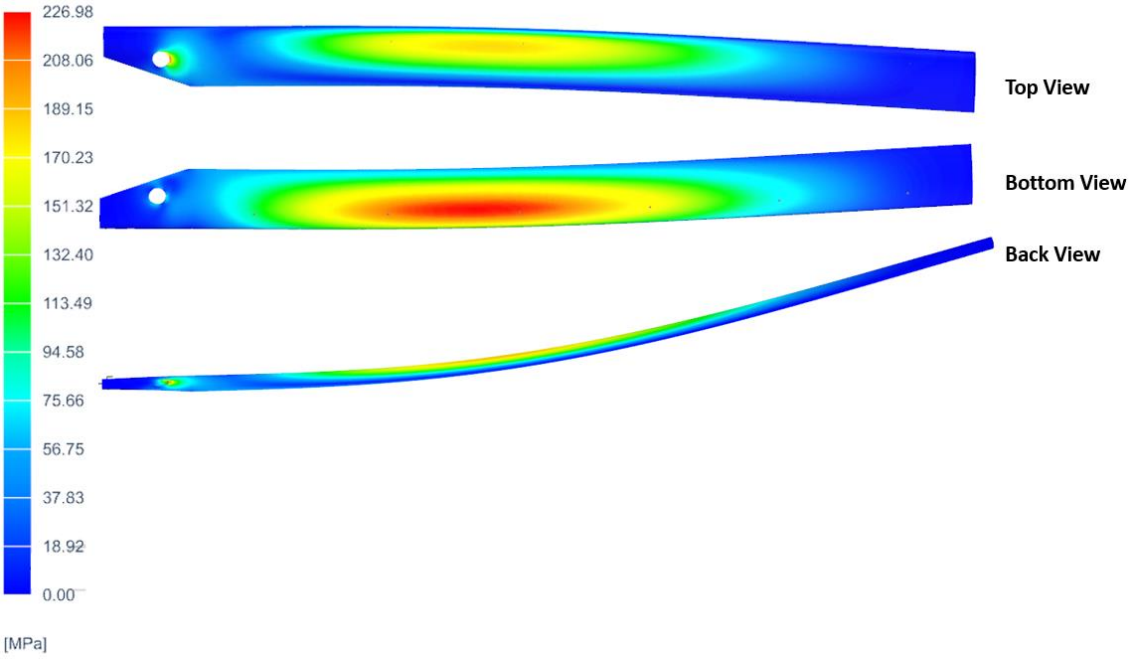

Figure 91: Von-Misses Stress Distribution on Blade for Flapping Up

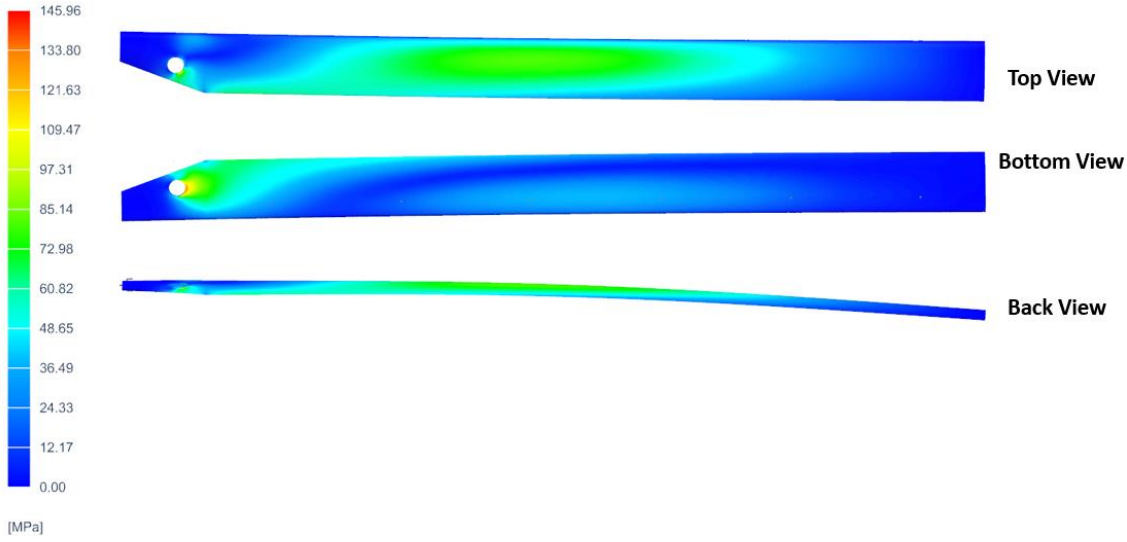

Figure 92: Von-Misses Stress Distribution on Blade for Fapping Down

Magnitudes of nodal von-misses stress distribution on blade are more in bottom of blade for flapping up and more in top of blade in flapping down because of majority of tensile stress on blade. Magnitudes of stress distribution on blade is more in flapping up motion since bending on blade is more in flapping up motion due to aerodynamic forces and moments.

3.3.2.2. Investigation of Forward Flight

In this simulation, helicopter main rotor model is put into a V_∞= 80 m/s airflow coming from 180-degree azimuth angle to 0-degree azimuth angle as shown in Figure 54. Same pilot inputs given in chapter 3.3.2.1 are applied in this section.

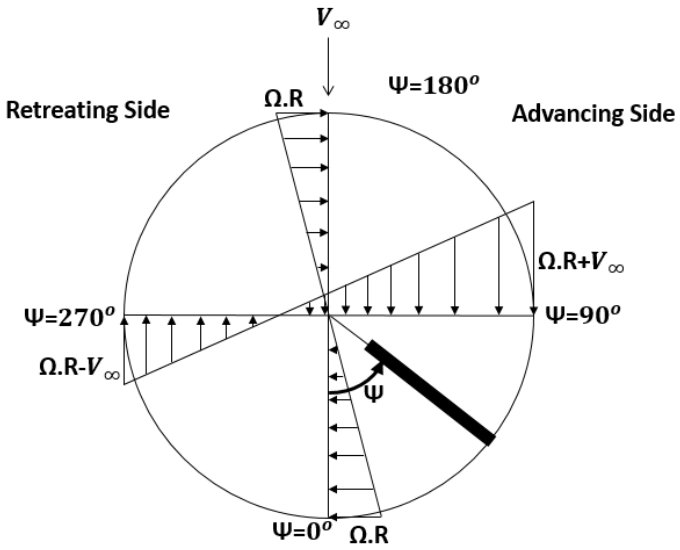

Figure 54: Airflow Distribution on a Rotor Blade in Forward Flight

The simulation results under the aerodynamic forces and moments effect are shown in Figure 93 to Figure 100. Parameters are investigated in some 720-degree azimuth angle range in steady part again.

Velocities on blade sections are varying in advancing side and retreating side due to forward velocity as shown in Figure 93. Since the rotor is rotating in counter clockwise direction, blade velocity is increasing in right hand side of rotor disk whereas it is decreasing in left hand side.

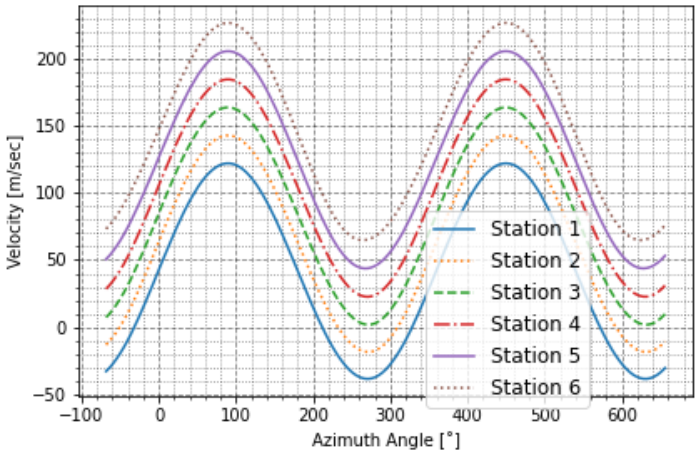

Figure 93: Sectional Velocities of Blade

Due to forward velocity, the lift is increasing on blade in advancing side. This concludes as the flap angle of blade is increasing in forward part of rotor disk as shown in Figure 94. In contrast, blade velocity is decreasing in retreating side of blade. This concludes as the flap angle of blade is decreasing in rear part of blade as shown in Figure 94.

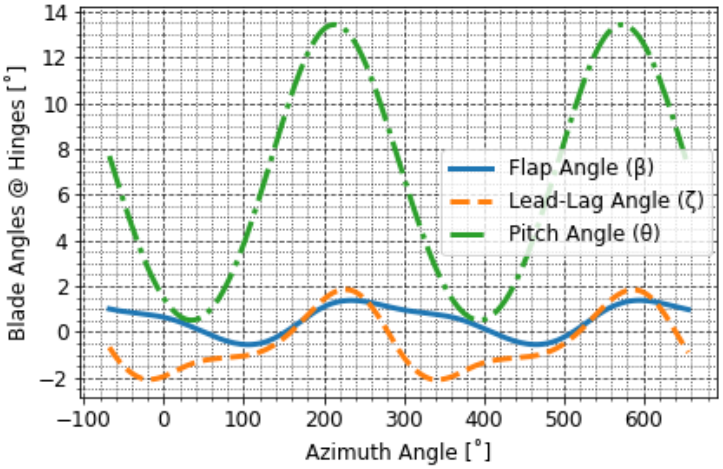

Figure 94: Pitch, Lead-Lag and Flap Angles of Blade

In forward flight, since completely different aerodynamic loads in advancing and retreating sides are observed, the blade is experiencing too much bending at each section. Therefore, flapping on blade should also be traced in each section of blade due to flexibility. Figure 95 shows flap angles of blade stations during flapping in each azimuth angle. Shapes of blade in flapping up and down are shown in Figure 101 and Figure 102 respectively.

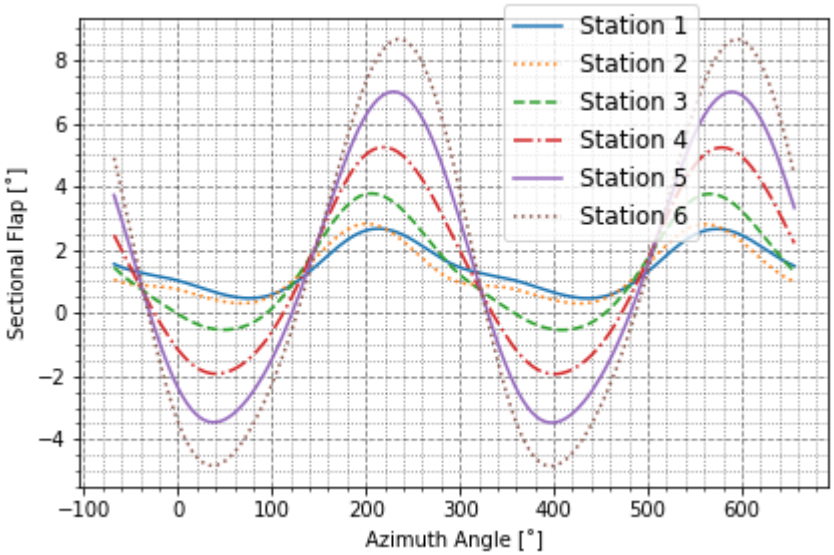

Figure 95: Displacement of Blade Stations in Global Z Direction

Angle of attack of blade is increasing at each azimuth angle and at each section of blade due to forward velocity as shown in Figure 96.

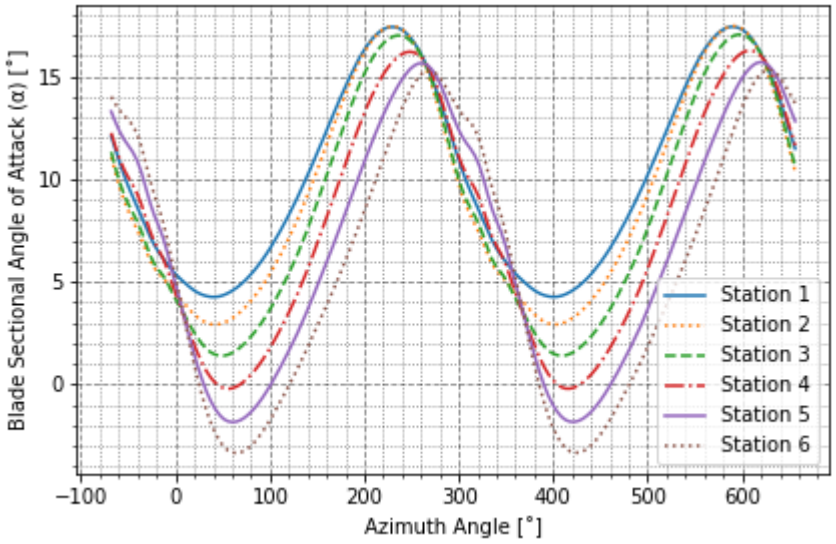

Figure 96: Angle of Attack

Elasticity is affecting the sectional FZ dramatically. While angle of attack is increasing, the lift and drag forces and pitching moments are increasing as shown in Figure 97, Figure 98, and Figure 99. Most amount of the FZ force is coming from advancing side which is around 0–180-degree azimuth angle range.

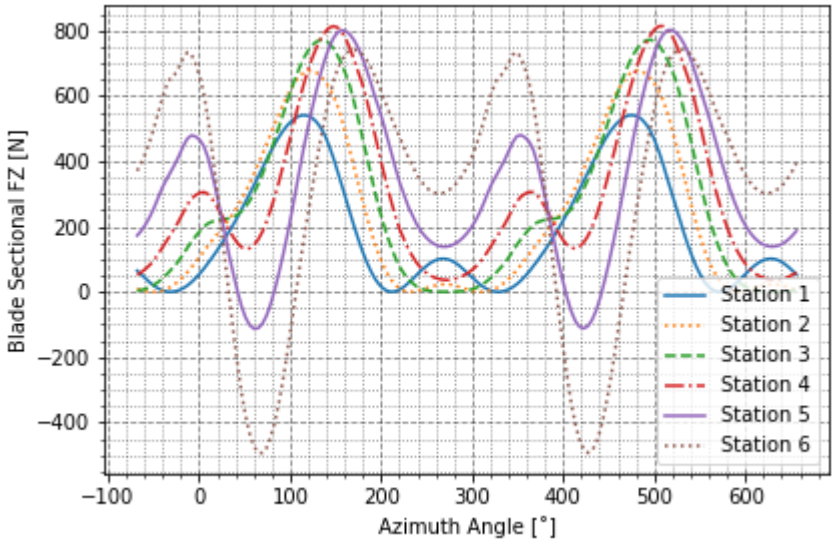

Figure 97: Aerodynamic Force Component in Z direction in Rotating Blade Axis

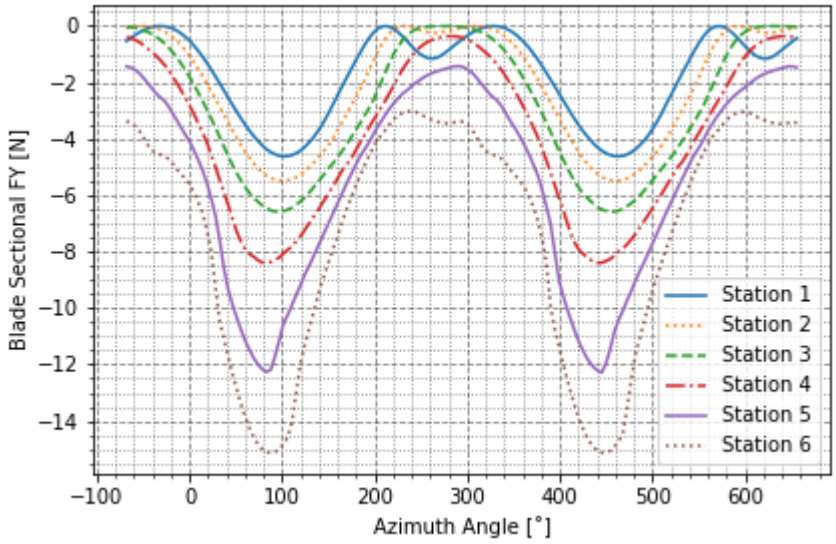

Figure 98: Aerodynamic Force Component in Y direction in Rotating Blade Axis

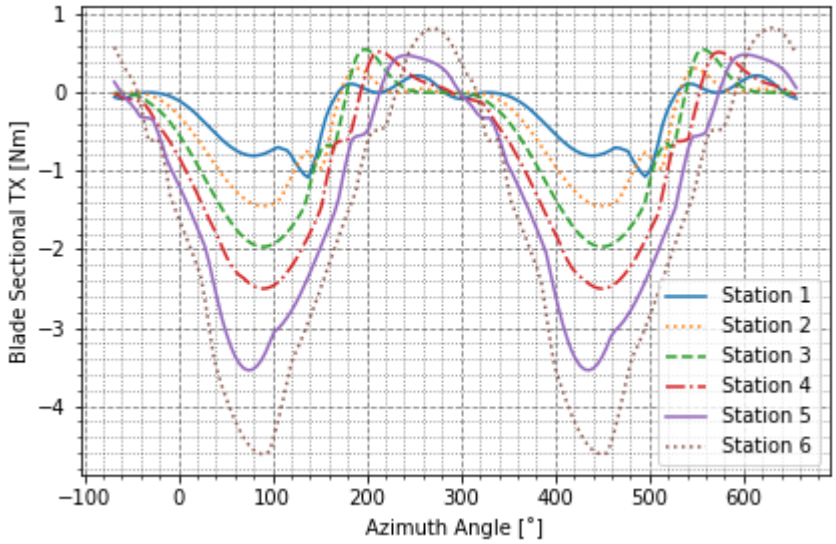

Figure 99: Aerodynamic Moment Component in X direction in Rotating Blade Axis

Amplitude of bending moment variation was approximately 20 Nm in hover flight and approximately 2000 Nm in pure longitudinal cyclic input. When the forward flight is included in the simulation, the aerodynamic forces are increases. This corresponds to approximately 4000 Nm bending moment variation in 80m/s forward speed condition.

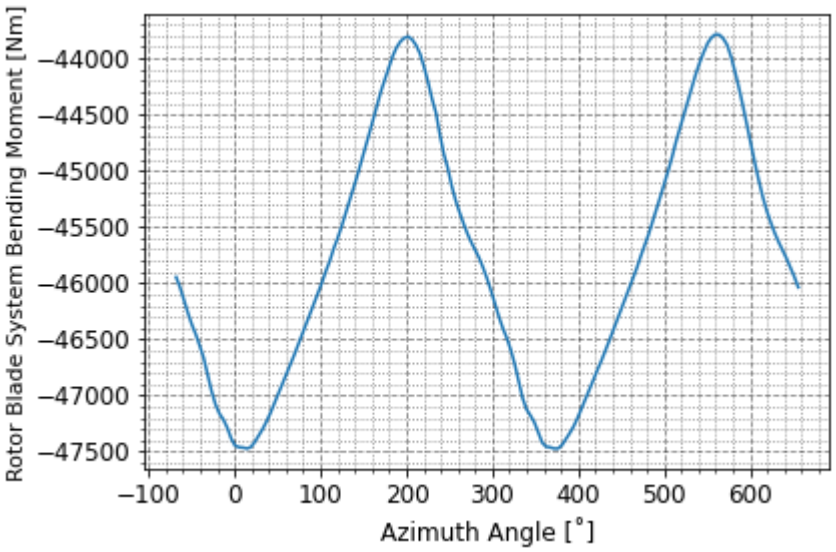

Figure 100: Rotor Blade System Space Connection Point Bending Moment in Y direction in Rotating Blade Axis for Forward Velocity and Longitudinal Cyclic Pitch Inputs

Von-Misses stress distribution on blade and blade shape during flapping up and down phases are given in Figure 101 and Figure 102 respectively.

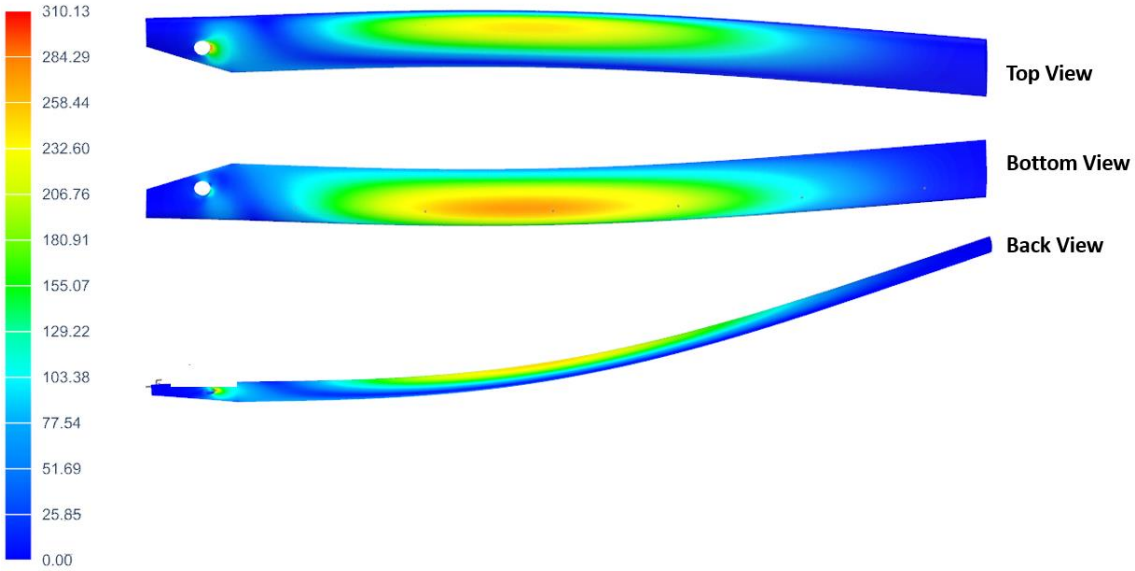

Figure 101: Blade Von-Misses Stress Distribution for Flapping Up

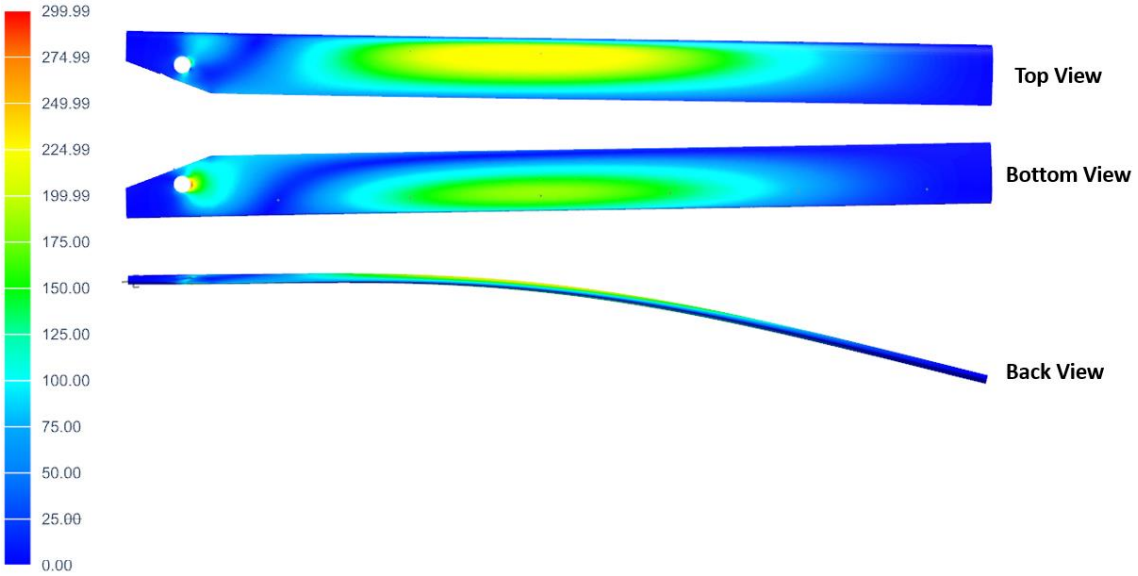

Figure 102: Blade Von-Misses Stress Distribution for Fapping Down

Magnitudes of nodal von-misses stress distribution on blade are more in bottom of blade for flapping up and more in top of blade in flapping down as in chapter 3.3.2.1. The magnitudes of stress distribution on blade and stressed area on blade are increased when forward velocity is come in to the case as expected.

4. COMPARISON OF DIFFERENT ROTOR DESIGNS

In this chapter, different rotor design solutions are compared. In this thesis, the 3D rotor CAD model is created with Simcenter 3D NX and with pointwise data output of airfoil shape in XFOIL. In the designing different rotor models, the rotor hub mechanism is kept the same but the blade design is varying according to the chord length, wing span, twist distribution, airfoil shape and material of the blade. The chord length, twist distribution, wing span and airfoil shape are directly affecting the aerodynamic loads. But material is not directly affecting. Since blade elasticity is changing due to the material type, elastic deformation can be observed on blade sections. Due to the elastic deformation of the blade, angle of attack, flapping angle, lag angle and freestream velocity of blade sections can change. Due to these changings, aerodynamic loads can be changed in each section. Therefore, blade elasticity is also important parameter for aerodynamic loads. In addition, blade material property is directly affecting the inertial forces occurred on blade. Inertial forces have also effects on blade motions. Therefore, change in blade motions due to material type can affect the aerodynamic loads. In this part, the rotor behaviors under these design parameters are investigated.

Rotor performances are also compared using thrust coefficient and solidity of rotor disk.

The rotor thrust coefficient is a dimensionless quantity used in analyses and design of a helicopter rotor. The quantity shows rotor thrust performance characteristics. The Thrust coefficient equation is given in equation (22):

$$C_T = \frac{T}{\rho A(\Omega R)^2} \tag{22}$$

Where T is thrust created by rotor disk, A is the rotor disk area, ρ is density of the air, Ω is the rotor rotstional velocity in radians per second, and R is the ratius of rotor disk.

In analyses and design of a helicopter rotor, the rotor solidity is also a used quantity. The solidity is also given as:

$$\sigma = \frac{Nc}{\pi R} \tag{23}$$

Where N is number of blades in rotor, c is the chord length of rotor blade, and R is again the radius of blade.

In order to have more accurate data, the blade is divided into 8 stations in this section. The aerodynamic forces and moments, pitch link loads, lead-lag damper loads, and rotor angular parameters are investigated and compared for different designs.

4.1. Effect of Different Materials

In this section, applications of different materials to rotor blades will be investigated. As discussed in chapter 2.6, the rotor blade is generated as one single isotropic material in this thesis since the concept of this thesis is not detail modelling of rotor blade. Pilot inputs discussed in Chapter 3.3.2.1 and 30 m/s flow to the rotor disk are performed with the rotor model for the investigation of different rotor designs. Used materials are listed in Table 17. These materials are randomly selected from default material list of Simcenter 3D.

Table 17: Used Materials in Investigation of Different Rotor Designs

Design #	Material Name	Category	Sub-Category	Mass Density (kg/mm^3)	Youngs Modulus (kPa)	Poisson's Ratio	Yield Strength (kPa)
Design 1	AISI_410_SS	Metal	Stainless Steel	7.73377e-06	219360000	0.27	483100
Design 2	Aluminum_2014	Metal	Aluminum Alloy	2.794e-06	73119000	0.33	393700
Design 3	Tungsten	Metal	Tungsten Alloy	1.93e-05	400000000	0.28	750000
Design 4	Titanium_Alloy	Metal	Titanium Alloy	4.454e-06	117270000	0.33	761500
Design 5	Aluminum_A356	Metal	Aluminum Alloy	2.67e-06	70000000	0.33	229000
Design 6	AISI_Steel_1005	Metal	Carbon Steel	7.872e-06	200000000	0.25	226000
Design 7	Aluminum_6061	Metal	Aluminum Alloy	2.711e-06	68980000	0.33	241700
Design 8	Aluminum_5086	Metal	Aluminum Alloy	2.66e-06	72000000	0.33	217000

In addition, other rotor design parameters which are kept constant are given in Table 18 and simulation inputs are given in Table 19.

Table 18: Other Rotor Design Parameters in the Study

Parameter Type	Parameter
Number of Blade Stations	8
Airfoil Profile	NACA23015
Chord Length (m)	0.120
Rotor Radius (m)	2
Linear Twist (˚)	4 at the root, -2 at the tip

Table 19: Simulation Inputs

Input Type	Input
Rotational Velocity (rad/sec)	80
Forward Velocity (m/s)	30
Actuator 1 Displacement	-14
Actuator 2 Displacement	2
Actuator 3 Displacement	-14

Total Lift/drag loads, maximum and minimum pitch link and lead-lag damper loads, and rotor system bending moment values given at a point discussed in Chapter 3.1.3 for each design are given in Table 20. Rotor system bending moment load is given with respect to the rotating hub axis system. In pitch link and damper loads, maximum means tension load whereas compression is minimum load.

Table 20: Loads on Rotor System for Different Material Designs

Designs	Lift (N)	Drag (N)	Rotor System Bending Moment (N/m)	Pitch Link Max (N)	Pitch Link Min (N)	Damper Max (N)	Damper Min (N)
Design 1	1056	-14	127449	5189	-5774	17572	-16449
Design 2	1123	-14	45952	6165	-5285	17688	-16794
Design 3	1085	-14	318159	5324	-6038	18435	-16937
Design 4	1068	-14	73367	5475	-5468	18006	-17140
Design 5	1134	-14	43907	6244	-5279	17596	-16758
Design 6	1047	-14	129740	5269	-5690	18065	-16812
Design 7	1140	-14	44581	6409	-5215	17732	-16851
Design 8	1124	-14	43735	6030	-5310	17465	-16562

In Table 20, rotor loads for 8 different material designs of blades are given. Lift and Drag loads are calculated using the sum average of lift and drag load distribution in 360-degree azimuth angle range on blade. Almost %9 difference is observed for these very different 8 materials. Minimum lift is generated as 1056N in design 1 whereas maximum is generated as 1140N in design 7. Material used in design 1 is almost 3 times bulky and stiff material than design 7. This makes design 7 more flexible. The flexibility of designs can also be investigated in Figure 103 and Figure 104 below.

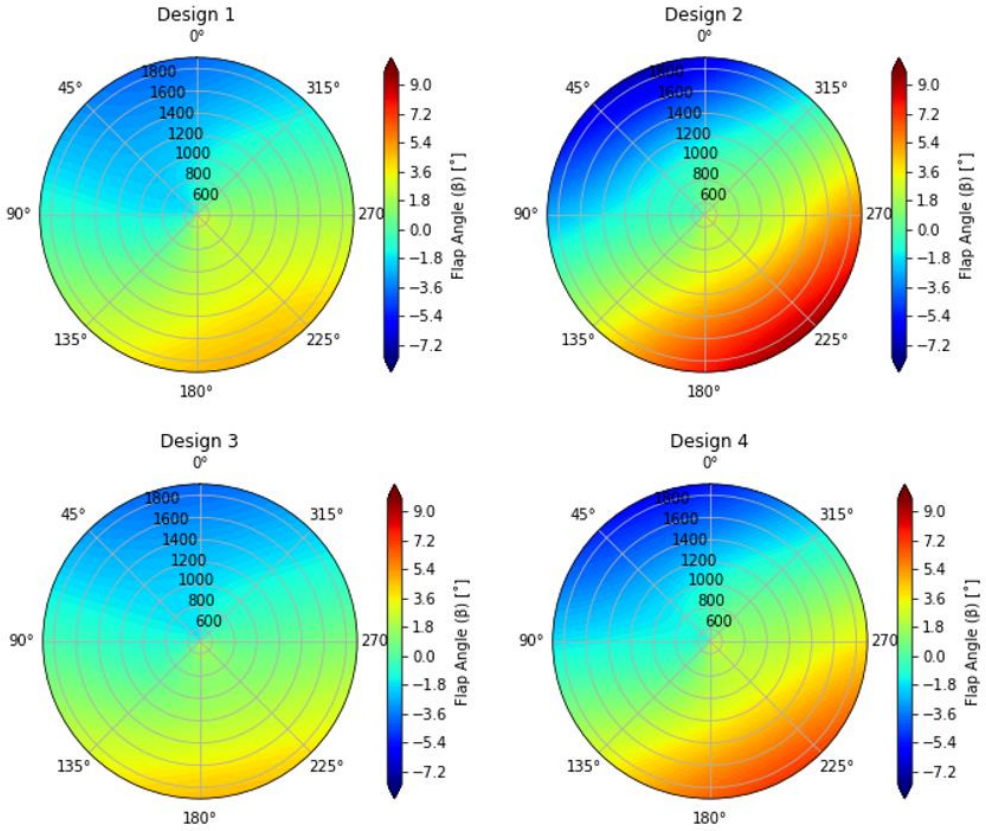

Figure 103: Flap Angle Contours of Design Numbers 1 and 4

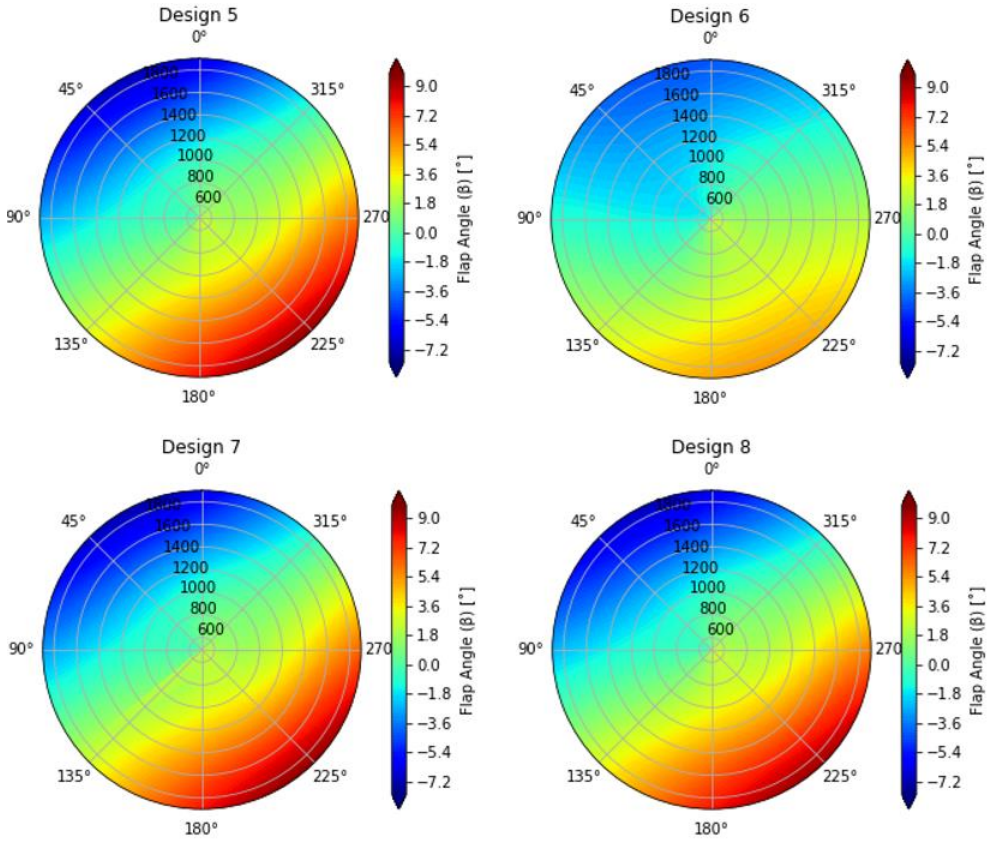

Figure 104: Flap Angle Contours of Design Numbers 5 and 8

Flap angle contours for each design can be compared in order to look at flexibility of blade since all 8 designs are simulated with the same maneuver inputs. For design 1 and 7, flap angle range of design 7 is wider than the design 1 since design 1 is more stiff material. Angle of attack contours are also given in Figure 105 and Figure 106 below. Blade angle of attack values are less in the advancing side because blade starts to perform flapping up motion in advancing side due to increasing of blade velocity with relative velocity. This flapping up motion can be seen in flap angle contour of designs. In design 7 compared to design 1 the angle of attack variation through the span of the wing is more visible due to flexibility.

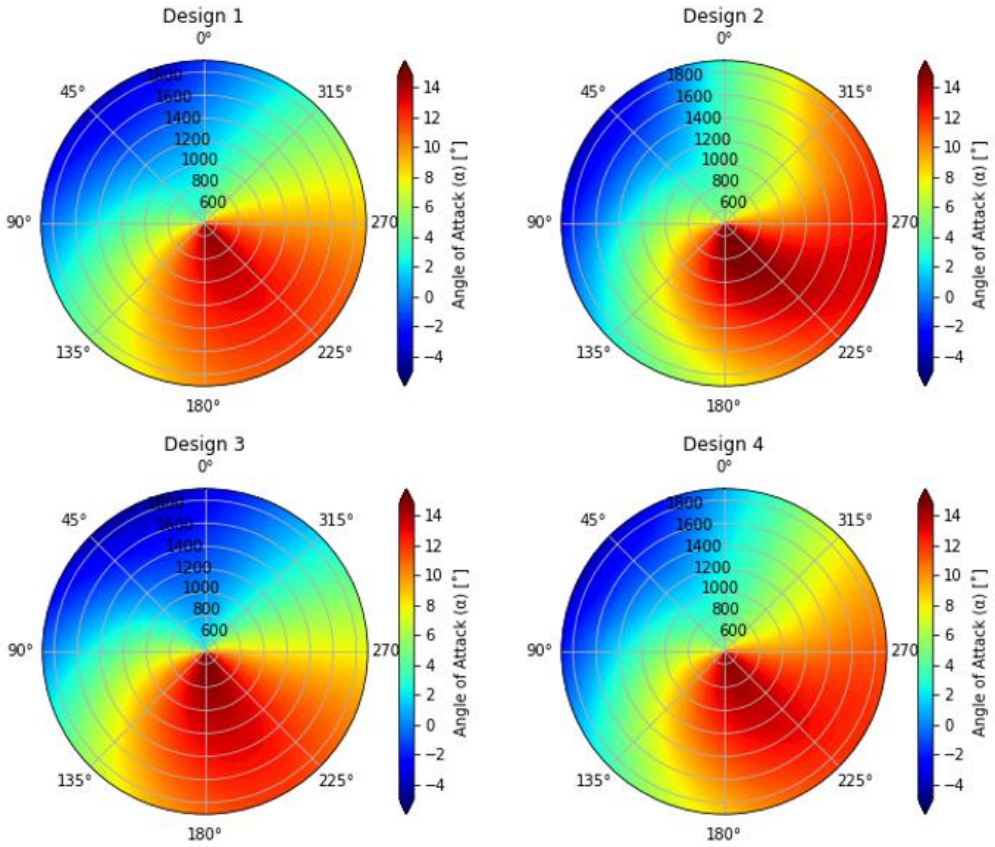

Figure 105: Angle of Attack Contours of Different Material Designs 1 - 4

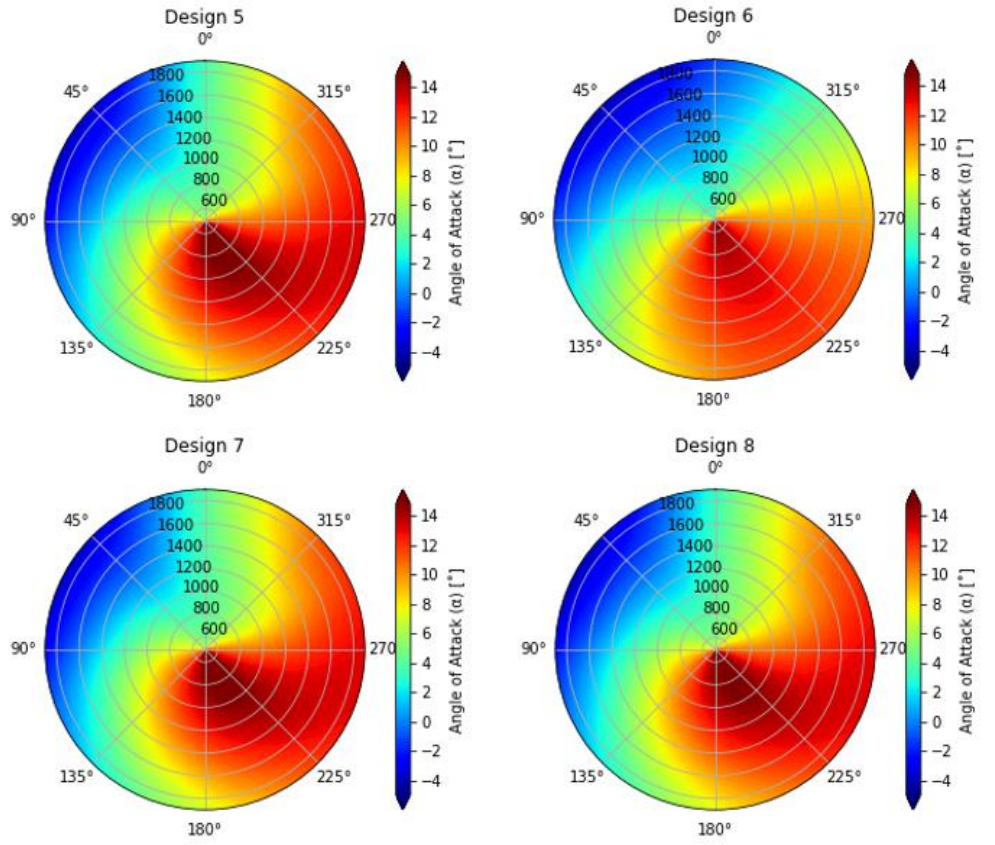

Figure 106: Angle of Attack Contours of Different Material Designs 5 - 8

Angle of attack difference between root and tip part of blade is more visible in design 7 contour compared to design 1 due to more structural twisting and more flapping motion in Figure 105 and Figure 106. As a conclusion, material selection, which are investigated in this thesis, are manipulating the rotor major aerodynamic loads since structural flexibility is varying the flap and angle of attack ranges. Total lift and drag loads are differing for each configuration. However, bending moment observed on rotor system is dramatically increasing for heavy materials due to inertial forces. Since hinges are main load carrying members of blade, inertial loads created by blade do not have significant effect on the loads of pitch links and dampers. Therefore, rotor blade harmonics due to aerodynamic forces are main load supplier of pitch link and damper of blades. Due to the harmonics of blade, the maximum and minimum loads on pitch link and damper are very close to each other.

4.2. Effect of c and R for Same Blade Solidity

In this section, blade will be designed for different values of chord length and blade radius while keeping blade solidity and other rotor design parameters are the same. The aerodynamic loads and structural loads will be discussed. Used c and R values for the same blade solidity are listed in Table 21. The specified solidity calculation is given below.

(24) $$\sigma = \frac{Nc}{\pi R} = \frac{4*0.12}{\pi*2} = 0.0764$$

(25) $$\frac{c}{R} = 0.0764 * \frac{\pi}{N} = 0.06$$

The rate of c/R is kept constant at 0.06 value. In summary, the design parameters and simulation inputs are given in Table 21, Table 22, and Table 23.

Table 21: Chord Length and Blade Span

Designs	Chord Length (m)	Blade Span (m)
Design 1	0.102	1.7
Design 2	0.114	1.9
Design 3	0.126	2.1
Design 4	0.138	2.3

Table 22: Other Parameters used in Rotor Design in the Study

Parameter Type	Parameter
Number of Blade Stations	8
Airfoil Profile	NACA23015
Chord Length (m)	0.120
Rotor Radius (m)	2
Linear Twist (˚)	4 at the root, -2 at the tip
Material	Aluminum_2014

Table 23: Simulation Inputs

Input Type	Input
Rotational Velocity (rad/sec)	80
Forward Velocity (m/s)	30
Actuator 1 Displacement	-14
Actuator 2 Displacement	2
Actuator 3 Displacement	-14

Material properties of "Aluminum_2014" are given in Table 17. For the constant solidity, the rotor simulation results are given in Figure 107.

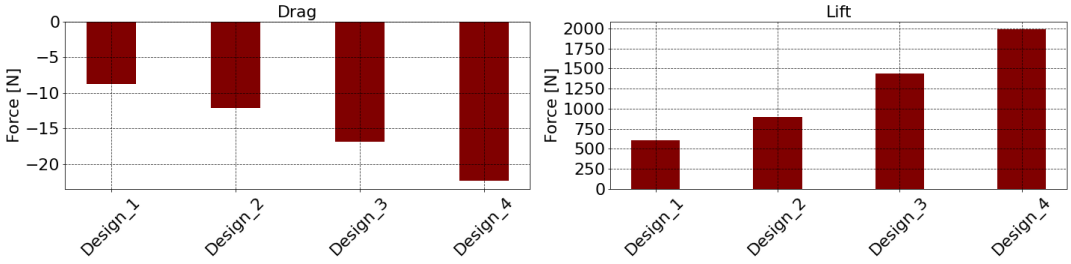

Figure 107: Total Lift and Drag Forces Created by Each Designs

Since the lifting surface of rotor disk is increasing with increasing chord and wing span, the total lift and drag created by blade are increasing for constant blade solidity as shown in Figure 107. Changing in other rotor loads are also shown in Table 24.

Table 24: Loads on Rotor System for Different Geometric Designs

Designs	Lift (N)	Drag (N)	Rotor System Bending Moment (N/m)	Pitch Link Max (N)	Pitch Link Min (N)	Damper Max (N)	Damper Min (N)
Design 1	609	-8	23130	3600	-5343	9132	-6913
Design 2	892	-12	36619	5027	-5333	16344	-13100
Design 3	1433	-16	55190	7855	-5064	19489	-17820
Design 4	1984	-22	80043	10675	-6468	21545	-19557

Rotor system bending moment is increasing with increasing wing span and chord length since blade aerodynamic loads, blade mass and inertial forces due to mass are increasing. Due to increasing aerodynamic and inertial forces, pitch link and damper loads are also increasing.

4.3. Effect of Twist Distribution

In this part, effect of linear twist distribution to blade sectional lift loads are investigated in hover maneuver with same actuator inputs discussed in Chapter 3.3.1.1. The blade is designed with the linear twist distribution. Since twist angle gives the angle difference between root and tip of the blade, the root and tip incidence values of each design are stated in Table 25. The twist distributions are selected for +9 and -9 incidence angle range in order to show the effect of twist distribution to the blade aerodynamic loads. In Addition, one of the blade designs, which is design 46, is not created with a twist distribution in order to show the comparison between aerodynamic loads of not twisted and twisted blades. The incidence angles of this design in root and tip are selected as (9,9) in order to show also the effect of high incidence angle.

Table 25: Twist Angles of Designs

Designs	Root Incidence (˚)	Tip Incidence (˚)	Designs	Root Incidence (˚)	Tip Incidence (˚)	Designs	Root Incidence (˚)	Tip Incidence (˚)
Design 1	0	-9	Design 17	6	-2	Design 33	5	-1
Design 2	1	-8	Design 18	7	-1	Design 34	6	0
Design 3	2	-7	Design 19	8	0	Design 35	0	-5
Design 4	3	-6	Design 20	0	-7	Design 36	1	-4
Design 5	4	-5	Design 21	1	-6	Design 37	2	-3
Design 6	5	-4	Design 22	2	-5	Design 38	3	-2
Design 7	6	-3	Design 23	3	-4	Design 39	4	-1
Design 8	7	-2	Design 24	4	-3	Design 40	5	0
Design 9	8	-1	Design 25	5	-2	Design 41	0	-4
Design 10	9	0	Design 26	6	-1	Design 42	1	-3
Design 11	0	-8	Design 27	7	0	Design 43	2	-2
Design 12	1	-7	Design 28	0	-6	Design 44	3	-1
Design 13	2	-6	Design 29	1	-5	Design 45	4	0
Design 14	3	-5	Design 30	2	-4	Design 46	9	9
Design 15	4	-4	Design 31	3	-3	Design 47	9	5
Design 16	5	-3	Design 32	4	-2			

Blade lift distributions are shown in Figure 108. The blade is divided into 8 aerodynamic stations as discussed. Therefore, lifts are calculated using area specifications of 8 distinct stations in order to create lines in Figure 108.

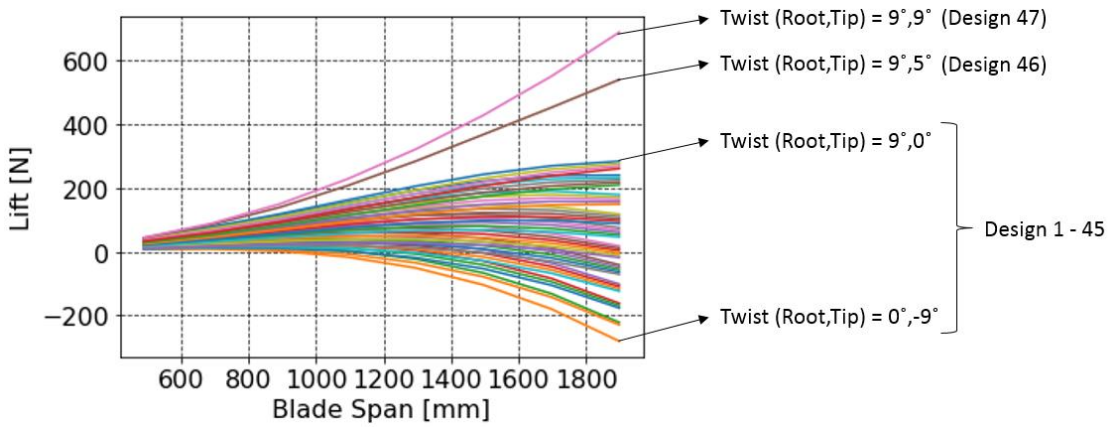

Figure 108: Sectional Lift Forces for Different Twist Distribution Designs

Each line in Figure 108 corresponds to a design specified in Table 25. The line in the top is created with (9,9) degree incidence angle (design 47). The line in the one lower of top line (design 46) is created with twist angle but overall incidence angle is kept high. Other lines are showing the Design numbers 1-45. Since no twist angle is given in design 47, the angle of attack values of blade sections has almost no change but the little change can be observed due to structural flexibility as shown in figure Figure 109. The pitch angle given to the blade is around 4.4 degree and blade incidence at each section is designed as 9 degrees. Therefore, the blade angle of attack is calculated as around 13.4 degrees. While

moving to blade tip from root, aerodynamic loads are increasing and the incidence angle of blade is increasing due to structural flexibility.

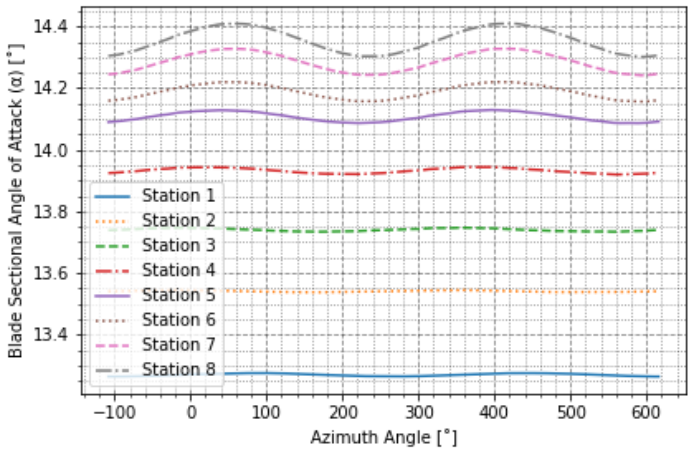

Figure 109: Sectional Angle of Attack for Non-Twisted Blade

The aerodynamic loads are increasing with square of velocity. This makes the parabolic increasing of aerodynamic loads in design 47. Design 46 is also close to design 47 since overall blade incidence is still high. For design 1-45, upper lines are created with high incidence angle at the root and not very low incidence angle but low incidence angle at the tip. For example, the incidence angle of 9 at the root and 0 at the tip. The line in the bottom for design 1-45 is then showing and opposite type of twist distribution design. These are the expected results for designs with different twist distributions.

Now, comparison of aerodynamic loads on rigid and elastic blades for different twist distribution designs will be discussed. 4 different twist distribution designs are compared for rigid and elastic blades given in Table 26. Material given in design 2 of Table 17 is used in order to create elastic blades. With this material, 4 different twist distribution designs, given in Table 26, are designed. In addition, rigid blades with these twist distributions are also designed. The designed blades are compared according to the lift generation capabilities given in Figure 110.

Table 26: Twist Angles of Designs

Designs	Root Incidence (˚)	Tip Incidence (˚)	Material
Design 1	9	0	Aluminum 2014 (Design 2 of Table 17)
Design 2	6	-3	Aluminum 2014 (Design 2 of Table 17)
Design 3	9	5	Aluminum 2014 (Design 2 of Table 17)
Design 4	9	9	Aluminum 2014 (Design 2 of Table 17)
Design 5	9	0	Rigid
Design 6	6	-3	Rigid
Design 7	9	5	Rigid
Design 8	9	9	Rigid

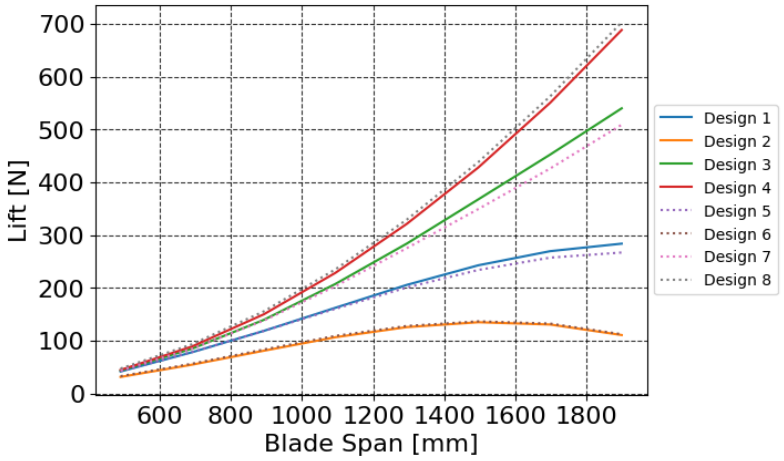

Figure 110: Lift Distribution Comparison of Rigid and Elastic Blades for Different Twist Distribution Design Study

In, Figure 110, solid lines are representing the elastic blades whereas dotted lines are representing the rigid blades. First, looking at the elastic and rigid blade design numbers 4 and 8. In these designs, blades are designed without twist distribution and with high incidence angle. Rigid blade creates high lift compared to elastic since angle of attack of blades are decreasing in elastic blade due to structural twisting and variance of sectional flap under high aerodynamic loads while going to tip from root as shown in the angle of attack comparison given in Figure 111 and Figure 112.

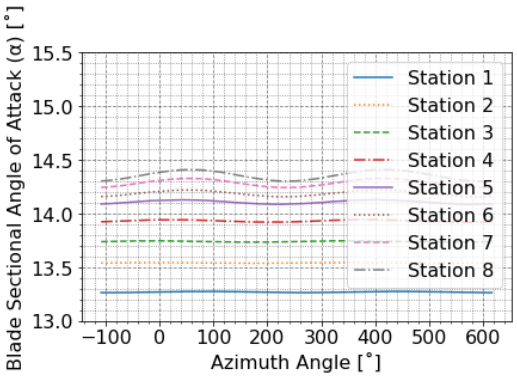

Figure 111: Sectional Angle of Attack for Design 4 (Elastic)

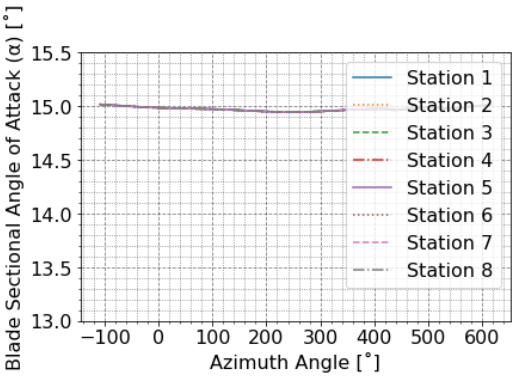

Figure 112: Sectional Angle of Attack for Design 8 (Rigid)

In contrast, for designs 1,3 and 5,7, elastic blades are creating more lift compared to rigid. These blades are generated with twist angle and twist angle is less at the tip. Structural twisting due to material elasticity is increasing the angle of attack while going to tip from root as shown in Figure 113 to Figure 116. Figure 113 is elastic version of Figure 114 and Figure 115 is elastic version of Figure 116.

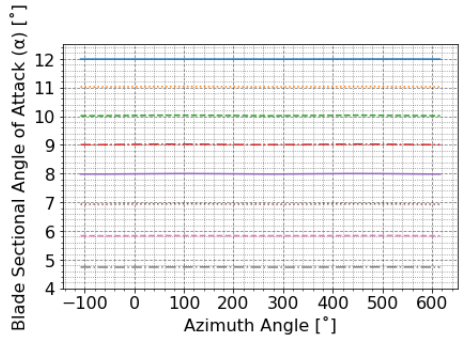

Figure 113: Sectional Angle of Attack for Design 1 (Elastic)

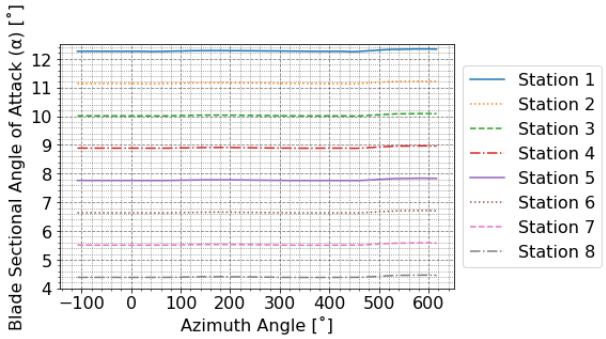

Figure 114: Sectional Angle of Attack for Design 5 (Rigid)

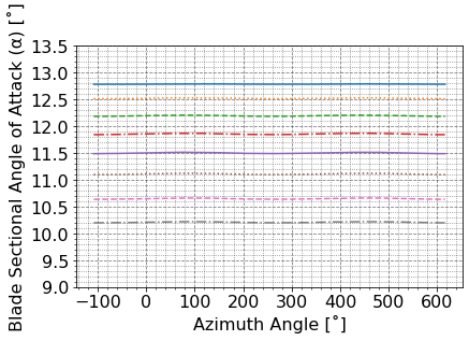

Figure 115: Sectional Angle of Attack for Design 3 (Elastic)

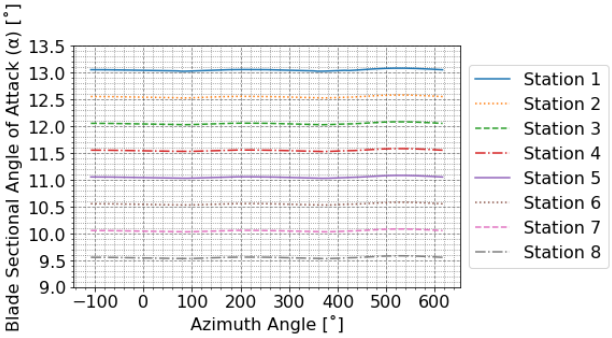

Figure 116: Sectional Angle of Attack for Design 7 (Rigid)

For designs 2 and 6, the blade positive degree at the root and negative incidence at the tip and almost the same lift for rigid and elastic is observed at each section compared to other blade designs. When compared angle of attacks of each design, almost no variance is observed as shown in Figure 117 and Figure 118 due to low twisting du to elasticity.

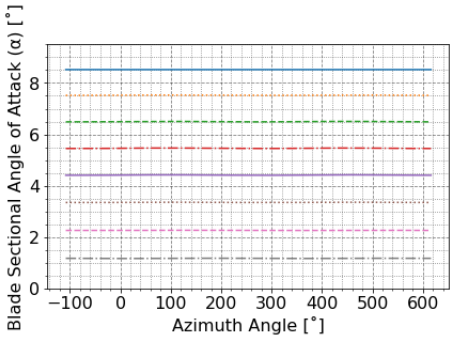

Figure 117: Sectional Angle of Attack for Design 2 (Elastic)

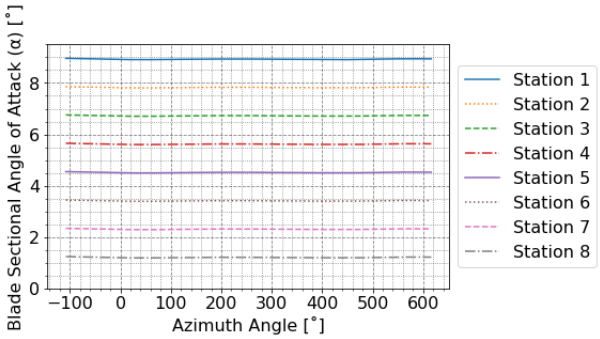

Figure 118: Sectional Angle of Attack for Design 6 (Rigid)

As a conclusion of twisting study, elasticity can affect the lift generation capability of blade in increasing way or decreasing way due to selection of twist distribution.

5. SUMMARY

In this thesis, a helicopter main rotor is modelled in aerodynamic and flexible multibody dynamics approach using Simcenter 3D software. Multibody dynamic simulation of main rotor mechanism is performed and parameters of the blade in some hover and forward flight maneuver conditions are investigated. In addition, FLIGHTLAB is used in order to verify the multibody model created in Simcenter 3D. The process begins with the generation of a kinematic model of the main rotor hub with rigid body components. A PYTHON algorithm is then developed and implemented to perform the tasks outlined in this thesis. The algorithm employs Simcenter 3D NX and XFOIL to create a 3D CAD model of the blades, and Simcenter 3D Motion to link the solid body of the 3D wing to the main rotor hub kinematic model via hinges. Furthermore, an aerodynamic model is applied to the kinematic model using Simcenter 3D Motion. The Simcenter Nastran component of the Simcenter 3D Pre/Post module is also linked to the algorithm to generate a flexible model of the blades. Simulation of the model and postprocess of simulation parameters are also performed with the algorithm. Therefore, a modelling, simulation and postprocess tool has been developed in this thesis.

In the literature, there exists a vast number of studies on main rotor models for helicopters. The primary focus of these studies is on the analysis and simulation of these models, which are often performed using commercial tools such as CAMRAD II, FLIGHTLAB, DYMORE, and MSC ADAMS. This thesis, however, employs the use of Simcenter 3D for the generation and simulation of a main rotor model. The use of Simcenter 3D in this context is unique, as there are few studies in the literature that have utilized this tool for the generation of rotor models.

Simcenter 3D is a multibody kinematic and dynamic analysis tool that offers similar capabilities to that of MSC ADAMS. Additionally, various types of main rotor exist, and all rotor types have been heavily researched in the literature to date. The model generated in this thesis is an articulated rotor model with all three types of hinges. The main rotor hub components are modeled as rigid, while the blades are modeled as flexible. Furthermore, the model includes stiffness and damping of the hinges, rigid actuators, and lead-lag dampers with damper specifications.

The blade shape is created as 2D point coordinates using XFOIL tool. Using these point coordinates, 3D wing is generated with a script for given span chord and twist angle

inputs. Then, solid model of 3D wing is generated by directly inserting this 3D wing data to Simcenter 3D NX. After modelling the 3D wing, finite element model (FEM) of the blade is created and inserted to the kinematic model in Simcenter 3D Motion. Linear and nonlinear modes for all 3 types of degree of freedoms (flapping, lead-lag, and feathering) are generated with the FEM model of blades. The simulation parameters are generated as more satisfying with finite element model of blade. Deformation in flapping up and down motions are giving more realistic simulation parameters. Stress distributions on blades are presented as compression and tension parts reasonably in flapping up and down motions.

An aerodynamic load application method called Blade Element Theory is also generated in order to create aerodynamic loads in Simcenter 3D. Blade element theory is directly created in Simcenter 3D motion. Airfoil aerodynamic database created by XFOIL tool is inserted to the model. This database is used in each section of the blades using sectional aerodynamic force and moment calculations. Other main rotor components are assumed as not creating any aerodynamic forces and moments in aerodynamic model. Forward flight and hover flight conditions are simulated using the blade element theory on the blades.

The aerodynamic effect of one blade to another blade is neglected in aerodynamic model. In addition, rotor bub mechanism does not contain a flexible part since the deflection of components of the rotor hub is negligible for this study. Due to these assumptions, in the rotor model, just one blade with the rotor HUB mechanism is used for simulation. The simulation of other blades is neglected in order to decrease the unnecessary complexity of the model and cost for the solution. The blade is created with positive linear twist angle. This makes the blade incidence negative at the tip and increasing from tip to root.

A FLIGHTLAB isolated main rotor model is also generated by selecting blade element theory. The same hinge locations and root cut-out value are used in order to implement the FLIGHTLAB model. The same twist distributions and the same airfoil profile with Simcenter 3D model are also used. However, the blade is modelled as rigid in both models for comparison since flap lag and pitch mode shapes could not be generated for FLIGHTLAB model. Inflow effect is closed in both models. Some hover and forward flight scenarios are simulated in Simcenter 3D rotor model and some hover trim and forward flight simulation results are generated in FLIGHTLAB rotor model. These results are compared.

Hover and forward flight maneuvers are then performed with the flexible Simcenter 3D model. Four flexible analyses are conducted, including two hover simulations with 4-degree and 8-degree blade pitch inputs, and two forward flight simulations examining cyclic pitch input and the effect of free stream velocity. In each hover simulations, constant rotational velocity input to rotor shaft and constant pitch up input to rotor blade are given. Also, constant rotor rotational velocity, constant collective and cyclic pitch inputs are implemented to the model in the first forward flight simulation. In addition, in second forward flight simulation, rotor model is putted into a constant freestream. The results, including flap, lag, pitch angle, sectional blade velocity, angle of attack, aerodynamic forces and bending moment, rotor blade system bending moment and von-Misses stress distributions, are presented in result plots with respect to azimuth angle.

After verification of the model is completed, rotor model simulation parameters under different design solutions are tested in this thesis. While the main rotor hub mechanism is kept constant, blade is designed with different design parameters. Then, wing span and chord length effect for constant blade solidity are investigated. Finally, linear twist distribution effect is also investigated.

6. CONCLUSION AND DISCUSSION

The developed model has undergone verification and design studies, and the results and conclusions of these studies are discussed in the following subchapters of the thesis.

6.1. Verification Results of Rotor Model

Pitch and flap angle response of FLIGHTLAB rotor model trim and simulations solutions and Simcenter 3D model simulations are showing great correlations for forward and hover flight scenarios as shown in Figure 60, Figure 61 and Figure 62.

Other parameters of rotor blade in hover flight are also investigated using elastic model. Flap angle of the blade remains constant during the simulation and this means the rotor model gets a coning shape. When the collective pitch input is increased, the aerodynamic forces and moments are increased so that the rotor blade flap, lead-lag and pitch angles are increased. The discussed results are expected results for hover condition.

Other parameters of rotor blade in forward flight are also investigated using elastic model. When a helicopter main rotor is in forward flight or if a pilot gives a cyclic pitch input to the rotor, the rotor started to perform flapping motion since the aerodynamic forces and moments are started to be different at each azimuth angle. Therefore, the flapping, lead lagging and pitching angles of blade should be periodically vary during a 360-degree azimuth angle range. In the simulations, it is shown in the parameters that, the blade is performing periodic motions with cyclic pitch input. When rotor mechanism is put into a freestream, difference of rotor aerodynamic loads in right-hand side and left-hand side of rotor disk with respect to the freestream direction is increased since blade velocity is increased in advancing side and decreased in retreating side. This situation increases blade angle variations during 360-degree azimuth angle range. These are expected results for a helicopter rotor simulation.

In each run it is demonstrated that blade angle of attack values are decreased from root to tip because of twist angle. However, blade aerodynamic loads are increased from root to tip due to the majority of linear velocity of each station. Also, blade stress distributions in hover flights are almost the same in each azimuth angles whereas in forward flight conditions, the periodic variations on blade stress distributions are observed. These are also an expected results for helicopter main rotor simulations.

The thesis work shows modelling and analyses of a helicopter rotor model in Simcenter 3D. A rotor model in Simcenter 3D shows a reasonable dynamic result as shown in blade angle parameters and as shown in the comparison with FLIGHTLAB model. In addition, flexible 3D model of a helicopter main rotor blade is also generated in Simcenter 3D and stress distributions on blade are traced in different maneuvers and reasonable results are generated. Rotor loads with different design solutions are also compared. PYTHON tool is used in order to make the work efficiently. The work concludes that a rotor model can be generated and analyzed using Simcenter 3D features and almost all dynamic features of a rotor model can be analyzed using Simcenter 3D.

6.2. Rotor Aerodynamic and Structural Responses to Design Solutions

Simulation responses to variety of blade material is checked. Since flexibility of the blade is changing for different materials, changing of angle of attack and flapping angle are traced. For stiff materials, blade is performing a behavior closer to rigid body whereas for less stiff materials, the changings in angles are more visible. Increase in angle of attack means increase aerodynamic forces. Due to more flexibility in less stiff materials, angle of attack and flap angles of blades are increasing. This concluded as lifting force on blades are increasing for less stiff materials. Effect of material on pitch link and damper loads are very small since main load carrying members are hinges of blade. But rotor system bending moment loads are increasing for more stiff material due to contribution of more mass and inertial properties.

The aerodynamic forces are increasing for increasing rotor blade radius and chord as expected.

Without twist, the blade aerodynamic loads are parabolically increasing from root to tip as expected. With twist angle, aerodynamic loads distribution on blade are varying and varying distribution of lifts are given in related figures. Effect of elasticity on different twist distribution designs are also checked in the study. It is concluded that, elasticity can increase the lift generation of blade if a good selection of twist distribution is performed.

6.3. Future Studies

Static CFD solutions of the modelled blade for each angle of attack(α) and sideslip angle(β) combinations can be performed and aerodynamic database created with the CFD solutions can be implemented to the model. Coupling methodology together with CFD can be performed. Rotor parameters created in this study are intended to be compared with the parameters of the model of future work. Design optimization algorithm can be implemented. Using design optimization, best design tried to be created for some performance criteria. Fatigue life of designed blades can also be investigated in the future work. The rotor model can be validated with and appropriate test data.

7. REFERENCES

[1] Johnson, W. (2013) Rotorcraft Aeromechanics. Cambridge University Press.

[2] Sankar, Lakshmi. (2018). ERF 2016 Coaxial Rotor Paper.

[3] Yaakub, Mohd & Wahab, A.A. & Abdullah, Aslam & Nik Mohd, Nik Ahmad Ridhwan & Shamsuddin, S.S. (2017). Aerodynamic prediction of helicopter rotor in forward flight using blade element theory. JOURNAL OF MECHANICAL ENGINEERING AND SCIENCES. 11. 2711-2722. 10.15282/jmes.11.2.2017.12.0246.

[4] Paul J. C. (1958). Lift and Profile-Drag Characteristic of an NACA0012 Airfoil Section as Derived from Measured Helicopter Rotor Hovering Performance. Report/Patent Number: NACA-TN-4357.

[5] Ilkko, Juho & Hoffren, Jaakko & Siikonen, Timo. (2011). Simulation of a helicopter rotor flow. Rakenteiden mekaniikka. 44. 186-205.

[6] Skiba, Krzysztof. (2019). Designing and FEM simulation of the helicopter rotor and hub. IOP Conference Series: Materials Science and Engineering. 710. 012003. 10.1088/1757-899X/710/1/012003.

[7] "Aerodynamic Coefficients." [Online]. Available: http://airfoiltools.com/airfoil/details?airfoil=naca23015-il

[8] P. Persson, P. Weinerfelt, and S. Aeronautics, "A coupled aero and structural dynamics model for computation of unsteady loads on the helicopter skeldar v200"

[9] J. Gordon L. (2006) Principles of Helicopter Aerodynamics. 2nd edition, Cambridge University Press.

[10] Bramwell A. R. S, Gorge D. and David B. (2000) Bramwell's Helicopter Dynamics 2nd edition.

[11] Shinoda, Patrick & Norman, Thomas & Jacklin, Stephen & Bernhard, A.P.F. & Yeo, Hyeonsoo & Haber, Axel. (2023). Investigation of a Full-Scale Wide Chord Blade Rotor System in the NASA Ames 40-by 80-Foot Wind Tunnel.

[12] Romander, Ethan & Meyn, Larry & Norman, Thomas & Barrows, Danny & Burner, A. (2014) Blade Motion Correlation for the Full-Scale UH-60A Airloads Rotor.

[13] Park, Jae-Sang. (2013). Multibody analyses for performance and aeromechanics of a rotor in low-speed flight. Aircraft Engineering and Aerospace Technology: An International Journal. 86. 10.1108/AEAT-09-2012-0150.

[14] Kunz, Donald & Jones, Henry. (2001). Modeling and Simulation of the Apache Rotor System in CAMRAD II.

[15] Sun, Tao & Tan, J. & Wang, Haowen. (2013). Investigation of rotor control system loads. Chinese Journal of Aeronautics. 26. 1114–1124. 10.1016/j.cja.2013.07.029.

[16] S-61 Sea King Rotor Head Animation. [Online]. Available: https://www.youtube.com/watch?v=83h6QK-oJ4M&t=161s

[17] Simcenter 3D Motion Documentation on Support Center. [Online]. Available: https://docs.sw.siemens.com/en-US/product/289054037/doc/PL20201029134623742.motion/html/id563081

[18] Castillo-Rivera, S. & Tomas-Rodriguez, M.. (2016). Helicopter nonlinear aerodynamics modelling using VehicleSim. Advances in Engineering Software. 100. 252-265. 10.1016/j.advengsoft.2016.08.001.

[19] G. D. Padfield, Helicopter Flight Dynamics: The Theory and Application of Flying Qualities and Simulation Modeling, American Institute of Aeronautics and Astronautics, Inc., Washington DC, 2007.
[20] "From Wood to Composite Materials the Evolution of the Rotor Blade." [Online]. Available: https://helicoptermaintenancemagazine.com/article/wood-composite-materials-evolution-rotor-blade
[21] Garinis, Dimitrios & Dinulovic, Mirko & Rasuo, Bosko. (2012). Dynamic Analysis of Modified Composite Helicopter Blade. FME Transactions. 40.
[22] Loutun, Mark & Didane, Djamal & Mohideen Batcha, Mohd Faizal & Abdullah, Kamil & Ali, Mas & Mohammed, Akmal Nizam & Afolabi, Lukmon. (2021). 2D CFD Simulation Study on the Performance of Various NACA Airfoils. CFD Letters. 13. 38-50. 10.37934/cfdl.13.4.3850.
[23] "XFOIL Subsonic Airfoil Development System" [Online]. Available: https://web.mit.edu/drela/Public/web/xfoil/
[24] "Product Overview" [Online]. Available: https://www.flightlab.com/flightlab.html
[25] Wall, Berend & Junker, B. & Burley, Casey & Brooks, T.F. & Yu, Y. & Tung, C. & Raffel, M. & Richard, Hugues & Wagner, W. & Mercker, Edzard & Pengel, K. & Holthusen, H. & Beaumier, P. & Delrieux, Yves. (2002). The HART II Test in the LLF of the DNW - a Major Step towards Rotor Wake Understanding. 42.1-42.16.